Reynolds number effects in wall-bounded turbulent flows

Mohamed Gad-el-Hak

University of Notre Dame, Notre Dame, IN 46556-5637

Promode R Bandyopadhyay

Naval Undersea Warfare Center, Newport, RI 02841-5047

This paper reviews the state of the art of Reynolds number effects in wall-bounded shear-flow turbulence, with particular emphasis on the canonical zero-pressure-gradient boundary layer and two-dimensional channel flow problems. The Reynolds numbers encountered in many practical situations are typically orders of magnitude higher than those studied computationally or even experimentally. High-Reynolds number research facilities are expensive to build and operate and the few existing are heavily scheduled with mostly developmental work. For wind tunnels, additional complications due to compressibility effects are introduced at high speeds. Full computational simulation of high-Reynolds number flows is beyond the reach of current capabilities. Understanding of turbulence and modeling will continue to play vital roles in the computation of high-Reynolds number practical flows using the Reynolds-averaged Navier-Stokes equations. Since the existing knowledge base, accumulated mostly through physical as well as numerical experiments, is skewed towards the low Reynolds numbers, the key question in such high-Reynolds number modeling as well as in devising novel flow control strategies is: what are the Reynolds number effects on the mean and statistical turbulence quantities and on the organized motions? Since the mean flow review of Coles (1962), the coherent structures, in low-Reynolds number wall-bounded flows, have been reviewed several times. However, the Reynolds number effects on the higher-order statistical turbulence quantities and on the coherent structures have not been reviewed thus far, and there are some unresolved aspects of the effects on even the mean flow at very high Reynolds numbers. Furthermore, a considerable volume of experimental and full-simulation data have been accumulated since 1962. The present article aims at further assimilation of those data, pointing to obvious gaps in the present state of knowledge and highlighting the misunderstood as well as the ill-understood aspects of Reynolds number effects.

CONTENTS

Nomenclature 308
1. Introduction 309
   1.1 Field versus laboratory flows 309
   1.2 Reynolds number 309
   1.3 Outline of present review 310
2. Contemporary relevance 311
   2.1 Primary issues 311
   2.2 Turbulence modeling 311
   2.3 Flow control and post-transition memory 312
3. Flow regimes 313
   3.1 Viscous region 313
   3.2 Constant-Reynolds stress region 314
   3.3 Outer Layer 315
4. Comparison to other shear flows 316
5. Mean flow 319
   5.1 Streamwise velocity 319
   5.2 Von Kármán constant 320
   5.3 The illusory asymptotic state 321
   5.4 Is self-preservation ever achieved? 322
   5.5 Alternatives to the logarithmic profile 324
6. Higher-order statistics 325
   6.1 Root-mean-square velocity fluctuations 325
   6.2 Reynolds stress 330
      6.2.1 Reynolds number effects 330
      6.2.2 Peak location 332
      6.2.3 Asymptotic theory 333
   6.3 Spectra 333
   6.4 Skewness and flatness factors 335
   6.5 Wall-pressure fluctuations 338
7. Coherent structures 339
   7.1 Overview 340
   7.2 Open issues 341
      7.2.1 Origin of different structures 341
      7.2.2 Inner/outer interaction and regeneration mechanisms 342
   7.3 Reynolds number effects 344
      7.3.1 Bursting period 344
      7.3.2 High Reynolds number 345
      7.3.3 Small structures in outer layer 346
      7.3.4 Inner structures 348
8. Flow control 350
   8.1 Introductory remarks 350
   8.2 Riblets 351
   8.3 Recovery response 351
      8.3.1 Disturbances in outer layer 352
      8.3.2 Disturbances close to wall 352
   8.4 Control of high-Reynolds number flows 353
9. Numerical simulations 353
   9.1 General remarks 353
   9.2 Direct numerical simulations 355
10. Non-canonical boundary layers 356
11. Concluding remarks 358
Acknowledgment 359
References 359
Biographies 365

Transmitted by Associate Editor HJS Fernando

ASME Reprint No AMR148 $38
Appl Mech Rev vol 47, no 8, August 1994

NOMENCLATURE

a	pipe radius or channel half-width
c_x	longitudinal phase velocity
C_f	local skin-friction coefficient $= \tau_w / \left(\frac{1}{2}\rho U_o^2\right)$
C_{fo}	skin-friction value for negligible freestream turbulence
C_x, C_y, C_z	typical eddy lengths along x, y, and z
d	vortex diameter
$D_{\text{K.E.}}$	dissipation of turbulence kinetic energy
DR	drag reduction with respect to reference (unaltered) case
E	energy
f	bursting frequency, Hz
f_s	freestream turbulence parameter $= \left\{\left[u'/U_o\right]/\left[(L_o/\delta)+2\right]\right\}$
f_β	freestream turbulence parameter modified by a damping factor $= f_s\beta^n$
F_u	flatness factor (or kurtosis) of streamwise velocity fluctuations $= \left(\overline{u^4}\right)/\left(u_{\text{rms}}\right)^4$
F_υ	flatness factor of normal velocity fluctuations
G	Clauser's velocity-profile shape parameter $= \int_0^\delta \left(\frac{U_o-U}{U_\tau}\right)^2 dy \Big/ \int_0^\delta \left(\frac{U_o-U}{U_\tau}\right) dy$
h	riblet height
H	shape factor $= \delta^*/\theta$
k	wavenumber
k_z	spanwise wavenumber
ℓ	mixing length or hot-wire length
L	size of largest eddies in the flow
L_o	longitudinal dissipation length-scale in the freestream
M_∞	freestream Mach number
p'	root-mean-square value of the pressure fluctuations
P_{KE}	production of turbulence kinetic energy
$\boldsymbol{P}$	two-dimensional spetrum $= \boldsymbol{P}\left(k_z^+, \omega^+\right)$
q^2	twice the turbulence kinetic energy
$R_{u\upsilon}$	shear correlation coefficient $= -\overline{u\upsilon}/\left(u_{\text{rms}}\upsilon_{\text{rms}}\right)$
Re_a	channel or pipe Reynolds number based on centerline velocity and channel half-width or radius
Re_c	a critical value of Re above which the turbulence structure changes
Re_L	Reynolds number based on plate length and freestream velocity
Re_t	turbulence Reynolds number $= u'L/\nu$
Re_x	surface-length Reynolds number $= U_\infty x/\nu$
Re_Γ	vortex Reynolds number $= \Gamma/\nu$
Re_θ	momentum-thickness Reynolds number $= U_\infty\theta/\nu$
Re^*	ratio of outer length-scale (δ or a) to inner length-scale (ν/U_τ) (δ^+ or a^+ is also used to notate same quantity)
s	spanwise spacing of V-groove riblets
S_u	skewness factor of streamwise velocity fluctuations $= \left(\overline{u^3}\right)/\left(u_{\text{rms}}\right)^3$
S_υ	skewness factor of normal velocity fluctuations
$S_{(du/dt)}$	skewness factor of velocity derivative with respect to time
t	time
T	bursting period
T_u	freestream turbulence intensity $= u_{\text{rms}}/U_\infty$
u, υ, w	components of velocity fluctuations along x, y, and z, respectively
u'	root-mean-square value of the streamwise velocity fluctuations
$-\overline{u\upsilon}$	time-mean (kinematic) Reynolds shear stress
U	mean velocity within the boundary layer in the x-direction
U_ℓ	centerline velocity in pipe or channel
U_τ	local friction velocity $= (\tau_w/\rho)^{1/2}$
U_o	velocity at edge of shear layer
U_∞	freestream velocity in boundary layer
$W(y/\delta)$	universal wake function
x, y, z	longitudinal, surface normal, or spanwise coordinates, respectively
y_p	location of peak Reynolds stress
β	damping factor $= \left[1+3\ e^{-(\text{Re}_\theta/425)}\right]$
γ	intermittency factor
$\gamma(x)$	circulation per unit length of a vortex sheet
Γ	total circulation in a vortex tube
δ	boundary-layer thickness
δ^*	displacement thickness
ΔU^+	strength of the wake component in wall units
ΔC_f	change in skin friction due to freestream turbulence
θ	momentum thickness
η	appropriately normalized transverse distance in a wake flow
κ	von Kármán's constant
λ_x, λ_y, λ_z	Taylor's micro-scales or wavelengths along x, y, z, respectively
μ	coefficient of dynamic viscosity
ν	kinematic viscosity $= \mu/\rho$
ρ	density
τ_w	wall-shear stress $= \mu(\partial U/\partial y)_w$
Φ	power spectrum of turbulent velocity or Reynolds stress fluctuations
ω	radian frequency $= 2\pi f$
ω_x, ω_y, ω_z	components of vorticity fluctuations along x, y, and z
Ω_x, Ω_y, Ω_z	mean vorticity components along x, y, and z

Subscripts:

max	maximum value
ref	reference (unaltered) case
rms	root mean square
w	variable computed at wall
τ	value based on the shear stress at the wall
∞	freestream condition

Superscript:

+ non-dimensionalized with wall-layer scales, viz U_τ for velocity, ν/U_τ for length, and ν/U_τ^2 for time

′ root-mean-square (rms) value

1. INTRODUCTION

1.1 Field versus laboratory flows

It is difficult to overstate the technological importance of the turbulent wall-bounded flow. Vast amount of energy is spent in overcoming the turbulence skin-friction drag in pipelines and on air, water and land vehicles. For blunt bodies, *eg*, trucks and trains, the pressure drag resulting from boundary layer separation can be several orders of magnitude higher than the skin friction, and even more energy is wasted. Heat transfer and mixing processes crucially depend on the turbulent transport for their efficient attainment. The Reynolds numbers encountered in many practical situations are typically orders of magnitude higher than those studied computationally or even experimentally (Fig 1). Yet, our knowledge of high-Reynolds number flows is very limited and a complete understanding is yet to emerge. The existing knowledge base, accumulated mostly through physical as well as numerical experiments, is clearly skewed towards low Reynolds numbers. For many practical applications the key question is then what are the Reynolds number effects on the mean and statistical turbulence quantities and on the organized motions of turbulence? One always hopes that the flow characteristics become invariant at sufficiently high Reynolds number. That merely shifts the question to what is high enough?

Consider the simplest possible turbulent wall-bounded flow, that over a smooth flat-plate at zero incidence to a uniform, incompressible flow or its close cousin the two-dimensional channel flow. Leaving aside for a moment the fact that such idealized flow does not exist in practice, where three-dimensional, roughness, pressure-gradient, curvature, wall compliance, heat transfer, compressibility, stratification, and other effects might be present individually or collectively, the canonical problem itself is not well understood. Most disturbing from a practical point of view are the unknown effects of Reynolds number on the mean flow, the higher-order statistical quantities and the flow structure. The primary objective of the present article is to review the state of the art of Reynolds number effects in wall-bounded shear-flow turbulence, with particular emphasis on the canonical boundary layer and channel flow problems.

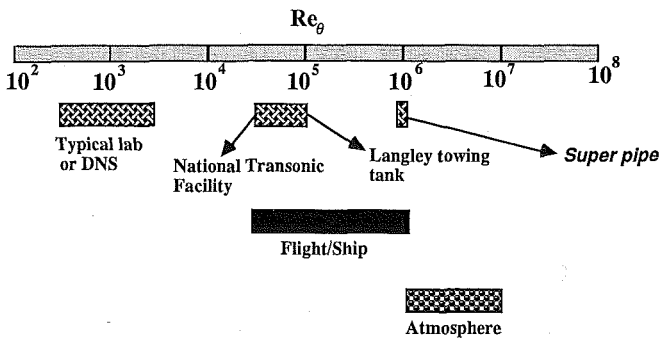

Fig 1. Ranges of momentum-thickness Reynolds number for different facilities and for field conditions.

1.2 Reynolds number

Reynolds number effects are intimately related to the concept of dynamic similarity. In a given flow geometry, if L and U are the length and velocity scales, respectively, the non-dimensional equation of motion for an effectively incompressible fluid is given by:

$$\frac{\partial \vec{u}}{\partial t} + (\vec{u}.\nabla)\vec{u} = -\nabla P + \frac{1}{\mathrm{Re}}\nabla^2\vec{u} \qquad (1)$$

where $\mathrm{Re} = UL/\nu$, P is pressure and ν is kinematic viscosity. This seemingly superficial non-dimensionalization reveals two important properties. The first is the concept of *dynamic similarity*. No matter how L, U, and ν are varied, as long as Re is the same in two geometrically similar flows, they have the same solution. Small-scale model testing of large-scale real-life flows is based on this property. Secondly, for a given geometry and boundary condition, the effect of changing L, U, or ν, or any combination of them,

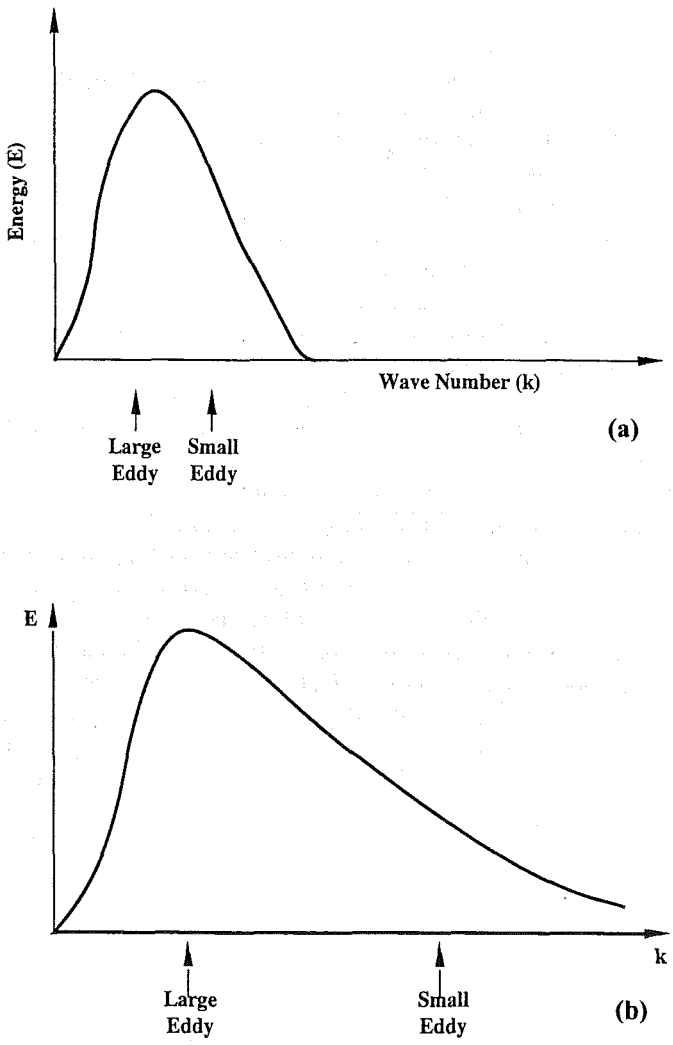

Fig 2. Energy spectra at low and high Reynolds numbers: (a) Low Reynolds number; (b) High Reynolds number

can be described uniquely by the change of Re alone. Although, the importance of Re was recognized earlier by Stokes, it has come to be termed Reynolds number in recognition of Osborne Reynolds' telling demonstration of its effect on the onset of turbulence (Reynolds, 1883). Even today, the laminar-to-turbulent transition is one of the most dramatic Reynolds number effects and its rational computation continues to be a research challenge.

Equation 1 shows that Re represents the relative importance of viscous and inviscid forces. Since three forces, *viz* inertia, pressure, and viscous, are in equilibrium, the balance can be described by the ratio of any two, although it has become customary to characterize the flow by the ratio of inertia to viscous forces.

In this paper, only turbulent flows are considered because they are widely prevalent. The recent report by Bushnell *et al* (1993) treats Reynolds number similarity and scaling effects in laminar and transitional flows. The understanding of the effects of Reynolds number relies on our understanding of viscous forces. For a wall-bounded flow, this is true no matter how high the Reynolds number is. Experience shows that there is no practical Reynolds number where the no-slip boundary condition, which owes its origin to viscous effects, switches off. Since the net viscous force on an element of incompressible fluid is determined by the local gradients of vorticity, the understanding of the vorticity distribution is the key to determining Reynolds number effects. Vorticity can be produced only at a solid boundary and cannot be created or destroyed in the interior of a homogeneous fluid under normal conditions.

The qualitative effects of Reynolds number on the scales of turbulence are demonstrated in the two velocity-fluctuations spectra depicted in Fig 2. The large scale is only weakly dependent on Reynolds number (Townsend, 1976). However, as Reynolds number increases, the small scales become physically smaller (larger wavenumbers) and the diversity of intermediate scales between the large and small increases. In terms of organized motions in a turbulent boundary layer, the effect of Reynolds number on the omnipresent elongated vortex loops (horseshoes) is as sketched in Fig 3, from Head and Bandyopadhyay (1981). With increasing Reynolds number, the aspect ratio of the constituent hairpin vortices increases while the vortices become *skinnier*. The related result, viz. the relative shrinking of the inner layer where viscous effects are stronger is shown in the mean-velocity profiles depicted in Fig 4. Significantly, the two flows have approximately the same boundary layer thickness (13 cm). While the inner layer occupies most of the boundary layer for the low-Reynolds number flow, it shrinks to a very small proportion at high Reynolds number.

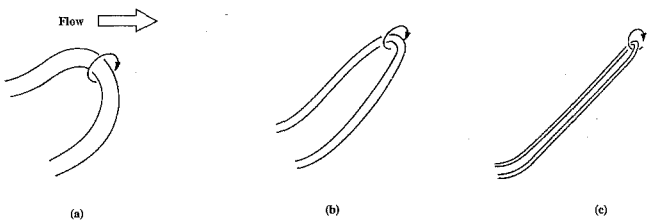

Fig 3. Qualitative effect of Reynolds number on features composing the outer region of a turbulent boundary layer (from Head and Bandyopadhyay, 1981): (a)Vortex loop at very low Re; (b) Elongated loop or horseshoe at low to moderate Re; (c) Hairpin or vortex pair at moderate to high Re.

1.3 Outline of present review

In this article, the effects of Reynolds number on the mean flow, coherent structures and statistics of turbulent boundary layers and channel flows are reviewed. Published data are re-examined in light of the following questions. (1) Does the boundary-layer turbulence structure change after the well known Reynolds number limit, *viz* when $Re_\theta > 6x10^3$? (2) Is it possible to disturb a high-Reynolds number, flat-plate turbulent boundary layer near the wall such that the recovery length is O[100δ]? (3) How close is the numerically simulated low-Reynolds number, flat-plate turbulence structure to that observed experimentally? The turbulence structure appears to change continuously with Reynolds number virtually throughout the boundary layer and sometimes in unexpected manners at high Reynolds numbers (Bandyopadhyay, 1991).

It is relevant to acknowledge in here two recent doctoral theses by Kailasnath (1993) and Smith (1994), which came to our attention after the bulk of the present paper was written. Both dissertations address somewhat similar questions to those raised in here. Kailasnath (1993) amplifies on the notion of scale similarity using a statistical approach for obtaining valuable information on the structure of the instantaneous momentum flux within laboratory as well as atmospheric turbulent boundary layers. Smith (1994) emphasizes Reynolds number effects on the structural aspects of boundary layers.

The present paper is organized into 11 sections. Following the present introductory remarks, the contemporary relevance of the general topic of Reynolds number effects and of the specific problems of flow control and post-transition memory is given in Section 2. The different regions of the boundary layer are reviewed in the following section. Section 4 highlights the qualitative differences between wall-bounded layers and free-shear flows. Reynolds number effects on the mean flow and on higher-

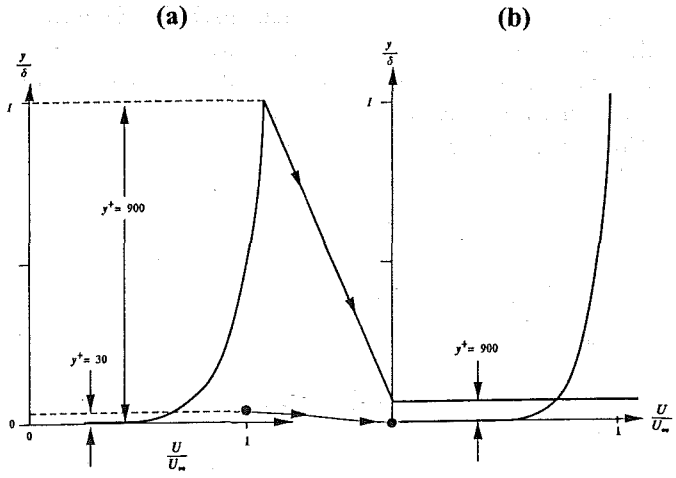

Fig 4. Mean-velocity profiles at low and high Reynolds numbers: (a) Re_θ = 2060; δ^+ = 887; δ = 13.1 cm (from Kline *et al*, 1967); (b) Re_θ = 38,000; δ^+ = 17,350; δ = 12.8 cm (from Tu and Willmarth, 1966).

order statistics are given in Sections 5 and 6, respectively. Outer and inner coherent structures and their interactions are recalled in Section 7. Brief remarks are made on flow control, numerical simulations, and non-canonical boundary layers in the following three sections. Finally, concluding remarks are given in Section 11.

2. CONTEMPORARY RELEVANCE

2.1 Primary issues

Most studies on the structure of flat-plate turbulent boundary layers are being carried out at rather low Reynolds numbers (Fig 1). The few existing high-Reynolds number wind- or water-tunnels are expensive to build and operate and are heavily scheduled with mostly developmental work. Full computational simulation of high-Reynolds number turbulent flows is beyond the reach of current computers. Since many practical flows have very high Reynolds numbers, the question is how relevant are the low-Reynolds number studies to practical situations? For this reason alone the issue of Reynolds number effects is important. The Reynolds number scaling laws are usually given by the wall-layer, outer-layer, or any mixed-layer length, time, and velocity scales which govern the variation of a mean or turbulence quantity with Reynolds number.

The subject is too broad and here it is discussed mostly in light of five questions. One of the earliest studies of the Reynolds number effect in turbulent boundary layers was due to Coles (1962). When measurements of mean-velocity profiles were expressed in inner-layer form based on *directly measured* local friction values, a logarithmic region was found to exist even at an Re_θ of $50x10^3$, where Re_θ is the Reynolds number based on momentum thickness and freestream velocity. The wall-layer variables appear to describe the mean flow in the inner layer universally in flat plates, pipes, and channels at all Reynolds numbers.

On the other hand, in a boundary layer, the behavior of the outer layer, when expressed in terms of wall-layer variables by the strength of the wake component ΔU^+, which is the maximum deviation of the mean-velocity profile from the log law, appeared to reach an asymptotic value for $Re_\theta > 6x10^3$. Above this limit, the inner- and outer-layer mean flows are expected to reach an asymptotic state which the turbulence quantities are also hypothesized to follow. This is, however, not the case since the wake component starts decreasing, albeit slowly, at about $Re_\theta > 15x10^3$. This raises the question, does the mean flow ever achieve true self-preservation?

The situation is murkier for higher-order statistics. Measurements in pipes (Morrison *et al* 1971), channels (Wei and Willmarth 1989), and boundary layers (Andreopoulos *et al* 1984; Erm *et al* 1987) are beginning to show that the turbulence quantities do not scale with wall-layer variables even in the inner layer. Therefore, the question arises, can we apply the mean-flow scales to turbulence?

Furthermore, the outer-layer-device drag reduction experiments of Anders (1990a) show that above this Reynolds number limit, the maximum skin-friction reduction and the recovery length (the latter with some exception) do not remain constant but reduce with increasing Reynolds number. The loss of performance at higher Reynolds numbers is puzzling and Anders attributed it to a significant change in the turbulence structure. In this background, the question does the turbulence structure change when $Re_\theta > 6x10^3$, is discussed.

Consider another puzzling high-Reynolds number behavior. In the fifties, Clauser had experimentally shown that in a turbulent boundary layer at a given Reynolds number, disturbances survive much longer in the outer layer than in the inner layer. He demonstrated this by placing a circular rod in the outer and inner layers of a fully-developed wall layer. In viscous drag-reduction techniques where a device drag penalty is involved, a recovery length of $O[100\delta]$ is desirable to achieve a net gain. To date, with outer-layer devices, such recovery lengths have been achieved only at low Reynolds numbers as mentioned earlier. One normally expects the recovery length to be far less if the disturbances are applied near the wall, and the length to reduce even more as Re_θ is increased. However, published data are re-examined here which shows that, in fact, at higher Reynolds numbers, an opposite trend sometimes takes place. This unexpected result indicates a serious difficulty in the extrapolation of low-Reynolds number results. The fourth question is concerned with this aspect of the Reynolds number effect.

Spalart (1986) has numerically simulated a smooth flat-plate turbulent boundary layer at $Re_\theta = 300$, 670, and 1410. Robinson *et al* (1989) have analyzed the data base at $Re_\theta = 670$ and identified the organized structures. In the last part of the paper, the numerically obtained low-Reynolds number structures are compared with experimental observations.

2.2 Turbulence modeling

Full computational simulation of high-Reynolds number turbulent flows is beyond the reach of current capabilities. Understanding of turbulence and modeling will continue to play vital roles in the computation of high-Reynolds number practical flows using the Reynolds-averaged Navier-Stokes equations (Reynolds, 1895). The mean flow review by Coles (1962) has had a great impact on turbulence modeling. However, that article did not cover any turbulence quantities. Additionally, as will be discussed in Section 5, the effects of Reynolds number on even the mean flow at truly high Reynolds numbers (momentum thickness-based Reynolds number $Re_\theta \geq 1.5x10^4$) are still, unfortunately, not understood and are, surprisingly, even misunderstood and erroneously simplified.

After the work of Coles, interest in organized motion or the so-called coherent structures, had increased. The coherent structures of turbulent boundary layers, particularly for low-Re flows, have been reviewed several times (Willmarth, 1975a; 1975b; Willmarth and Bogar, 1977; Blackwelder, 1978; Cantwell, 1981; Hussain, 1983; Fiedler,

1986; Robinson, 1991). In these reviews, the kinematic features of coherent structures are discussed but, the Reynolds number dependence is by and large not covered. Furthermore, although these developments have greatly improved our understanding of the turbulence production mechanism, their impact on turbulence modeling and flow control have been minimal. The *structural modeling* works of Perry and Chong (1982), Nagano and Tagawa (1990), and Bandyopadhyay and Balasubramanian (1993; 1994) are exceptions and hold some promise.

The Direct Numerical Simulation (DNS) of turbulent boundary layers have so far been carried out up to an Re_θ of 1410 (Spalart, 1986). Since the computational resource required varies approximately as the cube of the Reynolds number, it would not be possible to simulate very high-Reynolds number turbulent shear flows any time soon (Karniadakis and Orszag, 1993). This has created a resurgence of interest in turbulence modeling particularly for high-Reynolds number wall-bounded flows. Thus, there is a need to review the state of the art of Reynolds number effects on the mean flow, turbulence statistics, and coherent structures, so that the flow physics input to any new turbulence model or flow control device is up to date. To be useful to modeling or to flow management, seven requirements of this review paper can be specified:

1. Evaluate the state of the art of aspects of the mean flow at truly high Reynolds numbers left open by Coles (1962).

2. Examine experimental and numerical simulation data to determine the Reynolds number effects on conventional *statistical turbulence quantities*, particularly those which appear in the various forms of the Reynolds-averaged Navier-Stokes equations.

3. Determine if the scaling laws of the mean flow apply to the higher-order turbulence statistics as commonly assumed.

4. Critically investigate the issues of post-transition memory and probe resolution of existing turbulence measurements, including such statistical quantities as root mean square and spectrum.

5. Establish the state of the art of Reynolds number effects on the coherent structures or organized motions, while keeping an eye on the need of *structural modeling*.

6. Attempt to bridge the gap between the coherent structure flow physics and Reynolds-averaged quantities, and thereby make the former useful to a practicing engineer.

7. Finally, it is more useful to review the mean flow, the turbulence quantities and the organized motions in a unified manner than to treat them separately. The advantage is that it will then be possible to examine if the mean-flow scaling laws can indeed be extrapolated to turbulence.

2.3 Flow contrtol and post transition memory

Apart from that in turbulence modeling, knowledge of the Reynolds number effects is useful to flow control. This is because experimental investigations at low Reynolds numbers, *ie* lower speeds and/or smaller length scales, are less expensive. Most flow control devices are, therefore, developed and tested at rather low speeds. Extrapolation to field conditions is not always straightforward though, and it often comes to grief. The relevance of Reynolds number effects to flow control is particularly telling in case of full numerical simulation because it is currently limited to Reynolds numbers that are not that far from transitional values.

One of the objectives of this review article is to highlight the misunderstood and ill-understood aspects of the Reynolds number effects. This should help guide flow control, turbulence modeling research, and data gathering for code validation in the right direction. Two examples would serve to make the point.

In viscous drag reduction techniques where a device drag penalty is involved, as with outer layer devices (OLD), a recovery length ~100δ is desirable to achieve a net gain. As indicated in Section 2.1, this does happen at low Re_θ ($< 6x10^3$) (Anders, 1990a). However, when Anders examined his outer layer devices at higher Reynolds numbers, to his surprise, the drag reduction performance was reduced and the device was no longer a viable candidate for viscous drag reduction. For both low Re_θ ($< 6x10^3$) and high ($> 6x10^3$), the effectiveness of OLD diminishes with the increase of Reynolds number (Bandyopadhyay, 1986a; Anders, 1990a).

The continued drop in the drag reduction comes as a surprise because the mean flow analysis of Coles (1962) indicates an asymptotic state of the outer layer to have been reached above $Re_\theta > 6x10^3$. Anders attributed the irreproducibility of the low-Reynolds number behavior at higher values to a significant change in the turbulence structure at higher Re_θ. As discussed by Head and Bandyopadhyay (1981), a continuous change in the ratio of the outer to the inner layer, $U_\tau\delta/\nu$, is observed even beyond $Re_\theta = 6x10^3$. This also suggests that $U_\tau\delta/\nu$ may be more important to turbulence production than the wake component ΔU^+.

The above example shows that the 1962 review work of Coles is not always providing sufficient guidance on the Reynolds number effects to the research application engineer. The reason seems to be that our knowledge of the Reynolds number effects on the mean flow is not enough for many applications (and modeling), and that we also need to know the *Reynolds number effects on the turbulence*. Considerable amount of statistical mean and turbulent flow data have come out of the experimental and numerical simulations since 1962 and it would be useful to review the state of the art.

That, being armed with the knowledge of Reynolds number effects on the mean turbulent flow alone does not allow one to address all practical problems, can be demonstrated in the unexpected post-transition result reported by Klebanoff and Diehl (1952). Their measurements on artificially thickened boundary layers (see Section 8.3.2 of the present article) showed that the return to the "equilibrium" state is slowed down as the reference Reynolds number is *increased and not decreased!* This raises the question, are the near-wall transition-trip disturbances surviving for increasingly large x/δ as the Reynolds number is increased? This question is clearly important to model testing and code validation data, where roughness is used to trip and thicken

the boundary layer to simulate high Reynolds numbers or flight conditions. Thus, there is also a need to review available experimental data containing the Reynolds number dependence of the distance up to which transition memory survives.

3. FLOW REGIMES

An inspection of the distribution of viscous and turbulence shear stresses in a typical wall-bounded flow demonstrates the presence of three distinct regions. Figure 5, adapted by Sreenivasan (1989) from the smooth-pipe-flow data of Nikuradse (1932) and Laufer (1954), shows such distribution in wall units (friction velocity, $U_\tau = (\tau_w/\rho)^{1/2}$, used as velocity scale, and the ratio of kinematic viscosity to friction velocity used as length scale).

Pipe (or channel) flow data are preferable to flat-plate boundary layer experiments since the Reynolds stress, a rather difficult quantity to measure accurately, can be computed exactly for fully-developed channel flows from the relatively simple measurements of mean-velocity profile and pressure gradient (see Section 6.2). The semi-log plot in Fig 5 enhances the importance of the thin near-wall region relative to the rest of the shear layer.

The broken line in the figure is the time-averaged viscous stress distribution computed by differentiating the mean-velocity profile. Note that this laminar flow concept of shear may not be relevant to the time-dependent turbulent flow, since turbulence models based on the mean velocity gradients have not been widely successful (*eg*, Bradshaw *et al* 1967). Nevertheless, it is clear from the figure that the mean viscous stress, $\mu\ (\partial U/\partial y)$, is important only near the wall. This wall layer is followed by a region of approximately constant Reynolds stress. Finally, an outer layer[1] is characterized by a diminishing turbulence shear stress, reaching zero at the centerline of the pipe. Unlike the second and third regimes, the extent of the first region does not depend on Reynolds number. Both the viscous region and the constant-Reynolds stress region are similar in all wall-bounded flows. In contrast, the outer layer is different in internal flows and boundary layers. Profiles of the mean velocity and other turbulence statistics can be constructed from scaling considerations of the three distinct regimes, as will be seen in the following three subsections.

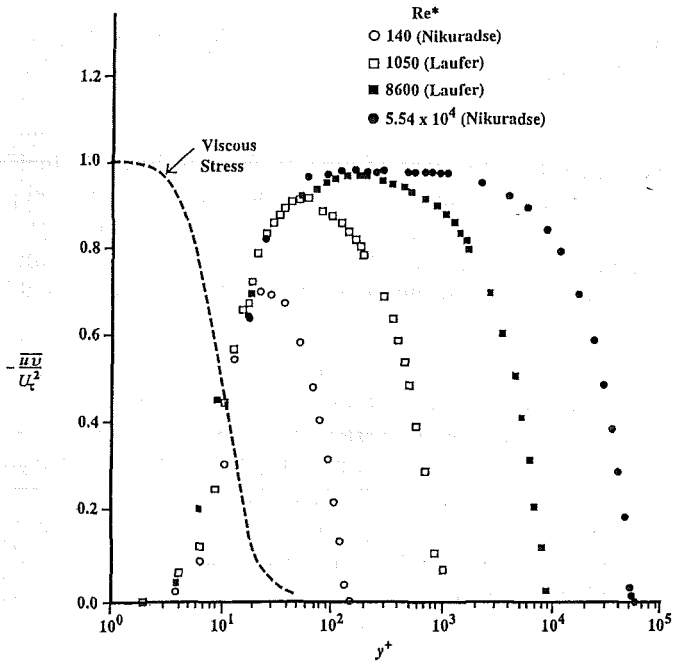

Fig 5. Distribution of viscous and turbulence shear stresses in wall-bounded flows (from Sreenivasan, 1989).

Note that the Reynolds number used as a parameter in Fig 5 is defined as $Re^* = U_\tau a/\nu$; that is the channel half-width (or boundary-layer thickness) expressed in wall units: a^+ (or δ^+). Although numerically Re^* and δ^+ are the same, their difference in significance and usage should be clarified. The variable δ^+ denotes the ratio of the outer- to inner-layer thickness, and represents the degree of shrinking of the latter with respect to the former which changes little with Reynolds number (see Fig 4). It emphasizes the disparity of the two scales and the diversity of the intermediate and interacting scales at higher Reynolds numbers. As will be seen in Section 7, δ^+ indicates the reduction of the hairpin vortex diameter and the increase in its aspect ratio as the Reynolds number increases (Head and Bandyopadhyay, 1981). The value of δ^+ in a typical laboratory experiment is O[1000], while it approaches 100,000 in the boundary layer developing over the space shuttle (Bandyopadhyay, 1990). This variable is pertinent to the understanding of the mechanism of drag reduction by outer-layer devices (Anders, 1990b). On the other hand, Re^* is a Reynolds number, also called a stability parameter by Black (1968). In Black's work and later in Sreenivasan's (1988), Re^* indicates a Reynolds number associated with the quasi-periodic instability and breakup process that is hypothesized to be responsible for the regeneration of turbulence in a wall-bounded flow (Sections 4 and 7). Note that, for a smooth wall, Re^* increases monotonically with Re_θ and never reaches an asymptote.

3.1 Viscous region

Viscosity appears to be important only up to $y^+ = 30$. The viscous region can be subdivided into two subregions: the viscous sublayer and the buffer layer (Fig 6). Very close to the wall, $0 \le y^+ \le 5$, the turbulence shear stress is nearly zero which implies that the only relevant quantities there are the kinematic viscosity ν and friction velocity U_τ.[2] In this viscous sublayer, several turbulence statistics can be asymptotically estimated from considerations of the no-slip condition and continuity and dynamical equations. Following Monin and Yaglom (1971) and using experimental data, Sreenivasan (1989) gives the following Taylor's series expressions, in wall units, for the root-mean-square value of the three fluctuating

[1] Called core region in internal flows.

[2] For *hydraulically rough* walls, *ie* where the average roughness height is greater than the viscous sublayer thickness, the relevant scaling parameters are the characteristic roughness neight and friction velocity.

velocity components and for the Reynolds stress, respectively:

$$U^+ = y^+ - 1\text{x}10^{-4}\, y^{+4} + 1.6\text{x}10^{-6}\, y^{+5} + ... \quad (2)$$

$$u'^+ = 0.3\, y^+ + c_1\, y^{+2} + ... \quad (3)$$

$$v'^+ = 0.008\, y^{+2} + c_2\, y^{+3} + ... \quad (4)$$

$$w'^+ = 0.07\, y^+ + c_3\, y^{+2} + ... \quad (5)$$

$$\overline{-uv}^+ = 4\text{x}10^{-4}\, y^{+3} - 8\text{x}10^{-6}\, y^{+4} + ... \quad (6)$$

For $y^+ < 5$, the leading term of each of the above expansions suffices. Note however that the experimentally determined leading coefficients in Eqs 3-5 are lower than those computed from direct numerical simulations. Mansour *et al* (1988) analyzed the channel-flow data base generated by Kim *et al* (1987) and reported the following leading-term coefficients for u'^+, v'^+ and w'^+: 0.36, 0.0086, and 0.19, respectively. The last coefficient in particular is almost three times that of the corresponding leading term determined experimentally. The reason might be due to the rapid drop in the spanwise velocity fluctuations as the wall is approached, so a very small hot-wire probe or LDV focus would be needed to realize the true value.

With three terms, Eq 2 for the mean velocity is valid up to $y^+ = 20$. Note that the *constants* in the above equations are not necessarily universal. As will be discussed in Section 6, clearly discernible Reynolds number effects will be demonstrated for all higher-order statistical quantities even in the near-wall region.

The buffer layer is where both the viscous stress and the turbulence shear stress are important, and is where the peak production and dissipation of turbulence kinetic energy occur (at about $y^+ = 12$, seemingly independent of the global Reynolds number). In here, the characteristic local Reynolds number of $y\, U_\tau/\nu = 30$ is exceedingly low and turbulence cannot be maintained unless buffeted constantly by strong disturbances, presumably from the outer layer. This region merges with the constant-Reynolds stress layer.

3.2 Constant-Reynolds stress region

This region, loosely interpreted[3] to include all points within the - 3dB points of the peak Reynolds stress, extends from $y^+ = 30$ to $y/a = 0.2$, where a is the pipe radius. Here, the distance from the wall y is much larger than the viscous length-scale, ν/U_τ, but much smaller than the pipe radius (or the boundary layer thickness, δ, for an external flow). Note that the upper extent of this region is a constant fraction of the boundary layer thickness, but varies with Reynolds number when expressed in wall units (see Fig 6).

In this region, viscous stresses are negligible and the momentum flux is accomplished nearly entirely by turbulence. The only relevant length scale is y itself, and the square root of the nearly constant Reynolds stress, $(-\overline{uv}_{max})^{1/2}$, is the appropriate velocity scale. Therefore, the mean-velocity gradient can be expressed as:

$$\partial U/\partial y \sim (-\overline{uv}_{max})^{1/2}/y \quad (7)$$

The well-known logarithmic velocity profile follows directly from integrating Eq 7 and using the velocity at the edge of the viscous sublayer as a boundary condition:

$$U^+ = (1/\kappa)\ln(y^+) + B \quad (8)$$

where κ is the von Kármán constant. Both κ and B are presumably universal constants and are determined empirically for flat-plate boundary layers to be approximately 0.41 and 5.0, respectively. Slightly different values are used for the two constants in the case of pipe or channel flows. In that case, Eq 8 holds almost up to the centerline of the channel. As the Reynolds number increases, the extent of the logarithmic region (in wall units) increases and the maximum Reynolds stress approaches the value of the viscous stress at the wall ($-\overline{uv}_{max}/U_\tau^2 \rightarrow 1$).

Several other methods can be used to derive the logarithmic velocity profile. A mixing length, based on momentum transport, that simply varies linearly with distance from the wall, $\ell = \kappa\, y$, again yields Eq 8. Millikan's (1939) asymptotic analysis recovers the log relation by assuming the existence of a region of overlap where both the inner and outer laws are simultaneously valid (see also the rarely cited albeit relevant article by Izakson, 1937). All models invariably rely on the presence of the constant-stress layer

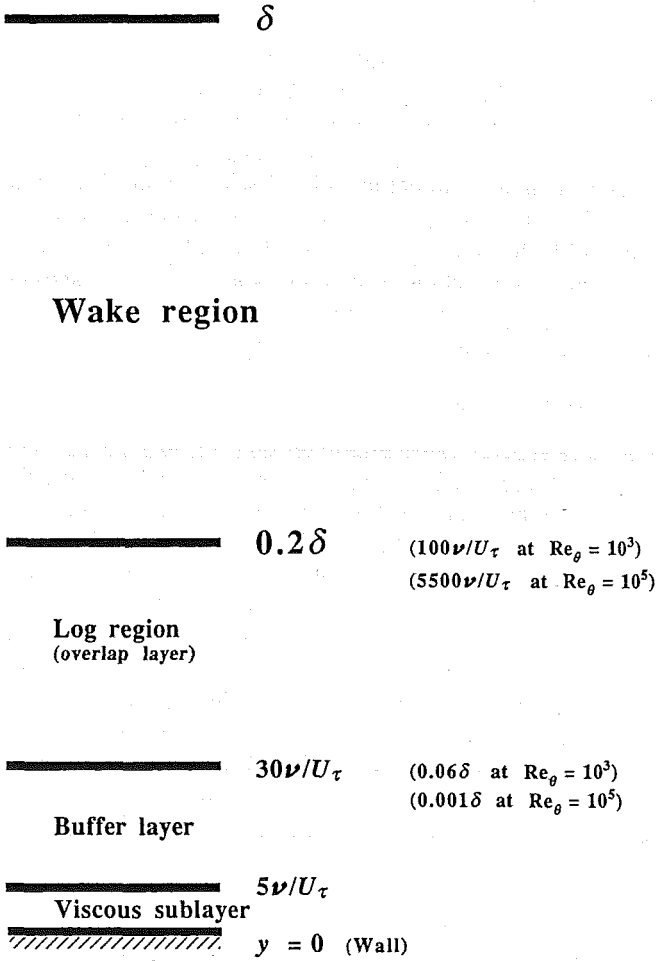

Fig 6. Schematic of the different regions within a wall-bounded flow at typical low and high Reynolds numbers.

[3] Strictly speaking, the Reynolds stress is not really constant anywhere in a pipe or channel flow.

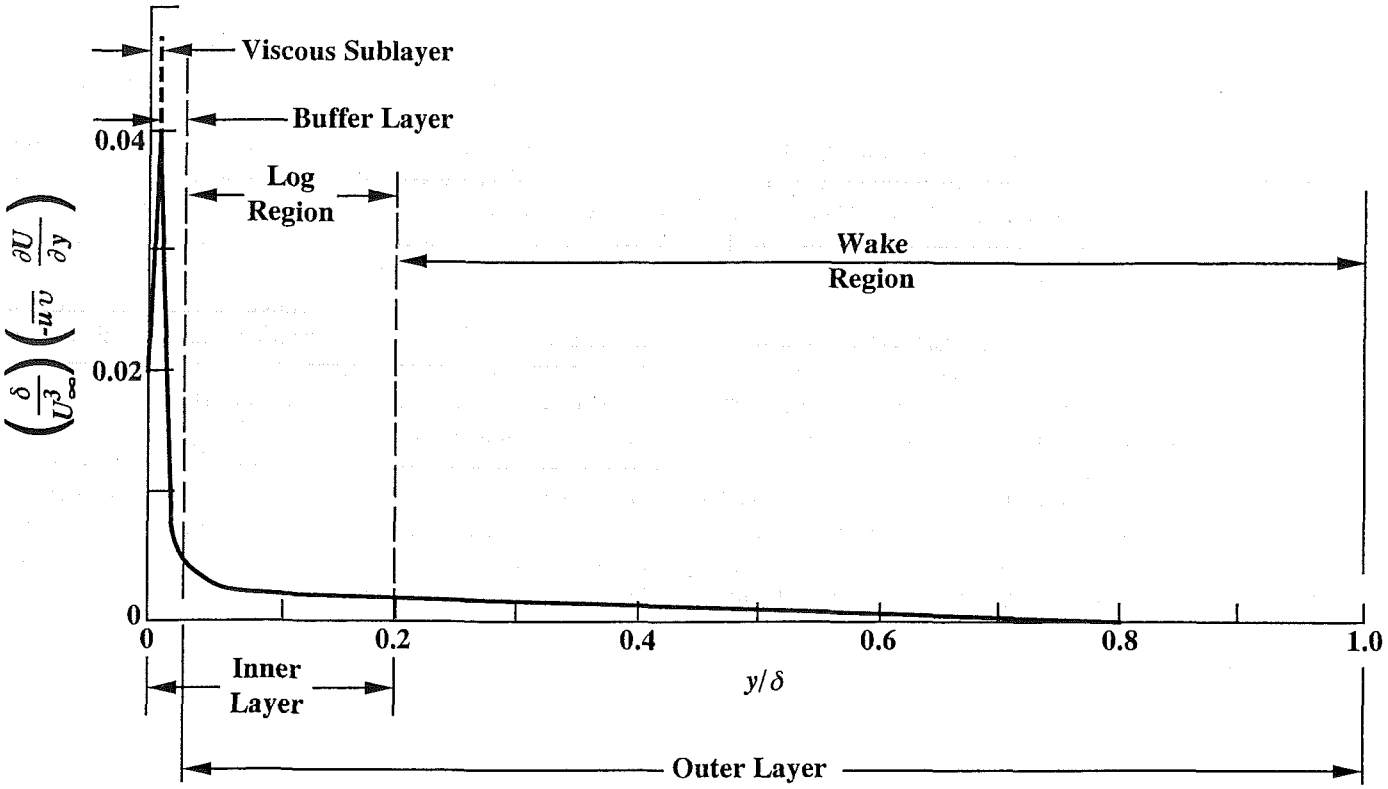

Fig 7. Normalized turbulence kinetic energy production rate as a function of normal distance from the wall. Data for a typical laboratory flat-plate boundary layer (from Kline *et al*, 1967).

experimentally observed at high Reynolds number. Despite copious evidence for the existence of a logarithmic region in the mean-velocity profile, the whole log-law scenario has been periodically questioned (see, for example, Barenblatt, 1979; 1993; Malkus, 1979; Long and Chen, 1981; George *et al*, 1992; 1994; Barenblatt and Prostokishin, 1993). We will return to this point in Section 5.5.

The arguments used by Millikan (1939) to derive the logarithmic relation for the boundary layer are analogous to those employed to establish the universal equilibrium theory of turbulence, called the theory of local similarity by its originator Kolmogorov (1941a; 1941b; 1941c; 1962). For the boundary layer, an *inertial sublayer* exists at sufficiently large Reynolds numbers and the overall flow dynamics is independent of viscosity, which merely provides a momentum sink of prescribed strength at the wall. Similarly, an *inertial subrange* exists in the turbulence energy spectrum when the Reynolds number is large enough. There, the wavenumber is larger than that for the large eddies but smaller than the dissipative wavenumbers. The viscosity again provides the dissipative sink for kinetic energy at the small-scale end of the turbulence spectrum. The spectral shape in the inertial subrange is completely determined by the energy flux across the wavenumber domain.

Similar scaling arguments to those leading to Eqs 7 and 8 can be used in the constant-turbulent stress region to show that:[4]

$$u'/U_\tau = \text{constant} = 2.0 \tag{9}$$

$$v'/U_\tau = \text{constant} = 1.0 \tag{10}$$

$$w'/U_\tau = \text{constant} = 1.4 \tag{11}$$

$$P_{\text{K.E.}} = D_{\text{K.E.}} = U_\tau^3/\kappa y \tag{12}$$

where $P_{\text{K.E.}}$ and $D_{\text{K.E.}}$ are the production and dissipation of turbulence kinetic energy, respectively. Additionally, a portion of the power spectrum for each of the three velocity components exhibits a -1 power law in this same region governed by a constant turbulence shear stress transmitted across its different fluid layers.

The total stress is approximately constant throughout the viscous layer and the constant-Reynolds stress region. This is the so-called inner layer (see Fig 7) and for a smooth wall the mean-velocity profile there is given by the unique similarity law of the wall, first formulated by Prandtl (1925):

$$U^+ = f(y^+) \tag{13}$$

where f is a universal function presumably independent of Reynolds number and streamwise location. The inner law is the same for both internal and external flows.

3.3 Outer layer

Beyond the constant-stress region, an outer layer is characterized by a diminishing turbulence shear stress. Note that

[4] The value of the constants in Eqs 9-12 are determined empirically from mostly low-Reynolds number experiments. Again, Section 6 will reveal that these *constants* depend in fact on the Reynolds number.

some researchers include the constant-Reynolds stress region as part of the outer region. This is perhaps an accurate inclusion since the part of the boundary layer where the logarithmic law is valid is, strictly speaking, the region of overlap between the inner and outer laws (see Fig 7).

In internal flows, intermittency of turbulence and interaction with potential freestream are absent. There is, however, an interaction of turbulence from the opposite wall in case of a two-dimensional channel and this is even more complex in case of a circular pipe. Furthermore, fully-developed conditions for pipes and channels are defined as that all time-averaged flow quantities (except static pressure) are independent of x. Therefore, the core region of a pipe or channel flow differs from the outer layer of a growing boundary layer.

The appropriate length scale in the core region is the pipe radius a (or the boundary-layer thickness, δ, for an external flow). The mean-velocity profile is characterized by the velocity defect $(U_o - U)$, where U_o is the velocity at the edge of the shear layer (centerline velocity U_ℓ for a pipe flow or freestream velocity U_∞ for a boundary layer). The velocity-defect (or, more appropriately, momentum-defect) law, formulated by von Kármán (1930), is given by a second universal function:

$$(U_o - U)/U_\tau = g(y/\delta) \tag{14}$$

This equation is valid even in the logarithmic region and appears to be well confirmed experimentally.

For a turbulent boundary layer, Coles (1956) combined the defect law and the inner law to give the following empirical velocity profile valid throughout the entire wall-bounded shear layer:

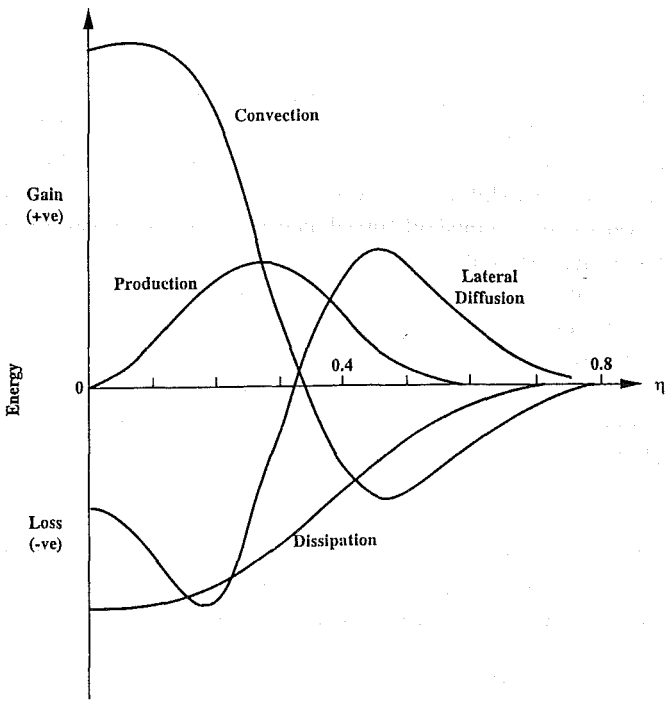

Fig 8. Turbulence energy balance in a typical plane wake (from Townsend, 1976).

$$U^+ = f(y^+) + (\Pi/\kappa)\, W(y/\delta) \tag{15}$$

where κ is the von Kármán constant and Π is a profile parameter that depends strongly on Re for small Reynolds numbers. Coles' idea is that a typical boundary layer flow can be viewed as a wake-like structure which is constrained by a wall. Intermittency and entrainment give rise to the wake-like behavior of the outer part of the flow, which is sensitive to pressure gradient and freestream turbulence. The wall constraint is closely related to the magnitude of the surface shear stress, and is sensitive to the wall roughness and other surface conditions.

For equilibrium flows (Clauser, 1954), the profile parameter Π is independent of streamwise location. The universal wake function $W(y/\delta)$ is the same for all two-dimensional boundary-layer flows. Its form is similar to that describing a wake flow or more precisely the mean-velocity profile at a point of separation or reattachment. For example, the wake function can be adequately represented by:

$$W\left(\frac{y}{\delta}\right) = 2 \sin^2\left[\frac{\pi}{2}\cdot\frac{y}{\delta}\right] \tag{16}$$

Note however that this simple expression obtained empirically by Coles (1969) does not yield zero velocity gradient at the edge of the boundary layer, as it should. Lewkowicz (1982) proposed an alternative quartic polynomial which removes this deficiency.

At the same Reynolds number, deviation of the actual mean-velocity distribution from the logarithmic profile in the core region of a pipe or channel flow is smaller than that in the outer region of a boundary layer. In fact, as mentioned in Section 3.2, the logarithmic velocity profile, Eq 8 with slightly modified constants κ and B, holds approximately up to the centerline of the pipe.

4. COMPARISON TO OTHER SHEAR FLOWS

Before proceeding to investigate the specific effects of Reynolds number on the mean and turbulence quantities of wall-bounded flows, it is instructive to give a coarse comparison between such flows on the one hand and free-shear flows on the other. As it will be illustrated, the presence of the wall is of paramount importance to the issue at hand. No matter how large the Reynolds number is, viscosity must be important in a progressively shrinking region close to the wall and *Reynolds number dependence persists indefinitely.*

Wakes, jets and mixing layers are profoundly different from channel and pipe flows and boundary layers. The absence of the wall in free-shear flows implies that at sufficiently high Reynolds numbers, the flow is nearly inviscid and by implication Reynolds number-independent (Dimotakis, 1991; 1993). For wall-bounded flows, on the other hand, there is always a small, progressively shrinking region near the surface where viscosity must be important, no matter how large the Reynolds number is.

In boundary layers and channel flows, the overall behavior and gross structure of turbulence is always affected by

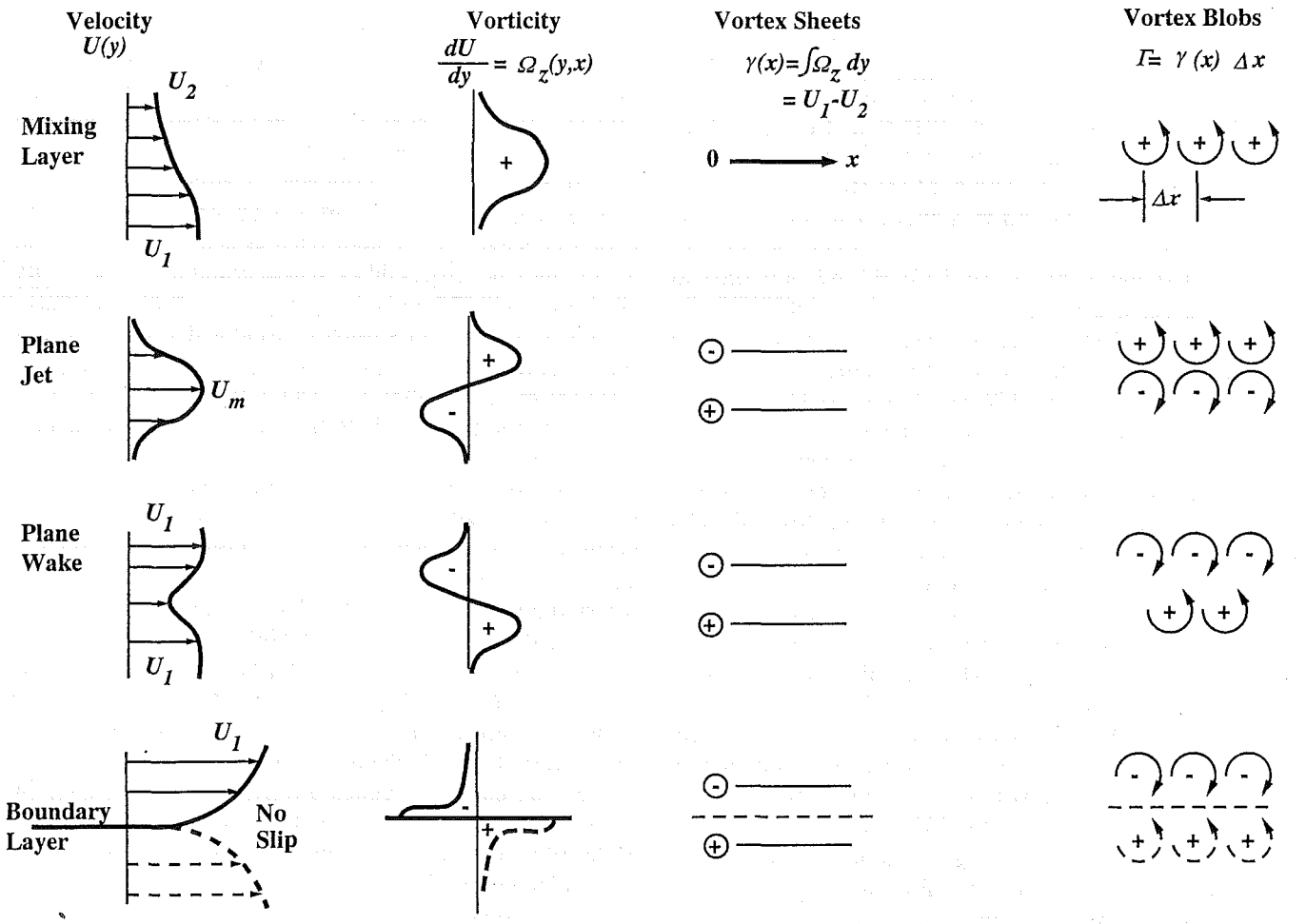

Fig 9. Mean streamwise velocity and mean spanwise vorticity distributions in different shear flows (from Roshko, 1992).

viscosity near the wall, while the direct effect of viscosity gradually diminishes away from the surface. This implies that the velocity and length scales must be different near the wall and away from it. The disparity of scales for wall-bounded flows increases with Reynolds number and true self-preservation may never be achieved, unless the inner and outer scales are forced to be proportional at all Reynolds numbers. This latter scenario can be realized, for example, in the very special case of flow between two planes converging at a prescribed angle.

In wall-bounded flows, very large levels of turbulent fluctuations are maintained close to the wall despite the strong viscous as well as turbulent diffusion. As indicated in Fig 7, at a typical laboratory Reynolds number of say $Re_\theta = O[10^3]$, more than about a third of the total turbulence kinetic energy production (and dissipation) occurs in the 2% of the boundary-layer thickness adjacent to the wall. The fraction of this thickness decreases as the Reynolds number increases (Fig 4). The near-wall region is directly affected by viscosity[5] and its importance to the maintenance of turbulence is clearly disproportional to its minute size.

The thinness of the viscous sublayer presents a great challenge to both physical and numerical experiments. Since this region is closest to the wall and is where drag acts, it is extremely important at all Reynolds numbers. Yet in contemporary direct numerical simulations, the viscous sublayer of 5 wall units is resolved only up to 1.4 wall units. In measurements, probe resolutions are even worse; other than in low-Reynolds number or oil-channel experiments, a probe length of $\ell^+ < 7$ is indeed rare (Bandyopadhyay, 1991).

In free-shear layers, on the other hand, energy production peaks near the inflection points of the mean-velocity profile. Both production and dissipation are spread over the entire flow width as shown in Fig 8 depicting the turbulence energy balance for a typical two-dimensional wake. Above a reasonably modest Reynolds number, $O[10^3]$, all turbulence quantities become invariant to additional changes in Reynolds number.

Despite these differences between boundary layers and free-shear flows, there are also some similarities. The outer region of a boundary layer is characterized by an intermittent rotational/irrotational flow, much the same as that observed in all free-shear flows. Moreover, the outer flow is more or less inviscid at sufficiently high Reynolds numbers,

[5] Through the action of viscous stresses for a smooth wall, or through the action of pressure drag resulting from the separated flow around discrete elements of sufficient size for rough walls.

again being similar to jets, wakes and mixing layers. The interaction between the outer, or *wake*, region of a turbulent boundary layer and the potential flow in the freestream is also similar to that in wakes and other free-shear flows. The above are observational similarities and differences between the wall-bounded turbulent flows and the free-shear layers. In the following, they are compared based on dynamic issues like the applicability of an inflectional inviscid breakdown mechanism, and it is shown that the subject is still wide open.

Inviscid stability theory has been successfully used to predict the observed coherent structures in turbulent free-shear flows, but it is not clear that similar arguments can be made when a wall is present. In other words, it is not obvious that the same inviscid, mean-flow breakdown mechanism responsible for generating the large eddies in, say, a mixing layer is operable in the case of a boundary layer. Consider the mean streamwise velocity and mean spanwise vorticity distributions sketched in Fig 9, from Roshko (1992), for four different shear flows. A two-dimensional mixing layer is modeled as a single vortex sheet placed at the location of peak vorticity (at the point of inflection of the mean-velocity profile). The local circulation per unit length of the vortex sheet, $\gamma(x)$, is equal to the integral of the mean spanwise vorticity, Ω_z, across the shear layer.

This vortex sheet is inviscidly unstable to two-dimensional perturbations and the resulting Kelvin-Helmholtz instability eventually evolves into the omnipresent two-dimensional vortices, observed even in high-Reynolds number mixing layers. The resulting vortex blobs correspond to the saturation state of this instability. As indicated in the sketch, circulation in the blobs is conserved, $\Gamma = \gamma(x)\ \Delta x$. Secondary instabilities of the roll-up structures result in smaller longitudinal vortices and other three-dimensional, hairpin-like eddies.

Similar reasoning lead to the in-phase counter-rotating vortices for plane jets and the staggered Kármán vortex street for two-dimensional wakes. As sketched in Fig 9, both jets and wakes can be modeled as two vortex sheets with opposite signs of vorticity. Again, each sheet is located at the location of spanwise vorticity extrema, and total circulation is conserved.

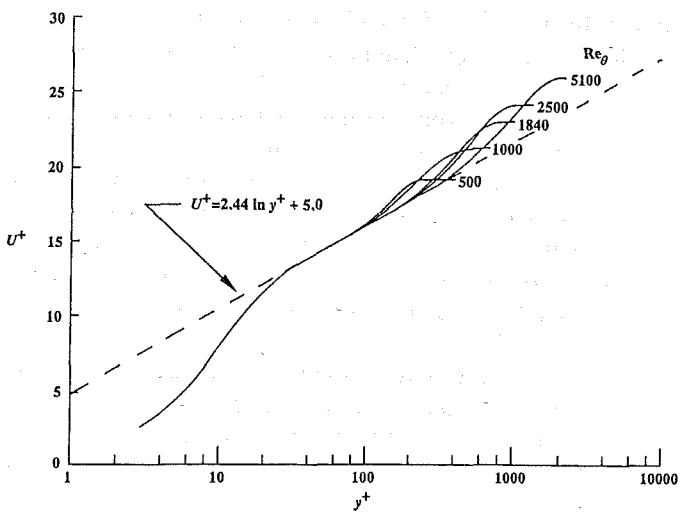

Fig 10. Comparison of mean-velocity profiles with logarithmic law at low Reynolds numbers. Boundary layer data from Purtell *et al* (1981).

For a turbulent wall-bounded flow, however, it is not obvious that the observed large-eddy structures (Section 7) can be derived using similar inviscid arguments. If the boundary layer is modeled by a vortex sheet in which the entire mean flow vorticity has been concentrated, the presence of the wall imposes a boundary condition that necessitates the use of an image vortex sheet of opposite sign of vorticity. Such considerations led Sreenivasan (1988) to propose that the large eddies are the result of an instability of a *caricature* of the real boundary layer. Two- and three-dimensional instabilities, both inviscid and viscous, of this caricature flow lead to a plausible explanation for many observed features including the double-roller structures, hairpin eddies and low-speed streaks (see Section 7 of the present article).

It turns out that a somewhat similar argument was advanced two decades earlier by Black (1968). He treats the mean-flow breakdown as an intermittent, three-dimensional, inviscid process, where a mechanism analogous to the starting vortex of an impulsively started airfoil is in play. He thereby successfully predicts the formation of an array of hairpin vortices due to a passing instability wave. Note that while Theodorsen (1955) *predicted* the formation of hairpin vortices, the aspect of an array of them is absent in his work. In Black's work $U_\tau\delta/\nu$ appears as an important *stability parameter*. Mention should also be made of the waveguide theory developed by Landahl (1967; 1972; 1977; 1980; 1990) to explain the cause and effect relationships for the variety of coherent structures observed in turbulent boundary layers.

In Sreenivasan's model a *fat* vortex sheet and its image are located on either side of the wall at a distance corresponding to the position of the peak Reynolds stress. Because of the absence of inflection points in the interior of the canonical turbulent flow, Sreenivasan (1988) chose the alternative location of peak based upon experience with transitional boundary layers.[6] From all available boundary layer as well as channel flow data, this location appears to scale with the geometric mean of the inner and outer scales. Sreenivasan (1988) termed that position the *critical layer*,[7] although any evidence for the existence of such a two-dimensional layer, where small perturbations are presumed to grow rapidly, is lacking. Using linear stability theory, Sreenivasan successfully showed that the primary instability of the vortex sheet and its image yields two-dimensional roll-up structures, which in turn excite low-speed streaks and bursting. Subsequent instability of the roll-up structures leads to hairpin eddies and double-roller structures. One problem with this picture is that, unlike the case of free-shear flows, the predicted two-dimensional structures have

[6] Note that in the past, both Clauser (1956) and Corrsin (1957) have also attempted to treat the turbulent regenerative process as primarily similar to the breakdown mechanism of a critical laminar layer.

[7] In a transitional wall-bounded flow, the location of peak Reynolds stress coincides with the critical-layer position. Since this location shows similar trends with Reynolds number to that in a turbulent flow (see the lowermost two data points in Fig 34b), Sreenivasan (1988) chose to place his proposed vortex sheet at this location.

never been observed in an actual turbulent wall-bounded flow. Sreenivasan (1988) himself allows that his simplistic model is unfinished and has a number of weaknesses but offers it as a target for useful criticism.

The arguments above indicate that the existence of an inviscid breakdown mechanism responsible for the self-sustenance of the turbulence has not been firmly established. In other words, it is not clear that the observed coherent structures in a boundary layer or channel flow are the result of an instability of the mean flow or its caricature. Until this issue is resolved, progress in the understanding of wall-bounded flows will remain lagging behind that of free-shear flows. Despite the importance of this dynamical issue, research on the organized nature of turbulent boundary layers has remained confined to the kinematics, and high-payoff turbulence control strategies are yet to be developed.

5. MEAN FLOW

Before investigating the issue of Reynolds number effects on coherent structures, available data for the mean velocity and higher-order statistics of wall-bounded flows are reviewed in the present and following sections. Section 5 focuses on the Reynolds number effects on the mean streamwise velocity, and Section 6 discusses these effects on rms velocity fluctuations, Reynolds stress, spectra, skewness and flatness factors, and rms and spectrum of wall-pressure fluctuations.

5.1 Streamwise velocity

The mean flow velocity in the streamwise direction is a relatively easy quantity to measure and almost every paper on wall-bounded flows has such measurements (see, for example, Preston and Sweeting, 1944; Laufer, 1951; Comte-Bellot, 1965; Eckelmann, 1974; Purtell *et al*, 1981; Andreopoulos *et al*, 1984; and Wei and Willmarth, 1989). Requirements for probe resolution are modest and, except very near the wall, most published data are reliable to better than 1%. This is obviously not the case for measurements of higher-order statistics, and this point will be revisited in the following section.

For a turbulent wall-bounded flow, the region directly affected by viscosity, the viscous sublayer plus the buffer layer, occupies progressively smaller proportion of the boundary-layer thickness as the Reynolds number increases (see Fig 6). The rest of the flow is dominated by inertia and the effect of viscosity enters only as an inner boundary condition set by the viscous region. It is not surprising, therefore, that the Reynolds number has a considerable effect on the velocity profile. As Re_θ increases, the mean-velocity profile becomes fuller and the shape factor, H, decreases accordingly. For example, at $Re_\theta = 2000$, $H = 1.41$, and at $Re_\theta = 10{,}000$, $H = 1.33$. The effect is even more pronounced at Reynolds numbers lower than 2000. In a laminar flat-plate flow, in contrast, viscosity is important across the entire layer and the shape factor is independent of Reynolds number.

Available data appear to indicate that the wall-layer variables universally describe the streamwise mean velocity in the inner layer of smooth flat plates, pipes and channels at all Reynolds numbers. Figs 10-12 illustrate this for boundary layers and channel flows for a wide range of

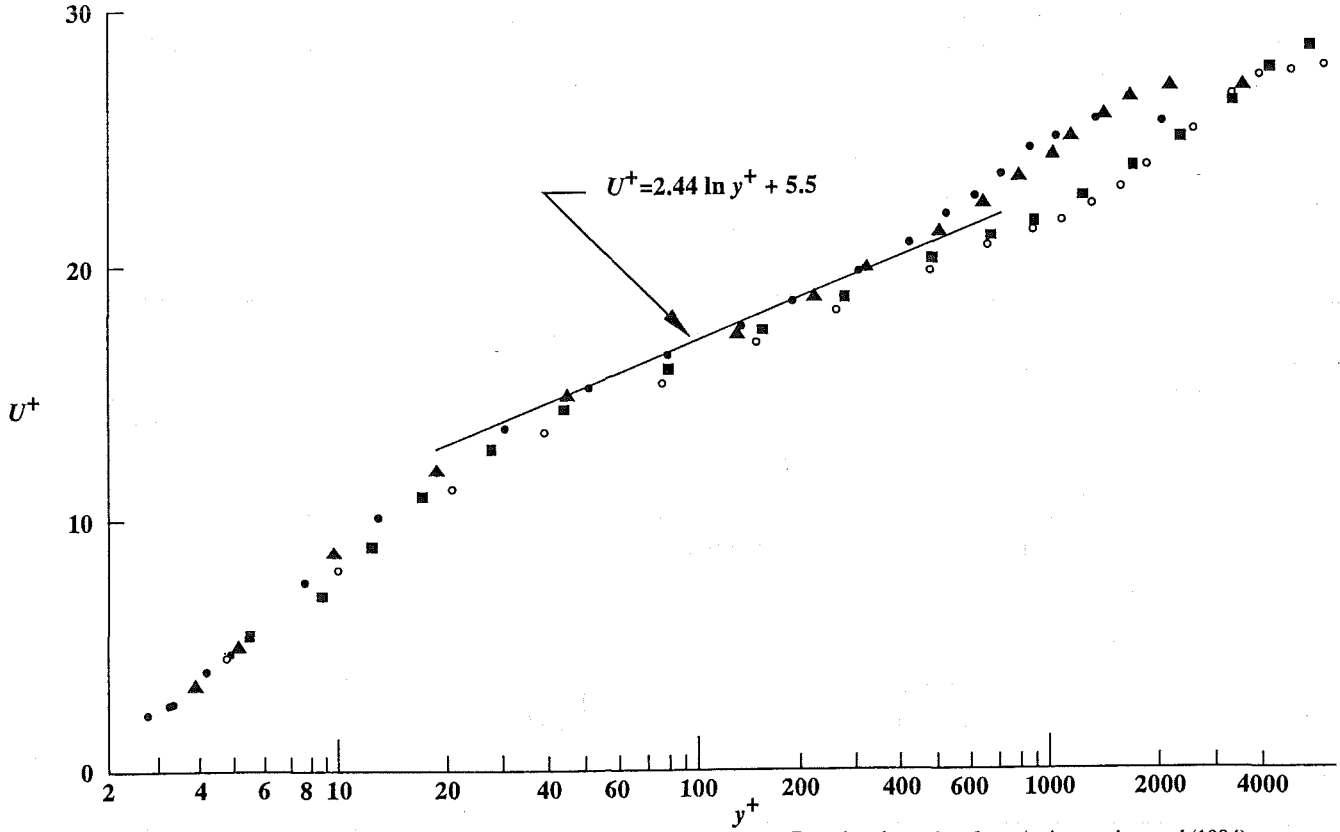

Fig 11. Non-dimensionalized mean-velocity profiles at high Reynolds numbers. Boundary layer data from Andreopoulos *et al* (1984).

Reynolds numbers. The low-Reynolds number boundary layer data of Purtell *et al* (1981) in Fig 10 indicate the presence of a logarithmic region for Re_θ as low as 500. This is rather surprising considering that at this Reynolds number a constant-stress region is virtually non-existent and the maximum Reynolds stress is substantially less than U_τ^2. However, in deriving the log law, Eq 8, the presumably constant velocity-scale has a weak, square-root dependence on the Reynolds stress. The extent of the log region, expressed in wall units, increases with Reynolds number but is a constant fraction of the boundary layer thickness (Fig 6).

The single straight line in Fig 10 does not support Simpson's (1970; 1976) claim that the law-of-the-wall, especially κ, varies with Reynolds number,[8] nor the assertion by Landweber (1953), Preston (1958) and Granville (1977) that the logarithmic region disappears all together at low Reynolds numbers. An important question is: What is the minimum Re_θ at which a log region is first established? Coles (1962) analysis of wake component indicates that it is zero at Re_θ 600. The data of Bandyopadhyay and Ahmed (1993) indicate that Clauser's outer-layer shape parameter, G, reaches zero at $Re_\theta = 425$. These can be regarded as two indications of a minimum value, supporting the experimental findings of Purtell *et al* (1981) depicted in Fig 10.

At low Reynolds numbers, the large scales of the turbulent fluctuations dominate its dynamics. The logarithmic region appears to be an inherent characteristic of the turbulent boundary layer and to be associated with the large eddies. Because of the persistence of the log region to Reynolds numbers just above transition, Purtell *et al* (1981) suggest that the large-scale structures in the turbulent boundary layer are related to, if not simply composed of, the hairpin eddies produced during the final stages of laminar-to-turbulent transition.

Andreopoulos *et al* (1984) provide mean-flow data for higher Reynolds number boundary layers. Figure 11 depicts their normalized data for the four Reynolds numbers Re_θ = 3624; 5535; 12,436 and 15,406. All three flow regimes described in Section 3 are apparent in the different mean-velocity profiles. Again, inner scaling appears to collapse the data in the inner layer (viscous plus logarithmic regions) onto a single curve.

Similar results are observed in the channel flow data of Wei and Willmarth (1989) depicted in Fig 12. Here the Reynolds number is based on the centerline velocity and the channel half-width and ranges from Re_a = 2,970 to Re_a = 39,582. As expected, the wake component in the mean-velocity profiles of the channel flow is much weaker than that in the boundary layer data.

5.2 Von Kármán constant

As discussed in Section 5.1, provided that a log region does indeed exist (see Section 5.5), Purtell *et al*'s (1981) measurements in low-Reynolds number boundary layers confirm that the law of the wall does not vary with Reynolds number, thus implying a truly constant value of the von Kármán's constant. Close to a decade earlier, Huffman and Bradshaw (1972) analyzed the data from several other low-Reynolds number experiments and arrived at the same conclusion. At the other extreme, Grigson (1992) used model and field data to show the constancy of κ for Reynolds numbers up to $Re_x = 4x10^9$. Both the low- and high-Reynolds number results refute an earlier claim by Simpson (1970) that the von Kármán constant varies with Reynolds number. Additionally, as illustrated below, a rather simple kinematic argument can be invoked to support the universality of κ (Bandyopadhyay, 1991).

Based on two-point velocity-correlation measurements, Townsend (1976) proposes the double-cone wall grazing eddy as the prototypal coherent structure in the near-wall region. This vortex, which satisfies the wall constraint, is the attached analog to his double-roller eddy of free-shear flows. The coherent structure is in contact with the wall over its whole length and vortex stretching is ignored. Its diameter must then be $d = 2y$, where y is the location of the vortex center.

Of relevance here is Robinson's (1990) observation that the near-wall streamwise vortices frequently detected in low-Reynolds number direct numerical simulations have mean diameters that vary with distance from the wall according to the linear relation:

$$d^+ = \kappa\, y^+ \tag{17}$$

where d is the mean vortex diameter and κ is the von Kármán constant. Now, the simple-momentum-transport model used in Section 3.2 to derive the log law assumes a local mixing length that varies according to:

$$\ell = \kappa\, y \tag{18}$$

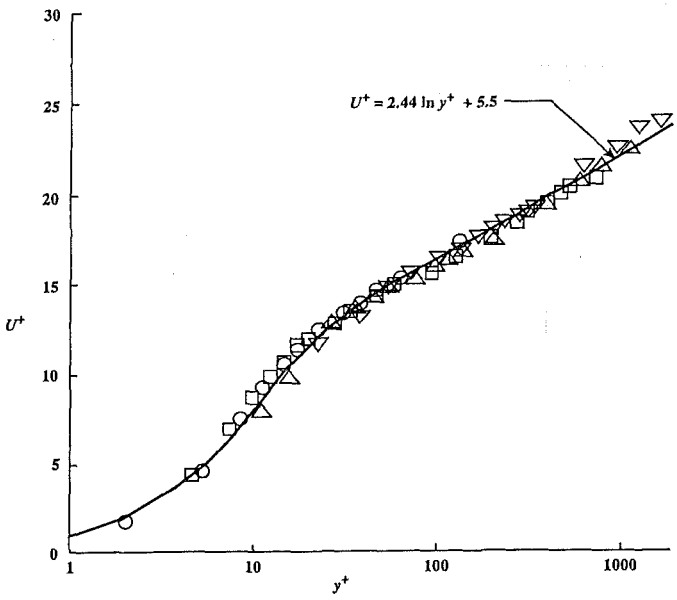

Fig 12. Mean-velocity profiles non-dimensionalized on inner variables. Channel flow data from Wei and Willmarth (1989).

[8] Note, however, the observation by George *et al* (1993), discussed in Section 5.5, that the superficial collapse in Purtell *et al*'s (1981) data results from *a priori* assuming the existence of a log region and using the velocity data to compute U_τ.

This means that in the constant-Reynolds stress region,

$$d^+ = \ell^+ = \kappa\, y^+ \tag{19}$$

Notice that ℓ reaches its maximum value at the end of the constant-stress region, *ie* at $(y/\delta) = 0.2$, such that:

$$(\ell/\delta)_{max} = \kappa\,(y/\delta)_{\text{top of log region}} = 0.082 \tag{20}$$

Thereafter ℓ is a constant throughout the rest of the boundary layer. Although $(\ell/\delta)_{max}$ is independent of the Reynolds number, it is clear that ℓ^+_{max} is not a constant. In fact, ℓ^+_{max} is a strong function of the Reynolds number for $\delta^+ < 10^3$ (Bushnell *et al*, 1975).

If the near-wall region within which ℓ_{max} is first reached is simply modeled to be composed of Townsend's double-cone eddies, it is then encouraging that the von Kármán constant of 0.41 is within the value of the constant of proportionality for the upper limit of the vortex size, *viz* 2. The kinematic behavior supports the contention that κ is independent of Reynolds number and type of flow (pipe, channel or boundary layer).

5.3 The illusory asymptotic state

While inner scaling appears to collapse wall-layer mean-flow data onto a single curve regardless of the Reynolds number, the situation is not that simple in the outer layer. As discussed in Section 3, Coles (1956) proposed to represent the entire mean-velocity profile in any two-dimensional turbulent boundary layer by a linear superposition of two universal functions, the law of the wall and the law of the wake. In fact, Coles suggested a simple extension of his empirical law to represent even yawed and three-dimensional flows. Recall Eq 15:

$$U^+ = f(y^+) + (\Pi/\kappa)\, W(y/\delta)$$

The first term on the right hand side is valid for any smooth wall-bounded flow, and available evidence appears to indicate that the function f is independent of Reynolds number, pressure gradient, and freestream turbulence. This term supposedly represents all mixing processes in the wall layer governed primarily by viscosity. The wall constraint is felt mainly in the viscous sublayer, the buffer layer and the logarithmic portion of the velocity profile. For rough walls, particularly when the roughness is sufficiently pronounced, the viscous length-scale is simply replaced by the characteristic roughness height. For both smooth and rough walls, the appropriate velocity scale is derived from the magnitude of the surface shear stress.

The second term, representing turbulent mixing processes dominated by inertia, is the product of the universal wake function $W(y/\delta)$ and the ratio of the profile parameter Π to the von Kármán constant κ. The parameter Π depends on the pressure gradient, the freestream turbulence and whether the flow is internal or external, but is not directly affected by wall conditions such as roughness, etc. For a flat-plate boundary layer, the profile parameter increases with Reynolds number but presumably asymptotes to a constant value at high enough Re. This is illustrated in Fig 13, from Coles (1962), depicting the change of the maximum deviation of the mean velocity from the logarithmic law, ΔU^+, with Reynolds number. In here, the maximum deviation, or the strength of the wake component, is expressed in wall units and the Reynolds number is based on freestream velocity and momentum thickness. The maximum Reynolds number shown is 15,000. Since the maximum deviation occurs close to the edge of the boundary layer and since $W(y/\delta)$ has been normalized such that $W(1) = 2$, the strength of the wake component is approximately related to the profile parameter by:

$$\Delta U^+ = 2\,\Pi/\kappa \tag{21}$$

It is clear that the strength of the wake depends upon the somewhat arbitrary way in which the logarithmic portion of the velocity profile is fitted, *ie* on the particular values of κ and B chosen.

Figure 13 shows that the strength of the wake component reaches a constant value for $Re_\theta \geq 6{,}000$. Coles (1962) termed the flow at this high Reynolds number "equilibrium," which led to the wide spread perception that the flow becomes independent of Reynolds number beyond

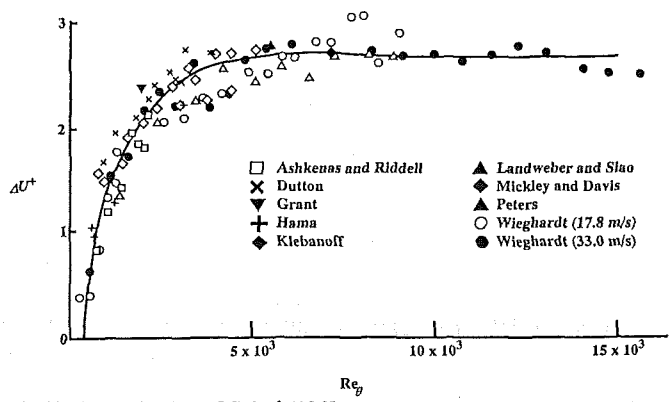

Fig 13. Reproduction of Coles' (1962) strength of the wake component in equilibrium turbulent boundary layers at low Reynolds numbers.

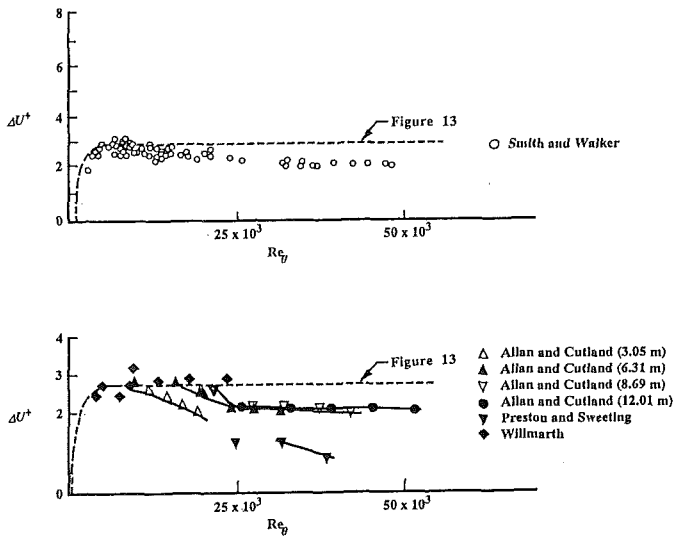

Fig 14. Reproduction of Coles' (1962) strength of the wake component at large Reynolds numbers.

this value. Unfortunately, when the plot in Fig 13 is extended to larger values of Reynolds numbers, it becomes clear that the presumed asymptotic state is merely an illusion. As shown in Fig 14, ΔU^+ starts decreasing again at about $Re_\theta > 15{,}000$, although very slowly compared to the rise rate for $Re_\theta < 6{,}000$. After excluding all data containing certain anomalies, Coles (1962) was puzzled by the persistent change in behavior and the variation between data sets for $Re_\theta > 15{,}000$. The drop can not be explained from experimental uncertainties such as those caused by probe calibration problems, improper tripping devices, three-dimensional effects, high levels of freestream turbulence and pressure-gradient effects, and Coles left the issue open.

The rapid rise and the subsequent gradual fall of ΔU^+ with Re_θ appear to be genuine and have been confirmed in several other experiments as summarized by Mabey (1979). The maximum ΔU^+, reached at about $Re_\theta = 6000$, is 2.7 for subsonic flows (Smith and Walker, 1959) but is higher by 30% or more for supersonic flows (Lee *et al*, 1962; Hopkins *et al*, 1972; Mabey *et al*, 1976).

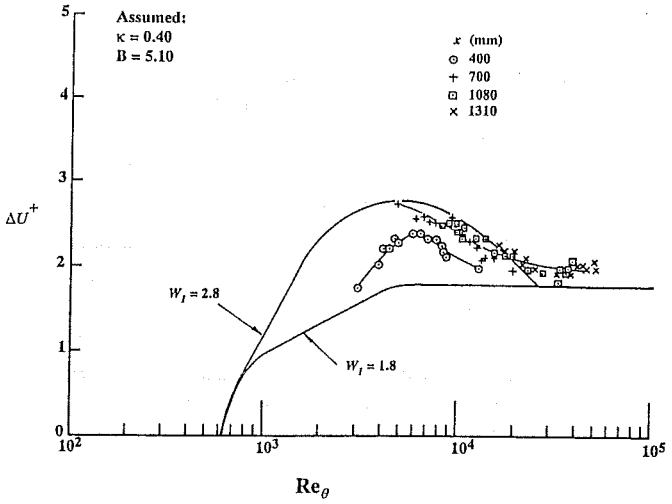

Fig 15. Strength of the wake component versus Reynolds number on a semi-log plot. Subsonic data of Smith and Walker (1959) at four different downstream stations. Figure reproduced from Mabey (1979).

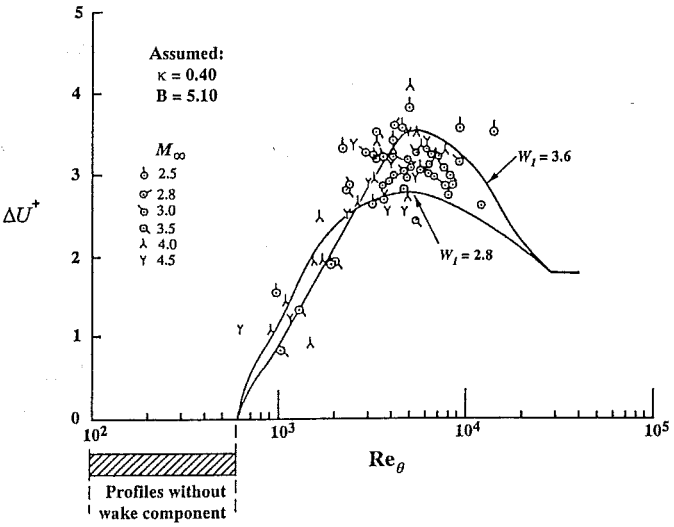

Fig 16. Strength of the wake component versus Reynolds number on a semi-log plot. Supersonic data of Mabey *et al* (1976) at six different mach numbers. Figure reproduced from Mabey (1979).

Smith and Walker's (1959) subsonic data, shown previously in the top part of Fig 14, are replotted on a semi-log scale in Fig 15, for four different measuring stations. The forward station, $x = 400$ mm, shows a different trend as compared to the three downstream locations. Using the two curves fitted to the data in Fig 15, Mabey (1979) analyzed the effects of the variation of the wake component with Reynolds number on skin-friction and total drag predictions. These are important parameters when extrapolating model tests to actual vehicle configurations. The curve marked $W_1 = 1.8$ corresponds to a constant wake component of 1.8 above $Re_\theta = 5600$, but falls to zero at $Re_\theta = 600$. The second curve marked $W_1 = 2.8$ peaks at $Re_\theta = 5600$, but drops at higher and lower Reynolds numbers. Particularly at low Re_θ, the skin-friction computed from the first curve fits the law-of-the-wall estimates, while predictions based on the second curve fit the directly measured drag better.

The supersonic data of Mabey *et al* (1976) are depicted in Fig 16, where there seems to be no significant variation with Mach number. Despite artificial tripping, the boundary layer was laminar or transitional for $Re_\theta < 600$, and no wake component can be extracted from the velocity profiles. As in the subsonic case, Mabey (1979) used the two fitted curves in Fig 16 to analyze the effects of the variation of the wake component with Reynolds number on skin-friction.

The Reynolds number effect on the mean flow can also be verified independently from Clauser's shape parameter:

$$G = \int_0^\delta \left(\frac{U_o - U}{U_\tau}\right)^2 dy \Big/ \int_0^\delta \left(\frac{U_o - U}{U_\tau}\right) dy \qquad (22)$$

where $U(y)$ is the velocity profile and U_o is the velocity at the dege of the boundary layer, $y = \delta$. Bandyopadhyay (1992) compiled the findings of several recent experiments to show the variation of G with Re_θ. The results are shown in Fig 17, and include the high-aspect ratio[9] data of Anders (1989). The trend parallels that of ΔU^+. The value of G first rises rapidly with Re_θ and then drops gradually. Figure 17 also corrects the loose notion found in the literature that G varies between 6.5 and 7.5.

5.4 Is self-preservation ever achieved?

At approximately $Re_\theta > 15 \times 10^3$, the gradual departure of ΔU^+ from the apparent low-Re_θ asymptote suggests that some new effects are gradually appearing in the turbulence production process. A new, lower asymptote appears to have been reached when $Re_\theta = 50{,}000$, but the boundary layer might also continue to change indefinitely as the inner and outer scales are forever disparting. The paucity of high-Reynolds number reliable data makes it difficult to make a definitive conclusion.

Without definitive experiments at even higher Reynolds numbers, one can never be sure of the universality of the

[9] Ratio of tunnel span to δ.

defect law. Very few existing facilities can deliver the required ultra-high Reynolds number flows, while maintaining relatively low Mach number (in the so-called low-speed, high-Reynolds number tunnels) as to avoid the added complication of compressibility effects. The world's largest wind tunnel, the 24 m x 37 m Full-Scale Aerodynamics Facility at NASA Ames, is capable of generating a boundary layer with a momentum-thickness Reynolds number as high as 3.7×10^5 (Saddoughi and Veeravalli, 1994).

The largest available water tunnels and towing tanks can deliver momentum thickness Reynolds numbers of approximately 3×10^4 and 9×10^4, respectively (Fig 1). Cryogenic tunnels, for example the National Transonic Facility at NASA Langley, typically use nitrogen and run as high as $Re_\theta = 6 \times 10^4$, but their Mach number is near one and are rather expensive as well as heavily scheduled (Bushnell and Greene, 1991). Tunnels using liquid helium I are an attractive, low-cost alternative to the much larger nitrogen tunnels (Donnelly, 1991). Helium facilities can match the Reynolds numbers of the transonic wind tunnels but with essentially zero Mach number and much smaller sizes (*eg*, 1 cm x 1 cm test section). Instrumenting the smaller facilities with high-resolution velocity or pressure probes is at present problematic, although the rapidly developing microfabrication technology has the potential for producing inexpensive megahertz-frequency and micron-size sensors (see, for example, Löfdahl *et al*, 1989; 1991; 1992).

A commonly accessible large-scale, high-Reynolds number facility is the atmospheric boundary layer. The flow is virtually incompressible and the momentum-thickness Reynolds number in the atmosphere can be as much as four orders of magnitude higher than that in typical laboratory experiments. Unfortunately, such a natural laboratory has several faults. Firstly, the "wall" in this case is almost always rough and direct comparison to the canonical boundary layer is difficult. Secondly, the atmospheric experiments are not well controlled, the flow conditions are neither precisely repeatable nor documentable to the needed detail (see however the recent thesis by Kailasnath, 1993, who was able to carry out useful comparison between low-Reynolds number laboratory data and high-Reynolds number atmospheric data).

The so-called *super-pipe* facility is currently being constructed at Princeton University (AJ Smits, private communications). The pipe has a diameter of 12.7 cm and a length-to-diameter ratio of 200. When completed, this high-pressure-air (200 atm.) pipe flow will provide a very high Reynolds number of up to $Re_a = 2.3 \times 10^7$ at a reasonably large scale and low Mach number, and hopefully will help in answering some of the questions raised in the present review.

For the present at least, it is simply not known if the mean flow in a wall-bounded flow ever achieves true self-preservation. As will be shown in Section 6, the situation is less clear for higher-order statistics.

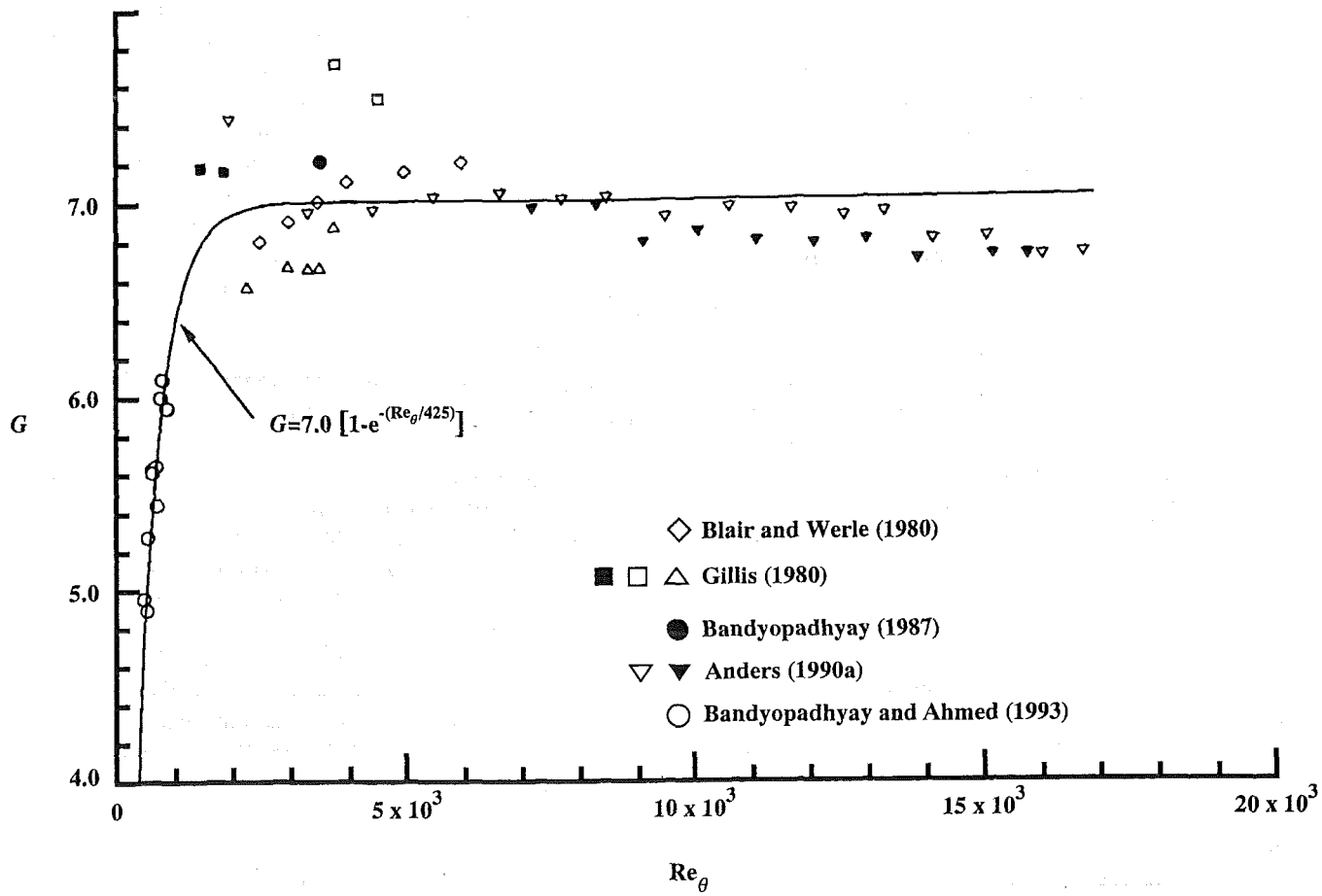

Fig 17. Low-Reynolds number effects on Clauser's shape parameter (from Bandyopadhyay, 1992).

5.5 Alternatives to the logarithmic profile

Despite copious evidence for the existence of the log law, the whole scenario leading to it has been questioned (see the references cited in Section 3.2). From a purely practical point of view, a portion of the streamwise mean-velocity profile could equally well fit either a logarithmic relation or a power law. If the mean-velocity profile for a pipe flow (or boundary layer) is to be fitted with a power law of the form:

$$\frac{U}{U_{\ell}} = c\left(\frac{y}{a}\right)^{\frac{1}{n}} \tag{23}$$

the value of the exponent ($1/n$) will decrease as the velocity profile becomes fuller. In other words, n increases as H decreases and Re increases. For example, the smooth-pipe-flow data of Nikuradse (1932) indicate that n changes from 6 to 10 as the Reynolds number varies in the range of $\mathrm{Re}_a = 2.53\text{x}10^3\text{-}1.85\text{x}10^6$ (Schlichting, 1979).

Sreenivasan (1989) argues that although the power law used by engineers to describe the mean-velocity profile has been discredited by scientists since Millikan (1939) derived the logarithmic law from asymptotic arguments, the basis for the power law is *a priori* as sound as that for the log law, particularly at low Reynolds numbers (see also Barenblatt, 1979; 1993; Barenblatt and Prostokishin, 1993). The behavior of the exponent ($1/n$) as $\mathrm{Re}_a \rightarrow \infty$ is of particular interest. If it tends to zero, the log law is recovered. If, on the other hand, the limiting value of the exponent is a non-zero constant, the log law does not strictly hold. This implies that an inertial sublayer is lacking and, therefore, that viscous effects persist even at infinitely large Reynolds number. Such a scenario is consistent with the suggestion by Long and Chen (1981) that the inner flow is the outcome of an interplay between wall effects and outer effects. According to them, it is strange that the matched layer between one characterized by inertia and another characterized by viscosity depends only on inertia. Long and Chen suggest that a "mesolayer" intrudes between the inner and outer regions preventing the overlap assumed in the derivation of the classical logarithmic velocity profile. Unfortunately, existing experimental or numerical mean-velocity data cannot readily be used to explore this important issue since the difference between a logarithmic relation and a power law with a large but finite n is imperceptible (see Kailasnath, 1993, for a comprehensive review of available data).

George *et al* (1992; 1993; 1994) provide the most serious challenge to the validity of the log law for external wall-bounded flows. They assert that boundary layer data taken at different Reynolds numbers collapse in the log region only if the shear stress is calculated from a method (*ie* the Clauser's method) which forces it to by assuming such a layer exists. Such superficial collapse compromises the collapse in the viscous sublayer where no adjustable constants or Reynolds number dependence should exist. As an alternative, George *et al* (1993) used measured shear stress to normalize the data of Purtell *et al* (1981), and showed that the profiles collapse well very close to the wall but not in the log region where clearly discernible Reynolds number dependence is depicted. To remedy the situation, George *et al* (1993) propose matching a new velocity-defect law with explicit Reynolds number dependence and the traditional law of the wall. The result in the matched region is a power-law velocity profile of the form:

$$\frac{U}{U_{\infty}} = C_o\left(\frac{y}{\delta}\right)^n + B_o \tag{24}$$

$$\frac{U}{U_{\tau}} = C_i\left(\frac{U_{\tau} y}{\nu}\right)^n + B_i \tag{25}$$

where the coefficients B_i, B_o, C_i, C_o and the exponent n are Reynolds number dependent, but all are asymptotically constant. In a subsequent paper, George *et al* (1994) have shown that the additive coefficients B_i and B_o are identically zero. Using Eqs 24 and 25, the friction coefficient is readily expressed as the Reynolds number to the power $-2n/(1 + n)$.

George *et al* (1994) assert that their approach removes many of the unsatisfying features of the classical Millikan's (1939) theory. Furthermore, they argue that a clear distinction should be made between internal and external wall-bounded flows. For fully-developed pipe and channel flows, the streamwise homogeneity insures that the pressure gradient and wall-shear stress are not independent, and thus U_{τ} is the correct scaling velocity for the entire shear layer including the core region. This results in a log law although the flow has no constant-stress layer. The growing, inhomogeneous boundary layer, in contrast, is governed by a power law even though it does, at least for zero pressure gradient and high Re, have a constant-stress layer. The matched region of a boundary layer retains a dependence on streamwise distance, and hence never becomes Reynolds number independent. The same arguments presented here for the mean flow could be extended to higher-order statistics.

The difference in the inner region between flat-plate boundary layers and fully-developed channel flows explored above might have serious implications on the principle and use of the Preston tube, a device widely used for measuring the local mean friction-coefficient. Such gauge is commonly calibrated in a pipe flow and relies on the universality of the inner layer to compute the skin friction in a flat-plate boundary layer. Such extrapolation is thus questionable, and direct measurements of wall-shear stress are clearly preferred.

George and Castillo (1993) have recently extended the new scaling law described earlier for the flat-plate flow to boundary layers with pressure gradient. Inclusion of roughness or compressibility effects could proceed along similar attempts made in the past for the classical theory (Hama, 1954; Coles, 1962).

The fresh look at the turbulent boundary layer by George and his colleagues is intriguing and deserves further scru-

tiny. Independent confirmation of their claims is needed, and carefully controlled boundary layer experiments over a wide range of Reynolds number would be most useful. Low-Reynolds number experiments in which the linear region is resolved and the wall-shear stress is measured directly would be particularly valuable. If validated, their new theory indicates that the boundary layer is governed by a different scaling law than commonly believed. Explicit, albeit weak, Reynolds number dependence is shown for the mean velocity profile all the way down to the edge of the viscous sublayer. The matched region retains a dependence on streamwise distance, and hence Reynolds number effects will always persist for all turbulence quantities.

6. HIGHER-ORDER STATISTICS

Compared to the mean flow, higher-order statistical quantities are more difficult to measure, and the issue of Reynolds number effects is murkier. For quantities such as root-mean-square, Reynolds stress, skewness and spectrum, the issues of spatial as well as temporal probe resolutions, three-dimensional effects and boundary-layer tripping devices become much more critical. In contrast to mean flow, reliable data for higher-order statistics are scarce.

A measurement probe essentially integrates the signal over its active sensing area or volume. This means that velocity or pressure fluctuations having scales smaller than the sensor size are attenuated by the averaging process, and the measured root-mean-square of the fluctuations, for example, is smaller than the true value. Several studies have shown the importance of probe size in the detection of small-scale structures in the near-wall region (for example, Willmarth and Bogar, 1977; Schewe, 1983; Johansson and Alfredsson, 1983; Blackwelder and Haritonidis, 1983; Luchik and Tiederman, 1986; Karlsson and Johansson, 1986; Ligrani and Bradshaw, 1987; Wei and Willmarth, 1989; Löfdahl *et al*, 1992). As a rule of thumb, probe length much larger than the viscous sublayer thickness is not acceptable for accurately measuring turbulence levels and spectra anywhere across the boundary layer, and even smaller sensing elements are required to resolve dynamical events within the sublayer itself.

The issue of sufficient probe resolution is particularly acute when studying Reynolds number effects. A probe that provides accurate measurements at low Re might give erroneous results when the Reynolds number is increased and the scales to be resolved become smaller relative to the probe size. The probe resolution should be expressed in wall units, and as mentioned above ℓ^+ should not be much larger than 5, where ℓ is the probe length.

The classic idea of inner scaling is that any turbulence quantity measured at different Reynolds numbers and in different facilities will collapse, at least in the inner layer, to a single universal profile when non-dimensionalized using inner-layer variables. In contrast to mean-velocity profiles, higher-order statistics do not in general scale with wall-layer variables even deep inside the inner layer. In the following five subsections, we review Reynolds number effects on the root-mean-square values of the velocity fluctuations, Reynolds stress, spectra, skewness and flatness factors, and rms and spectrum of the wall-pressure fluctuations.

6.1 Root-mean-square velocity fluctuations

The intensity of turbulent fluctuations is defined by its root-mean-square value. The streamwise velocity fluctuations are more readily measured using, for example, a single hot-wire probe or a two-beam laser Doppler velocimeter. Measuring the other two velocity components, in contrast, requires two hot wires either in an X-array or a V-array or four intersecting laser beams. Especially very close to the wall, few reliable measurements of the normal velocity components are reported in the literature, and even fewer are available for the spanwise component. A notable exception is the oil-channel data reported by Kreplin and Eckelman (1979), who measured all three velocity components inside the viscous sublayer. In here, boundary layer data for both low and high Reynolds numbers are presented followed by channel and pipe flow data.

Figure 18 shows the variation of the normal distribution of turbulence intensity in wall variables with Reynolds number. Measurements of the streamwise velocity component were conducted by Purtell *et al* (1981) in a low-Reynolds number, flat-plate boundary layer. Four Reynolds numbers based on momentum thickness are presented in the figure, ranging from Re_θ = 465 to 5100. It is clear that Reynolds number effects penetrate into the boundary layer much deeper in terms of the turbulence intensity than it does for the mean velocity. *Approximate similarity* in wall units is maintained only out to $y^+ \approx 15$, compared with mean velocity which is similar throughout the entire inner layer. Close inspection of the figure reveals that even in the viscous region itself, some weak dependence on Reynolds number is observed in the rms value of the streamwise velocity fluctuations, as seen at the lowest Reynolds number of Re_θ = 465. Purtell *et al* attributed the systematic decrease in u' across most of the boundary layer to the suppression of all but the largest turbulence eddies as the Reynolds number is reduced.

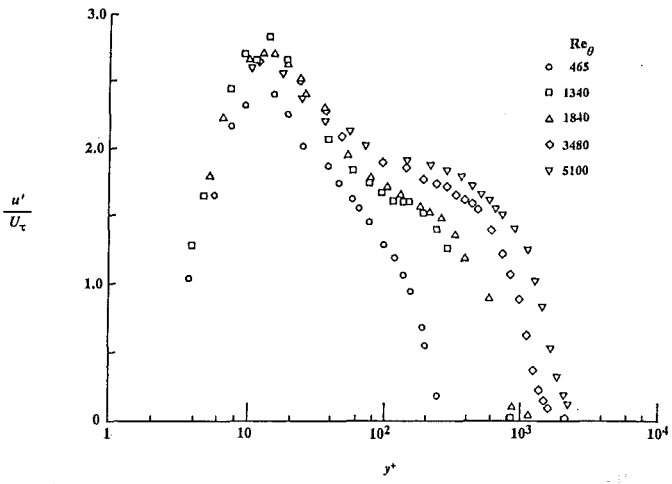

Fig 18. Variation of the distribution of turbulence intensity in wall variables with Reynolds number. Boundary layer data from Purtell *et al* (1981).

Reynolds number can of course be changed either by varying the freestream velocity at a fixed streamwise location or by holding the tunnel speed constant and conducting the measurements at increasing downstream locations. To check the state of development of the flow, Purtell *et al* (1981) measured, for a fixed freestream velocity, the mean-velocity profiles at four downstream distances from the tripping device. At the station closest to the distributed roughness, they report under-development in the outer region of the mean flow, but an undistorted logarithmic region that produces friction velocity values in agreement with directly measured U_τ-values computed from near-wall measurements of $\partial U/\partial y$. The same trends were observed at higher Reynolds numbers by Klebanoff and Diehl (1951).

When normalized with the freestream velocity, u' also shows distortion in the outer region for measurements not sufficiently far downstream of the tripping device. However, as shown in Fig 19, the rms data plotted in inner variables at a freestream velocity of 2.3 m/s and four downstream stations x = 91, 122, 152 and 183 cm, exhibit such a strong Reynolds number dependence in the outer layer that the distortion mentioned above is obscured. Close inspection of Fig 19 shows a small but systematic Reynolds number effect even below $y^+ = 10$. Barring the first measurement station (x = 91 cm), which is non-typical due to its close proximity to the tripping device, at a given y^+, u^+_{rms} increases with x, that is with Re_θ.

One might argue that the strong Reynolds number effects shown above will eventually subside at sufficiently high Reynolds number. This is not the case, at least up to Re_θ of 15,406, as shown in Andreopoulos *et al*'s (1984) flat-plate data depicted in Fig 20a. The rms-values of the longitudinal velocity fluctuations show strong Reynolds number dependence all the way to the edge of the viscous sublayer. In the buffer layer, u'/U_τ decreases as the Reynolds number increases from 3624 to 12,436, thereafter reaching what seems to be a constant value. An opposite trend, that continues for all four Reynolds numbers, is observed in the logarithmic and wake regions. Andreopoulos *et al* (1984) indicated that the behavior of their u'-data in the buffer region is in general agreement with the channel flow results of Laufer (1951), Comte-Bellot (1965) and Zaric (1972).

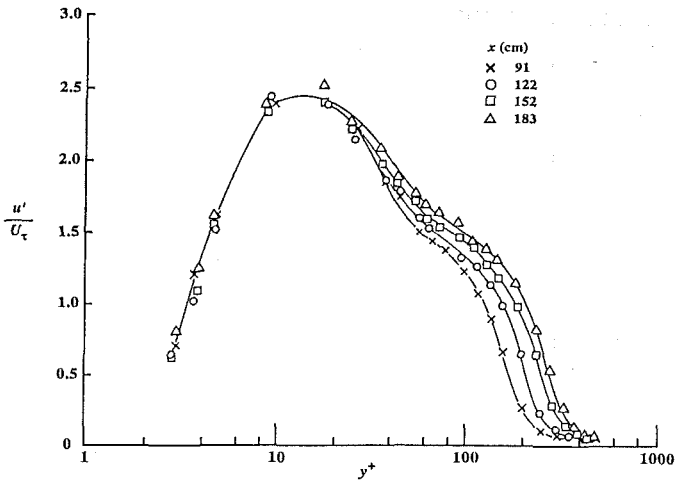

Fig 19. Distribution of turbulence intensity in wall variables at four different downstream locations. Flat-plate boundary layer at U_∞ = 2.3 m/s. (from Purtell *et al*, 1981).

Andreopoulos *et al* (1984) were able to measure the normal velocity component only at the lowest Reynolds number, Re_θ = 3620, as shown in Fig 20b. The weak second peak in v'/U_τ appearing at $y^+ = 4$ seems to be unique to this particular experiment, but the authors do not comment on this. Reliable v'- measurements could not be obtained by Andreopoulos *et al* for higher Reynolds numbers due to limitations of the applicable velocity range of their triple-wire sensor.

The effect of Reynolds number on the inner-layer turbulence in boundary layers is summarized in Fig 21, adapted by Bandyopadhyay (1991) from several different experiments. The peak value of u-turbulence intensity, which occurs at $12 \le y^+ \le 15$, is plotted normalized by wall variables versus the logarithm of Re_θ. In Ueda and Hinze's (1975) experiment, the freestream turbulence is 0.03%, hot wire ℓ^+ is between 2.4 and 6.7, and the measurements have been carried out at 3.4 m downstream of a trip wire. In Erm *et al*'s

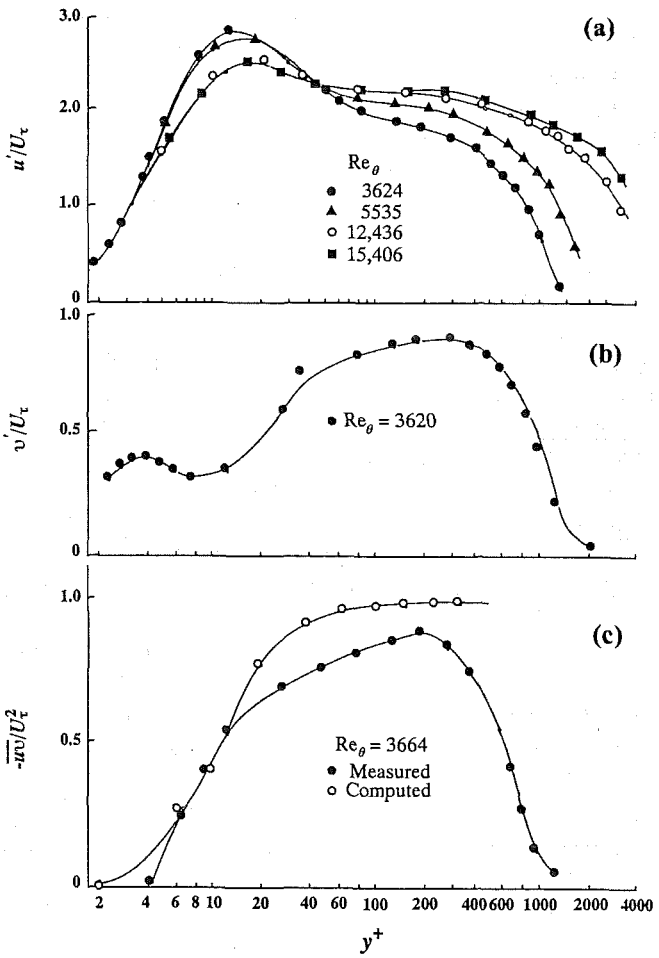

Fig 20. Normal profiles of rms streamwise velocity, rms normal velocity, and Reynolds stress (from Andreopoulos *et al*, 1984): (a) Root-mean-square values of longitudinal velocity fluctuations at four different Reynolds numbers; (b) Root-mean-square values of normal velocity fluctuations at Re_θ = 3620; (c) Measured and computed Reynolds stress distributions at Re_θ = 3664.

(1987) experiment, $\ell^+ < 5$ and the measurements have been carried out 0.18 to 1.94 m downstream of stimulator pins. Two sets of Purtell *et al*'s (1981) experiments are included where No. 4 floor sanding paper has been used to trip the boundary layer, $T_u = 0.05\%$, and $0.8 \leq \ell^+ \leq 3$. The $Re_\theta = 465$ data point is from a station 1.07 m downstream of a 15-cm long fetch of sand paper. The higher data points are from runs where the sand roughness extended over 61 cm and the measurements were carried out 2.69 m downstream. Note the higher value of the maximum turbulence intensity at the lowest Re_θ of the second data set. In Andreopoulos *et al*'s (1984) experiment, $1.7 \leq \ell^+ \leq 6.4$, and the measurements were carried out 3 to 4 m downstream of a 1 cm-long sandpaper trip (grit height $\approx$ 1 mm).

In Fig 21, T_u or ℓ^+ does not explain the variation between the different facilities. Despite the scatter in the different data sets, the general trend is for increasing values of the normalized peak value of u_{rms} with Reynolds number, at least initially. The paucity of data at $Re_\theta > 6000$ precludes making any definitive statement regarding the asymptotic behavior of u^+_{rms}. Since Re_θ represents outer layer scales, the figure shows that the outer layer affects the inner-layer u-turbulence. The outer-layer effect seems to be facility dependent even at $Re_\theta \sim 5\times10^3$ and 3.4 m from the trip. The stronger trip effects on turbulence at the higher Reynolds number is surprising, although as will be shown in Section 8.3.2, the mean flow also exhibits a similar behavior.

In Fig 21, in three experiments, the maximum value of u_{rms}/U_τ first increases rapidly (above 2.8) with Reynolds number before dropping slowly. This behavior is similar to the high Reynolds number mean flow behavior downstream of a trip. The reason for this is not understood; but like it is known for the effect of freestream turbulence, length scales O[δ] introduced into the outer layer by the trips could be involved. In that case, it is interesting that certain transition devices could affect the turbulence in a boundary layer at *high Reynolds numbers* even beyond 85δ. Three data points from the direct numerical simulation of Spalart (1986) are included in the figure and they indicate similar trends to those of the low-Reynolds number experiments.

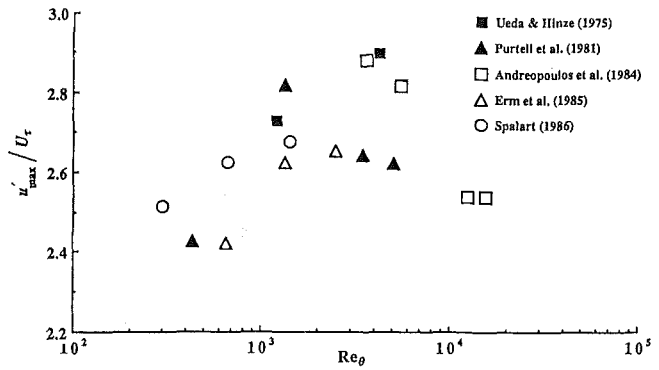

Fig 21. Peak value of u-turbulence intensity in turbulent boundary layers. The plot, from four different experiments and a single direct numerical simulation, demonstrates the effect of outer layer scales on inner-layer turbulence (from Bandyopadhyay, 1991).

Relatively more data are available for two-dimensional channel flows. Figure 22 depicts Reynolds number effects on the normal profiles of the streamwise turbulence intensity in four different channel flows. Laufer's (1951) experiments were conducted at three Reynolds numbers, based on channel half-width and centerline velocity, of Re_a = 12,300; 30,800; and 61,600. Comte-Bellot (1965) covered the higher range of Re_a = 57,000 and 230,000. Kreplin and Eckelmann's (1979) experiments were conducted at Re_a = 3850. Johansson and Alfredsson (1982) provided data for Re_a = 6900; 17,300; and 24,450.

Probe resolution problems appear to exist in both Laufer's and Comte-Bellot's high-Reynolds number data. In the former experiment, the hot-wire length increased from 3 wall units at the lowest Reynolds number investigated to 13 wall units at the highest Reynolds number, a fourfold loss in spatial resolution. Laufer (1951) observed (erroneously) a corresponding decrease in the peak value of u'/U_τ with increasing Reynolds number. Comte-Bellot's (1965) probe length increased from 13 to 36 viscous lengths as Re_a increased from 57,000 to 230,000. Correspondingly, she also observed (erroneously) a decrease in the peak value of the nondimensional streamwise turbulence intensity from 2.85 to 2.5. High-quality turbulence data obtained using sufficiently small probes and facilities void of significant trip-memory effects are clearly lacking. In any case, the data in Fig 22 indicate that the turbulence intensity profiles do not collapse even deep into the inner layer.

Similar trends are observed in the rms-values of the velocity fluctuations normal to the wall. Figure 23 depicts the υ' -profiles taken from four different facilities. Laufer's (1951) experiments were conducted at Re_a = 12,300; 30,800; and 61,600. Comte-Bellot (1965) covered the higher values of Re_a = 57,000 and 230,000. Eckelmann (1974) provided data for Re_a = 2800 and 4100. Alfredsson and Johansson's (1984) experiments were conducted at Re_a = 7500. The peak υ' is lower than that for the streamwise

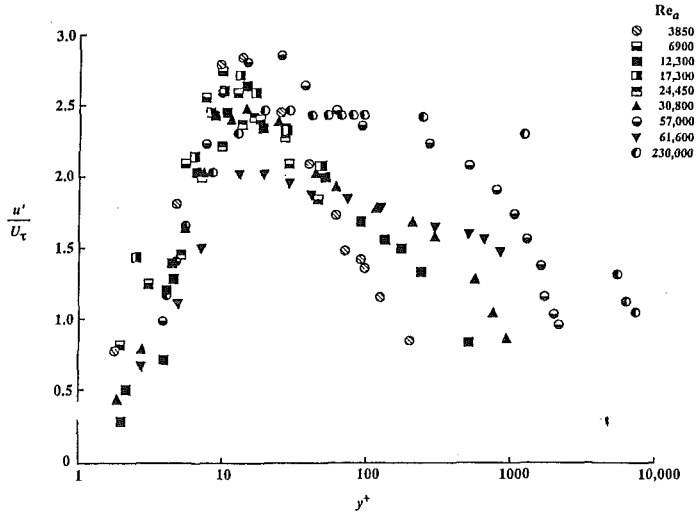

Fig 22. Streamwise turbulence intensity profiles non-dimensionalized with respect to inner variables. Channel flow data from four different experiments, compiled by Wei and Willmarth (1989).

fluctuations and occurs further away from the wall. Validity of inner scaling deep into the viscous region can not be ascertained from this figure because of the scarcity of data for $y^+ < 30$.

In view of the poor quality of most of the data in Figs 22 and 23, Wei and Willmarth (1989) systematically investigated the Reynolds number effects using a unique high-resolution, two-component laser-Doppler anemometer. To reduce the amount of ambient light in the vicinity of the measuring volume and thus to improve the signal-to-noise-ratio of the LDA system, four laser beams were entered and exited into the test section via two narrow slits located at the two side walls of a two-dimensional water channel. Both slots were covered with an extremely thin (17 microns) window of heat shrinking Mylar film, which virtually eliminated optical refraction by the window. The laser beams intersected at a single point away from the wall, and the effective probe length ranged from 0.66 to 6.43 wall units as the Reynolds number was varied in the range of Re_a = 3000-40,000. Beam refraction in the path between the laser source and the measuring station was minimized using a specially designed *optical head.*

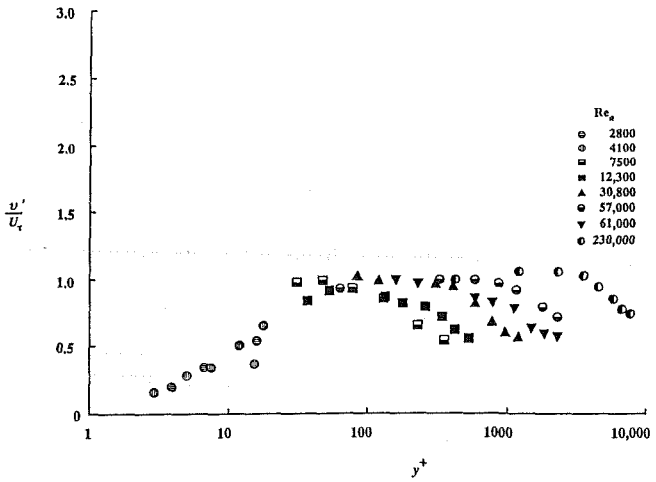

Fig 23. Normal turbulence intensity profiles non-dimensionalized with respect to inner variables. Channel flow data from four different experiments, complied by Wei and Willmarth (1989).

The combination of high spatial resolution and high data rates enabled Wei and Willmarth (1989) to reconstruct accurate time-dependent velocity traces. Their results for the streamwise and normal turbulence intensities are presented in Figs 24 and 25. In the former figure, u' and v' are nondimensionalized with the local mean velocity U, while U_τ is used as a velocity scale in Fig 25. In Fig 24, the intensity of turbulent fluctuations is described relative to the square root of the mean kinetic energy per unit mass at a given distance from the wall. The apparent increase in v'/U as the surface of the channel is approached violates the continuity equation and is probably caused by reduced measurement resolution very close to the wall.

The inner variable plot in Fig 25 allows some instructive comparison to other data in the literature (Figs 22 and 23). Wei and Willmarth (1989) ascribe the slight disagreement between the different data sets to a decreased spatial resolution of the hot wires used by Laufer (1951), Comte-Bellot (1965) and Johansson and Alfredsson (1982) at high Reynolds numbers. But, even in the newer data set, the fluctuating turbulence quantities do not scale with wall variables even at as close as 10 viscous lengths from the wall. In fact, inner scaling does not seem to apply to v' across the entire portion of the viscous region where measurements are available.

More recently, Harder and Tiederman (1991) have studied the behavior of the rms of the fluctuating streamwise and normal velocities as a function of distance from the wall of a two-dimensional water channel. Their results are depicted in Fig 26 for Re_a = 9019; 12,663; 19,013; and 21,650. In here, u^+_{rm} peaks at 2.76 for a $y^+ \approx 15$, while v^+_{rms} peaks at a $y^+ \approx 75$ with a value of 1.12. The data are generally 7% lower than those of Walker and Tiederman's

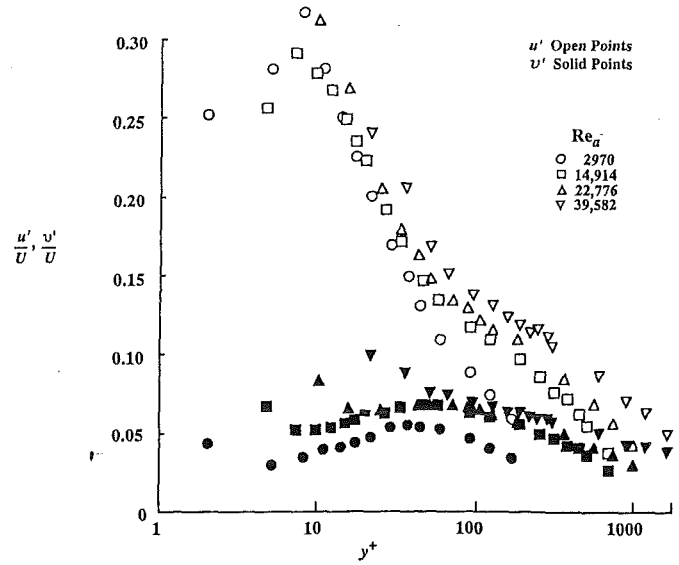

Fig 24. Profiles of turbulence intensity in streamwise direction (open points) and direction normal to wall (solid points), non-dimensionalized on local mean velocity. Channel flow data of Wei and Willmarth (1989).

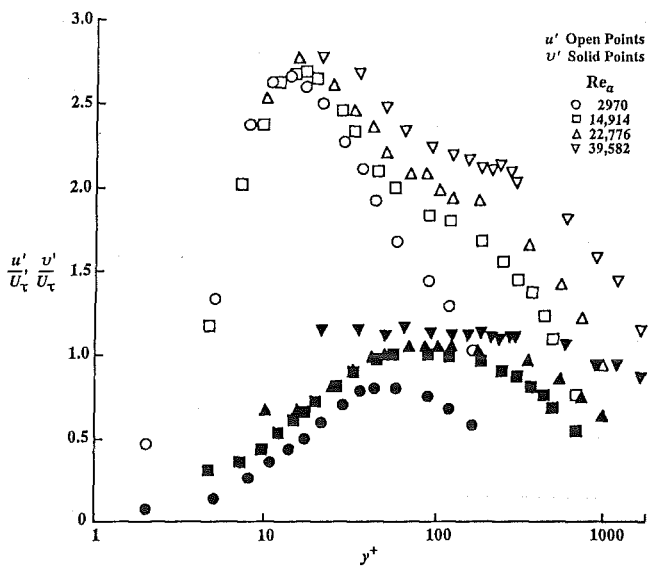

Fig 25. Profiles of turbulence intensity in streamwise direction (open points) and direction normal to wall (solid points), non-dimensionalized on inner variables. Channel flow data of Wei and Willmarth (1989).

(1990) experiments indicated by the solid lines in Fig 26, but 7% higher than the experimental values obtained by Hussain and Reynolds (1975) or the numerical simulation results of Kim *et al* (1987).

Harder and Tiederman (1991) assert that, in disagreement with Wei and Willmarth (1989), inner scaling does correlate the data for all Reynolds number in the wall region ($y^+ < 50$). However, in the present authors' opinion, the range of Reynolds numbers investigated by Harder and Tiederman (1990) is too narrow to make such a claim. The dependence on Reynolds number in the inner region is a rather weak one, and a substantial change in Re_a is needed to assure a measurable effect. Typically the turbulence intensity changes by only a few percentage points when the Reynolds number changes by 100%. The ratio of the largest to smallest Re_a in Wei and Willmarth's study is about 13, while it is only 2.4 in Harder and Tiederman's.

Additional support for Wei and Willmarth's (1989) basic conclusion that turbulence quantities in the near-wall region do not scale on wall variables comes from the boundary layer experiments of Purtell *et al* (1981) and Andreopoulous *et al* (1984), referenced earlier in this section, as well as from the physical and numerical channel-flow experiments conducted by Antonia *et al* (1992) and the flat-plate experiments of Murlis *et al* (1982), Wark and Nagib (1991) and Naguib and Wark (1992; 1994). It is, of course, conceivable that wall-layer scaling might apply over the entire inner layer provided that the Reynolds number is high enough, but at the moment at least such ultra-high-Reynolds number experiments cannot be conducted with sufficient probe resolution.

The effect of Reynolds number on the inner-layer turbulence in channel flows is summarized in Fig 27, compiled by Bandyopadhyay (1991). The peak value of u-turbulence intensity, which occurs at $12 \leq y^+ \leq 15$, is plotted normalized by wall variables. The data in the figure are compiled from the experiments conducted by Laufer (1951), Grass (1971), Eckelman (1974), Johansson and Alfredsson (1982), and Wei and Willmarth (1989) in five different facilities. For all the data points shown in Fig 27, probe resolution is better than 7 wall units. The data follows the general trends reported by Wei and Willmarth (1989), and the solid line in the figure is a least-square fit to all the points. The peak value in channel flows seems to be increasing monotonically with Reynolds number, at least up to Re_a = 23,000. Confidence in the data in this figure is, in general, higher than that for the boundary layer results summarized in Fig 21. There, post-transition memory effects may have played a role, that remains ill understood, in the observed trends.

Perry and Abell (1975) provide pipe flow data for the Reynolds number range of Re_a = 40,000-130,000. An example of their data is shown in Fig 28. The streamwise turbulence intensity in wall units is plotted versus y^+ for four different Reynolds numbers. As a consequence of the existence of a constant-stress regime, a distinct region of constant turbulence level appears for each of the four Reynolds numbers investigated [see Section 3.2 and Eq 9]. Although scaling with inner variables appears to collapse the pipe-flow data in the inner region, in contrary to the boundary-layer and channel-flow data discussed earlier, it

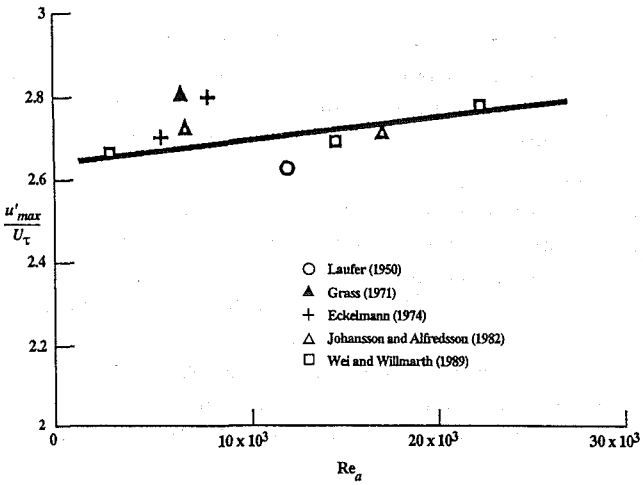

Fig 27. Peak value of u-turbulence intensity in two-dimensional channel flows. The plot, from five different experiments, demonstrates the effect of outer layer scales on inner-layer turbulence. Solid line represents the mean trend (from Bandyopadhyay, 1991).

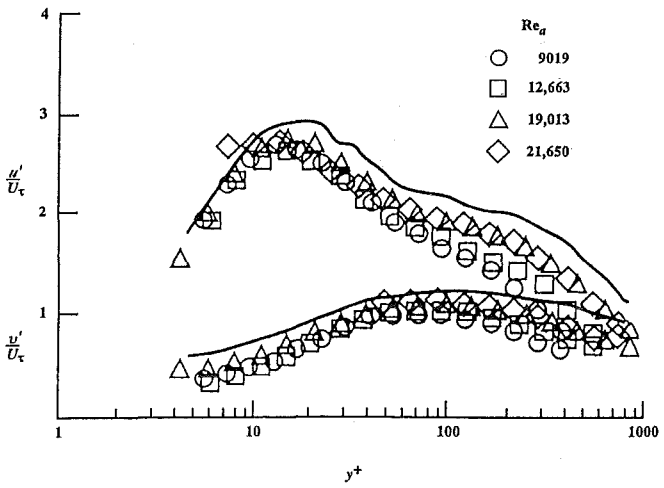

Fig 26. Profiles of turbulence intensity in streamwise direction and direction normal to wall, non-dimensionalized on inner variables. Channel flow data of Harder and Tiederman (1991). Solid lines in figure are best fit to Walker and Tiederman's (1990) data.

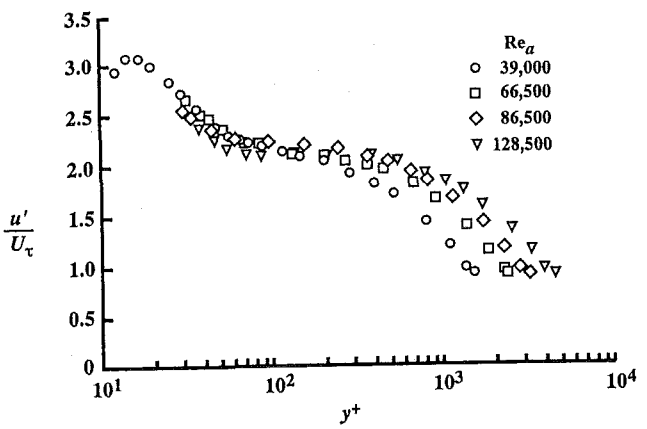

Fig 28. Streamwise turbulence intensity profiles non-dimensionalized with respect to inner variables. High-Reynolds number pipe-flow experiments of Perry and Abell (1975).

should be noted that the data in Fig 28 have been obtained with a hot-wire whose length has ranged from 35 to 100 wall units as the Reynolds number changed in the indicated range. According to the criterion that have been established earlier in this paper, Perry and Abell's probe resolution is insufficient to prove or refute the existence of similarity with inner variables.

Coles (1978) summarized the results of 50 different experiments conducted in circular pipes, rectangular channels and zero-pressure-gradient boundary layers. He does remark that not all experiments are equally reliable. Nevertheless, Fig 3 of Coles' paper indicates that, when the ratio of outer to inner length-scales, δ^+, increases from 100 to 10,000, the value of the rms streamwise velocity fluctuations measured at $y^+ = 50$ and normalized with the corresponding peak value measured at $y^+ \approx 15$ systematically increases from about 0.6 to 0.9. This result is consistent with a non-negligible Reynolds number effect on the turbulence just outside the viscous region.

6.2 Reynolds stress

6.2.1 Reynolds number effects

Turbulence shear stress, or Reynolds stress $-\rho\overline{u\upsilon}$, is the most important dynamical quantity affecting the mean motion. The major portion of the momentum transported in a two-dimensional turbulent wall-bounded flow is accomplished by $-\overline{u\upsilon}$. Therefore, modeling the behavior of Reynolds stress is one of the primary objectives of various prediction schemes. Simultaneous measurements of the streamwise and normal velocity fluctuations are required to compute the Reynolds stress at any particular point in the flow field. Provided this is done with high fidelity in the low- to moderate-Reynolds number laboratory experiments, extrapolation to the higher-Reynolds number field conditions is only possible if the Reynolds number effects are well understood. In this subsection, we review those effects in boundary layers, channels and pipes.

In boundary layers, the normalized cross correlation $-\overline{u\upsilon}$ is plotted in Fig 20c, for a single Reynolds number of $Re_\theta = 3664$. Again, Andreopoulos *et al* (1984) were unable to measure the Reynolds stress reliably at higher Reynolds numbers due to limitations of the applicable velocity range of their triple wire probe. The directly measured turbulence shear stress is on the average 10% smaller than the theoretical distribution deduced from the momentum balance and mean flow data and shown by the open symbols in Fig 20c.

More data are available for two-dimensional channel flows. The (kinematic) Reynolds stress normalized with the friction velocity is plotted versus the distance normal to the wall normalized with the channel half-width in Figs 29 and 30. In both figures, the data points are directly computed by averaging the product of the measured u- and υ-velocity fluctuations, and the solid line represents the theoretical total shear stress profile. In Fig 29, data from four different experiments are presented. Eckelmann (1974), using an oil channel, covered the low Reynolds numbers of 2800 and 4100. Alfredsson and Johansson (1984) conducted their experiment at $Re_a = 7500$, while Kastrinakis and Eckelmann (1983) conducted theirs at $Re_a = 12{,}600$. Comte-Bellot (1965) covered the higher range of Reynolds number of 57,000 and 230,000.

The data of Wei and Willmarth (1989) covered the Reynolds number range of 2970 to 39,582, and are reproduced in the linear plot shown in Fig 30. Their high-resolution LDA allows measurements very close to the wall where the Reynolds stress is decreasing. The maxima of the non-dimensional turbulence shear stress profiles increase in magnitude and are closer to the wall as the Reynolds number increases.

The same data above are plotted versus y^+ in Fig 31. Here, the semi-log plot allows closer inspection of the near-

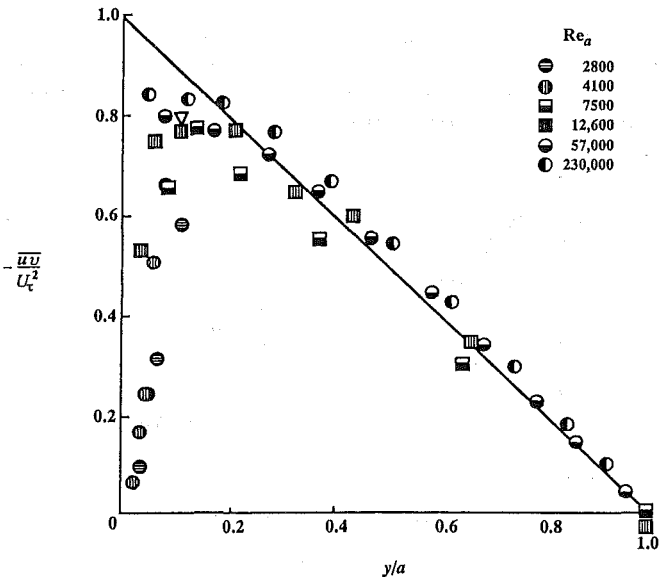

Fig 29. Reynolds stress profiles in wall units versus distance from wall normalized with channel half-width. Channel flow data from four different experiments, compiled by Wei and Willmarth (1989). Solid line represents total shear stress profile.

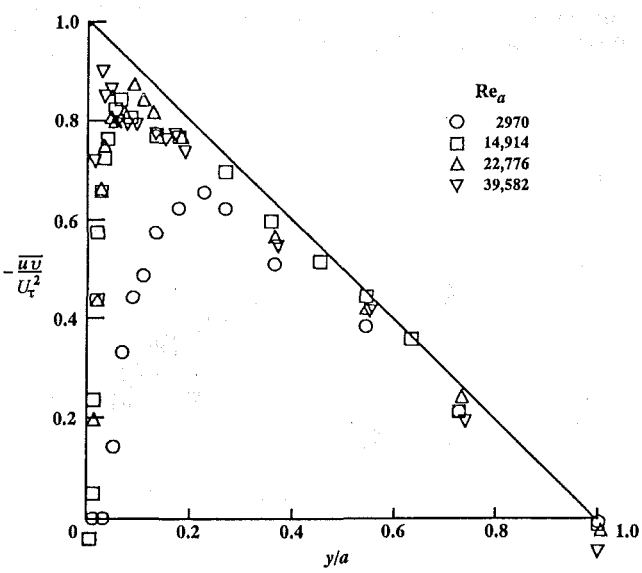

Fig 30. Reynolds stress profiles in wall units versus distance from wall normalized with channel half-width. Channel flow data of Wei and Willmarth (1989) at four different Reynolds numbers. Solid line represents total shear stress profile.

wall region, and Reynolds number effects are demonstrated more clearly. The maximum value of the normalized turbulence shear stress is not the same for each profile, indicating the lack of inner scaling in the Reynolds number range investigated. When expressed in wall units, the location of peak Reynolds stress moves away from the wall as the Reynolds number increases.

One advantage of investigating fully-developed pipe or channel flows is the ability to compare measurements with the computed Reynolds stress using the mean-velocity profile and pressure gradient, two quantities which are easier to measure. This has the advantage of being able to check the accuracy of the directly measured Reynolds stress, especially near the wall where probe resolution problems are particularly acute. In a fully-developed channel or pipe flow, the average normal and spanwise velocities vanish, there are no mean longitudinal velocity or Reynolds stress variations in the streamwise and spanwise directions, and the pressure gradient is a constant. The longitudinal momentum equation could then be integrated to give an exact relation between the Reynolds stress and mean-velocity distribution:

$$-\overline{uv} = -\nu\,(dU/dy) + U_\tau^2\,(1 - y/a) \tag{26}$$

where $U(y)$ is the streamwise mean-velocity distribution and a is the channel half-width or pipe radius. The friction velocity, or the slope of the velocity profile at the wall, is related to the constant pressure gradient through:

$$U_\tau^2 = \nu\,(dU/dy)_w = -\,(a/\rho)\,(dP/dx) \tag{27}$$

where P is the static pressure and ρ and ν are the fluid density and kinematic viscosity, respectively. In wall units the momentum balance Eq 26 reads:

$$-\overline{uv}^+ = -\,(dU^+/dy^+) + (1 - y^+/a^+) \tag{28}$$

Wei and Willmarth (1989) used Eq 28 to compute the Reynolds stress profiles shown by the solid lines in Fig 31. Again, the non-dimensional profiles at different Reynolds numbers do not collapse in the outer and logarithmic regions and even well into the viscous region. Except very close to the wall, the agreement between the directly measured Reynolds stress and that computed from the measured mean velocity and pressure gradient is very good, and attests to the accuracy of the instantaneous velocity traces reconstructed, filtered and smoothed from the Doppler burst detector and processor signals. Wei and Willmarth speculate that the divergence between the directly measured and computed Reynolds stresses is due to insufficient spatial and temporal resolution in the direct LDA measurement very close to the wall.

The Reynolds stress profiles measured in a water channel by Harder and Tiederman (1991) are reproduced, non-dimensionalized with inner variables, in Fig 32. The range of Reynolds numbers investigated, Re_a = 9019 to 21,650, is narrower than that studied by Wei and Willmarth (1989). Not surprisingly, then, Harder and Tiederman assert that, for $y^+ < 50$, inner scaling correlates their data for all four Reynolds numbers.

Wei and Willmarth (1989) also computed the turbulence kinetic energy production using both the directly measured

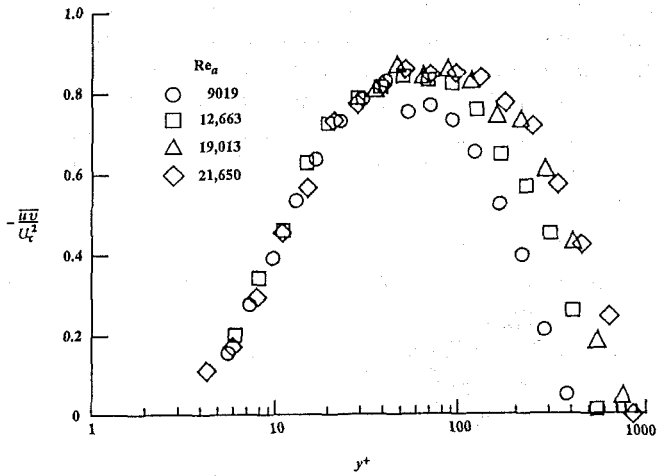

Fig 32. Reynolds stress profiles non-dimensionalized on inner variables. Channel flow data of Harder and Tiederman (1991) at four different Reynolds numbers.

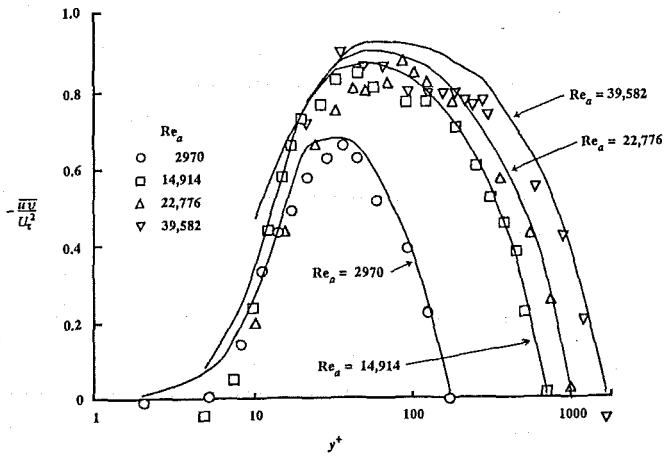

Fig 31. Reynolds stress profiles non-dimensionalized on inner variables. Channel flow data of Wei and Willmarth (1989) at four different Reynolds numbers. Solid line represents momentum balance calculations.

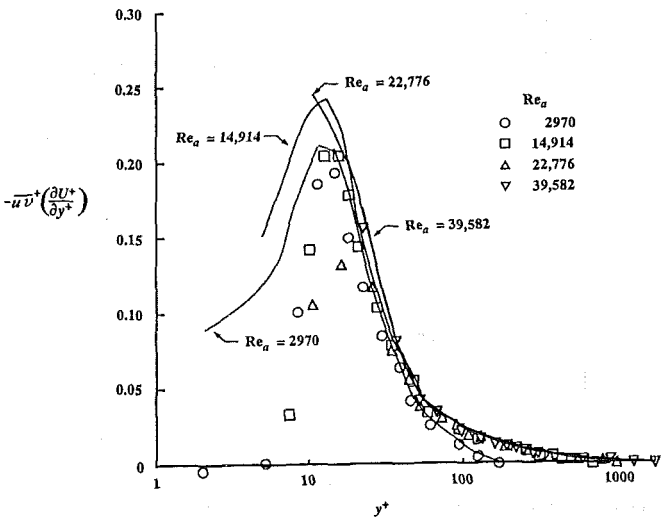

Fig 33. Turbulence kinetic energy production profiles. Channel flow data of Wei and Willmarth (1989) at four different Reynolds numbers. Solid lines represent momentum balance calculations.

Reynolds stress and the momentum balance equation. The profiles for four different Reynolds numbers are shown non-dimensionalized with inner variables in Fig 33. Excepting very close to the wall, the two methods of computing $-\overline{uv}$ (dU/dy) agree within 10%. Neither method leads to a profile collapse even in the viscous region. The maximum value of kinetic energy production obtained from the momentum balance increases with Reynolds number. The data point nearest to the wall measured at Re_a = 22,776 appears to be in error. Interestingly, while the position of peak Reynolds stress, expressed in wall units, moves away from the wall as the Reynolds number increases (Fig 31), the peak turbulence production seems to be fixed at $y^+ \approx$ 12-15. This point will be revisited later in this section and once more in Section 7.

The measurements of mean velocity and pressure drop in the smooth-pipe-flow experiments of Nikuradse (1932) and Laufer (1954) were used to compute the Reynolds stress profiles shown previously in Fig 5. The Reynolds number in that figure, $Re^* = U_\tau a / \nu$, is the ratio of the pipe radius to the viscous length-scale, and varies over the wide range of 140-55,400. A constant-turbulent-shear-stress region is clear at the highest Reynolds number. As in the channel flows, the peak value of normalized Reynolds stress increases and its location, relative to the viscous length-scale, moves away from the wall as the Reynolds number increases.

6.2.2 Peak location

Sreenivasan (1989) analyzed several different wall-bounded flow experiments. The distance from the wall, expressed in inner variables, where the streamwise turbulence intensity peaks appears to be independent of Reynolds number (Fig 16 of his paper). In contrast, the location where the largest normal fluctuations occur is a strong function of Reynolds number (Fig 17 of his paper):

$$[y^+]_{u'\text{-max}} = [Re^*]^{0.75} \tag{29}$$

where Re^* is the pipe radius or boundary layer thickness in wall units. Available data on the spanwise intensity are scarce and no conclusion can be reached on the scaling of its peak position. For the total turbulence kinetic energy, however, the position of its peak does scale on wall variables, much the same as u'. This is because the near-wall value of the total fluctuation energy is essentially overwhelmed by the streamwise component.

Similar to the normal fluctuations, the peak Reynolds stress occurs at increasingly higher values of y^+ as the Reynolds number increases as shown in Figs 34a and 34b, compiled from directly measured and computed turbulence shear stress data, respectively. The lowermost two data points in Fig 34b correspond to the location of the peak Reynolds stress, or the critical layer position, in typical transitional boundary layer and channel flows. A least-square fit of all the data points in both figures leads to the same equation:

$$[y_p^+] = 2\,[Re^*]^{0.5} \tag{30}$$

where y_p is the location of peak Reynolds stress. Note that although probe resolution has a significant effect on the magnitude of turbulence intensity, Reynolds stress or other higher-order statistics, a relatively long probe should have less effect on the accuracy of determining the peak location of these quantities. It is therefore not surprising that Sreenivasan (1989) could use a variety of data sources, including some with insufficient probe resolution, to arrive at the correlations in Eqs 29 and 30.

Equation 30 indicates that the location of the peak turbulence stress scales on the geometric mean of the inner and outer scales. Recall that, since this is the position in Sreenivasan's (1988) model discussed in Section 4, where all the mean vorticity of a turbulent boundary layer has been assumed to be concentrated into a single sheet, the correlation in Eq 30 gives some credence to his hypothesis.

Note that if a velocity profile is assumed for the case of fully-developed channel flow, exact expressions for the location of the peak Reynolds stress and turbulence kinetic energy production could be derived from Eq 26. For example, if the logarithmic mean-velocity profile,[10] Eq 8, is used, the peak Reynolds stress occurs at $y_p^+ = 1.56\ Re^{*0.5}$, while the peak production occurs at a fixed y^+.

At high Reynolds numbers the peak Reynolds stress occurs substantially outside the viscous region. Note however that, due to the shrinking of the inner layer as the Reynolds

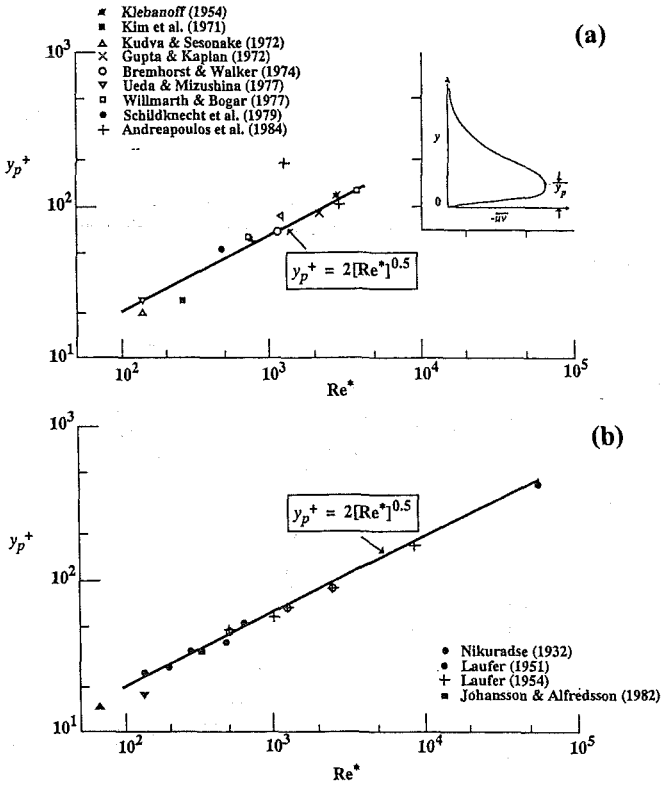

Fig 34. Location of peak Reynolds stress as a function of Reynolds number. Data compiled by Sreenivasan (1988) from various wall-bounded flow experiments. Solid lines are least-square fit: (a) Directly measured Reynolds stress; (b) Computed from measured mean velocity. The lowermost two data points correspond to the critical layer position in typical transitional flows.

[10] Not an accurate assumption for $y^+ < 30$.

number increases, this peak location moves closer to the wall as a fraction of the boundary layer thickness. Interestingly, while the most significant Reynolds-stress-producing activity does not occur at a universal value of y^+, the production of turbulence kinetic energy, $-\overline{uv}(dU/dy)$, does always peak at $y^+ \approx 15$. This implies that, at high Reynolds numbers where the two positions dispart, the scales producing the Reynolds stress are quite different from those responsible for the turbulence kinetic energy production. It is this observation that led Townsend (1961) to hypothesize the existence of an *active motion* and an *inactive motion* within the inner layer. The former is due to the vorticity field of the inner-layer proper and is responsible for Reynolds stress production. The statistical properties of the active motion are presumably universal functions of the distance from the wall. The inactive, larger-scale motion is partly due to the irrotational field sloshing associated with the pressure fluctuations in the outer layer and partly the large-scale vorticity field of the outer-layer turbulence which the inner layer sees as an unsteady external stream (see also the substantiative measurements of Bradshaw, 1967). The inactive motion does not scale with inner variables, and is characterized by intense velocity fluctuations. The effect of increasing the Reynolds number can then be thought of as the increasing significance of the inactive motion (see also Naguib and Wark, 1994).

The primary conclusion of this and the previous subsections is that Reynolds number does have an effect on the turbulence shear stress even in the inner layer. Inner scaling fails to collapse the Reynolds stress profiles. The peak value of $-\overline{uv}$ increases with Reynolds number and its position moves outward when expressed in wall units.

6.2.3 Asymptotic theory

The results depicted in Sections 6.1, 6.2.1 and 6.2.2 indicate that inner scaling fails to collapse the profiles for the Reynolds stress and for the root-mean-square values of the velocity fluctuations. Considerable Reynolds number effects are exhibited even for y^+ values less than 100. Panton (1990a) points out that a turbulent wall-bounded flow is fundamentally a two-layer structure, a classical single perturbation situation. At finite Reynolds numbers, neither the inner representation nor the outer representation is a uniformly valid approximation to the true answer in the matching region. As Re_θ varies, the overlap layer changes size and the proportions of inner and outer effects are altered.

A uniformly valid answer for the present singular perturbation problem could be obtained by forming an additive composite expansion from the inner and outer expansions. Matching essentially replaces the two lost boundary conditions at $y = 0$ and $y = \infty$, and the additive composite expansion is simply the sum of the inner and outer ones minus the common part (see, for example, Van Dyke, 1974). Systematic changes with Reynolds number that are considered anomalies when turbulent quantities are expressed as inner expansions could then be considered as proper first-order trends that are expected when viewed in the proper light. Such treatment were demonstrated for the mean flow (Panton, 1990b), for the rms turbulent fluctuations (Panton, 1991), and for the Reynolds stress (Panton, 1990a). Root-mean-square values of the velocity fluctuations or Reynolds stress expressed as additive composite expansions are equivalent in accuracy to the mean velocity expressed as the law of the wall plus the law of the wake.

For the mean flow, Panton (1990a) suggests the use of an inner velocity scale that is different from the friction velocity (see Eq 7 of the present article), the two being equal only in the limit of infinite Reynolds number. Within the framework of an asymptotic theory (Yajnik, 1970; Afzal, 1976; Afzal and Bush, 1985), the lowest-order equation for the mean flow shows weak Reynolds number dependence while that for the Reynolds stress indicates a much stronger effect. According to Panton (1990a), the logarithmic nature of the inner, outer and composite expansions for the mean flow dictates minimal Reynolds number effects. On the other hand, the Reynolds stress behaves algebraically and the inner/outer effects are mixed in different proportions and occur at different locations, resulting in strong Reynolds number dependency even in the first-order theory. Moreover, the additive composite expansion for the Reynolds stress does not evince a constant-stress region, only the inner expansion does so.

6.3 Spectra

It is often useful to analyze the kinetic energy of the turbu-

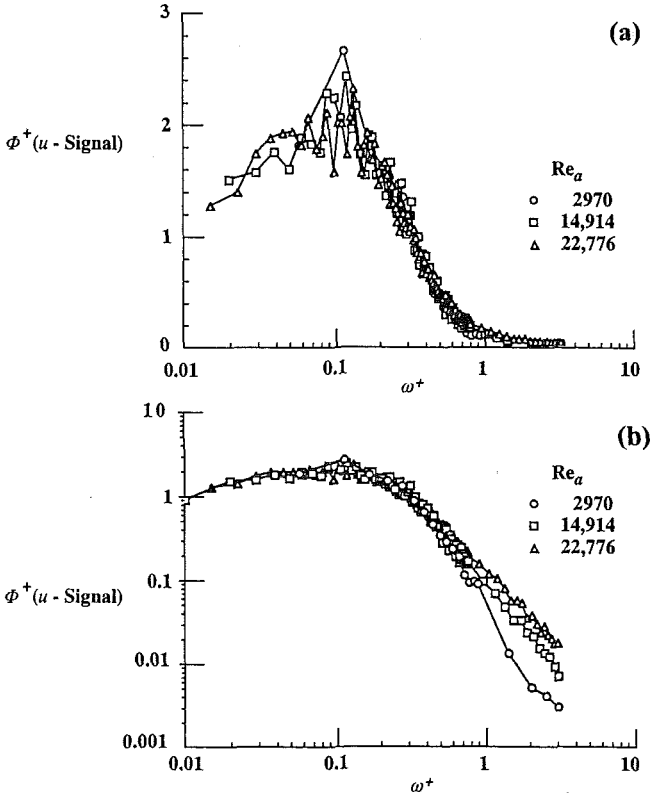

Fig 35. Power spectra of the streamwise velocity fluctuations at $y^+ = 15$. Inner variables scaling is used for normalization. Channel flow data at three Reynolds numbers; from Wei and Willmarth (1989): (a) Semi-log plot; (b) Log-log plot.

lent fluctuations according to its distribution over the various frequencies occurring in these fluctuations. The energy (or power) density spectrum of the fluctuating velocity components or Reynolds stress is computed from the respective instantaneous, digitized signals, and can yield information regarding structural evolution as the Reynolds number changes. Consider the channel flow data of Wei and Willmarth (1989) taken at $y^+ = 15$ at three different Reynolds numbers: $\mathrm{Re}_a = 2970$; 14,914; and 22,776. The power spectra of the streamwise velocity fluctuations nondimensionalized with inner variables are plotted versus the angular frequency in wall units on a semi-log scale in Fig 35a and on a log-log scale in Fig 35b. The normalization employed in these figures is that used by Perry and Abell (1975) and is such that the area under each curve is the mean-square of the velocity fluctuations in wall units. Essentially:

$$\Phi^+(\omega^+) = \omega^+ \Phi(\omega)/\nu \tag{31}$$

$$\omega^+ = \omega\, \nu/U_\tau^2 \tag{32}$$

where $\Phi(\omega)$ is the power spectral density of the velocity (or Reynolds stress) fluctuations, ω is the radian frequency, and ω^+ is the frequency scaled with inner variables.

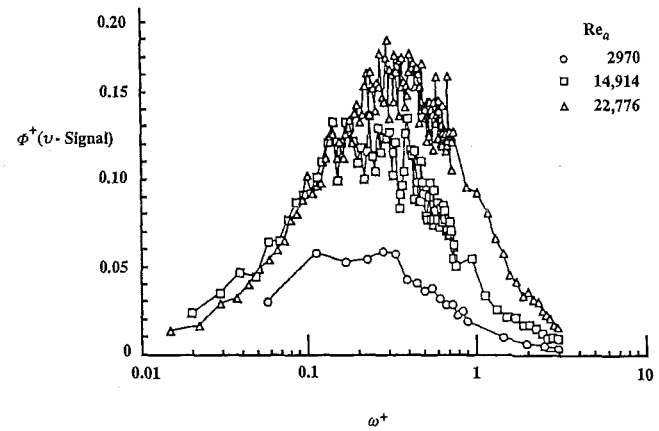

Fig 36. Power spectra of the normal velocity fluctuations at $y^+ = 15$. Channel flow data from Wei and Willmarth (1989).

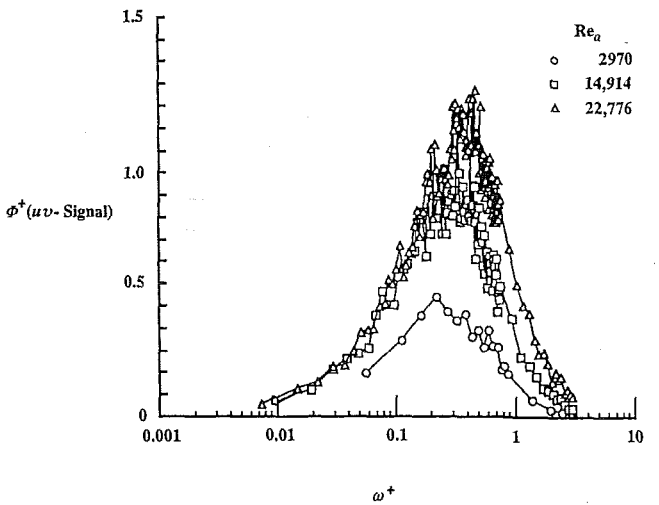

Fig 37. Power spectra of the Reynolds stress fluctuations at $y^+ = 15$. Channel flow data from Wei and Willmarth (1989).

Although there is appreciable scatter at lower frequencies (in the semi-log plot),[11] the u-power spectra in Figure 35 suggest that the energy-containing eddies scale on inner variables in the vicinity of the kinetic energy production peak, $y^+ = 15$. However, at high frequencies, the spectra begin to diverge from inner-layer scaling and greater energy is available with increasing Reynolds number (see the log-log plot in Fig 35b, which emphasizes the low-energy portion of the spectrum). This is consistent with the appearance of smaller eddies and increased vortex stretching at higher Reynolds numbers as will be discussed in Section 7. Notice that the increase in the streamwise turbulence kinetic energy with Reynolds number is very slight, consistent with the near-collapse of u'- data for $y^+ \leq 15$ in Fig 25.

Normalized plots similar to Fig 35a but for the near-wall normal velocity fluctuations and Reynolds stress are given in Figs 36 and 37, respectively. Neither set of plots scale on inner variables over a large portion of the energy-containing frequency range. This is consistent with Wei and Willmarth's (1989) assertion that neither the v'-profiles nor the $-\overline{uv}$-profiles scale on inner variables even very close to the wall (Figs 25 and 31).

The power spectra of the streamwise velocity, normal velocity and Reynolds stress in the same channel flow as above but near the edge of the inner layer, $y^+ = 125$, are shown in Figs 38, 39, and 40, respectively. Again, the area under each spectrum represents the mean square of the corresponding velocity or Reynolds stress fluctuations normalized with inner variables. Reynolds number effects on the high-frequency portion of the spectrum appear to be less pronounced at this distance farther away from the wall as compared to the spectra in the near-wall region depicted in Figs 35-37. Since the mean-velocity gradient decreases with increasing distance from the wall, Wei and Willmarth (1989) attribute the weaker Reynolds number-dependence to a diminished stretching of vorticity farther away from the wall. On the other hand, in the low-frequency portion of the spectra, Reynolds number effects are stronger. The lack of scaling with inner variables at $y^+ = 125$ is consistent with the measurements of Bradshaw (1967) and is due to the large-scale inactive motion.

The power spectra of the streamwise velocity fluctuations in the high-Reynolds number pipe flow experiment of Perry and Abell (1975) are shown in Fig 41. In this normalized log-log plot, $\Phi(ky)/U_\tau^2$ is plotted versus ky, where k is the wavenumber. The data points represent several Reynolds numbers in the range of $\mathrm{Re}_a = 40{,}000$-$130{,}000$, and several distances from the wall in the range of $y^+ = 150$-444. These distances correspond to the region of overlap where y is much larger than the viscous length-scale but much smaller than the outer scale (see Section 3.2). In this constant-Reynolds stress regime, the spectrum does not change with wall distance. The straight line in the log-log plot has the slope of -1, predicted for the equilibrium range of the spectrum using scaling arguments (see Sreenivasan,

[11] As will be shown in Figs 36 and 37, there is even more scatter in the v- and uv-spectra when similarly plotted on semi-log plots.

1989). The large-scale fluctuations outside this equilibrium range constitute the so-called inactive motion mentioned earlier. At the other end of the scale, the smaller eddies (high wavenumbers) either obey the usual -5/3 Kolmogorov-law provided the Reynolds number is high enough to create an inertial subrange, or simply be dominated by viscosity at low Reynolds numbers.

In summary, only the u-turbulence spectra scale with inner variables very close to the wall ($y^+ \leq 15$), while those for v and uv do not. In the constant- stress layer and over a wide range of Reynolds numbers, the spectrum of the longitudinal velocity fluctuations has a -1 slope in the equilibrium range of eddies.

6.4 Skewness and flatness factors

The third and fourth moments of a random signal give useful statistical information regarding the temporal distribution of its fluctuations around an average value. When nondimensionalized using the root-mean-square value of the fluctuations, these become the skewness and flatness factors, respectively. For example, for the streamwise velocity fluctuations the skewness and flatness factors are defined as follows:

$$S_u = \left(\overline{u^3}\right) / \left(u_{\text{rms}}\right)^3 \tag{33}$$

$$F_u = \left(\overline{u^4}\right) / \left(u_{\text{rms}}\right)^4 \tag{34}$$

Similar expressions can be written for the skewness and flatness factors for the other two velocity components, the Reynolds stress, the velocity derivative with respect to time, etc.

For a Gaussian signal, the probability distribution is symmetric around the mean value and those factors are respectively $S = 0$ and $F = 3$. A nonzero skewness factor indicates the degree of temporal asymmetry of the random fluctuations, *eg* acceleration versus deceleration or sweep versus ejection. Flatness factor larger than 3 is associated with a peaky signal as for example that produced by intermittent turbulent events.

Unlike the second and higher even moments, the third and all higher odd-number moments retain the sign information and thus contain valuable statistical information related to the coherent structures. The skewness of a turbulence quantity can be thought of as representing the flux of a stress which is directly attributable to coherent structures. For example, $\overline{u^3}$ is the streamwise flux of the streamwise turbulence kinetic energy $\overline{u^2}$, $-\overline{u^2 v}$ is the streamwise flux of the Reynolds stress $\overline{uv}$, $-\overline{uv^2}$ is the normal flux of $\overline{uv}$, etc.

A combination of positive $\overline{u^3}$ and negative $\overline{v^3}$ is associated with sweep events, while a combination of negative $\overline{u^3}$ and positive $\overline{v^3}$ is attributable to ejection events (see Section 7). Similarly, $-\overline{u^2 v}$ and $-\overline{uv^2}$ denote streamwise flux and outward transport of shear stress, respectively. Note that, via triple moments, structural information can be extracted without ambiguity. That is, without recourse to any subjective threshold setting as in the so-called VITA and VISA--variable-interval time- or

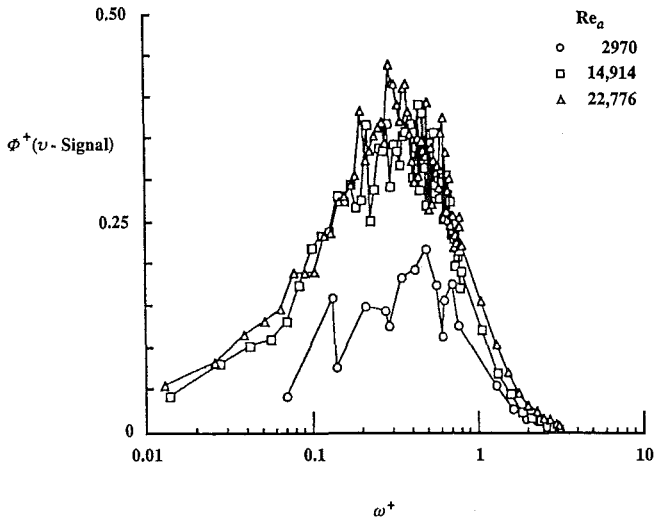

Fig 39. Power spectra of the normal velocity fluctuations at $y^+ = 125$. Channel flow data from Wei and Willmarth (1989).

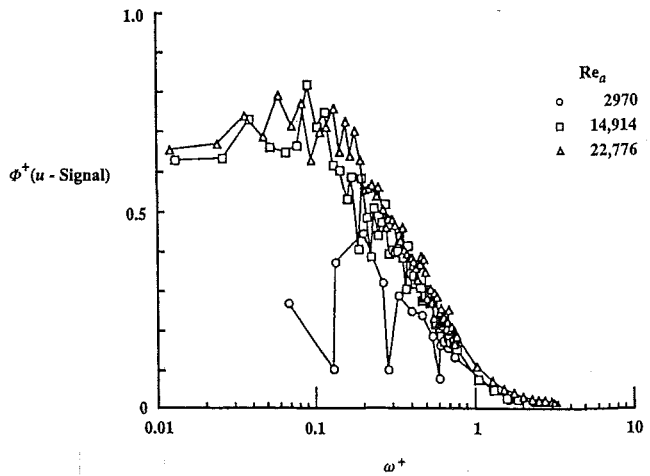

Fig 38. Power spectra of the streamwise velocity fluctuations at $y^+ = 125$. Channel flow data from Wei and Willmarth (1989).

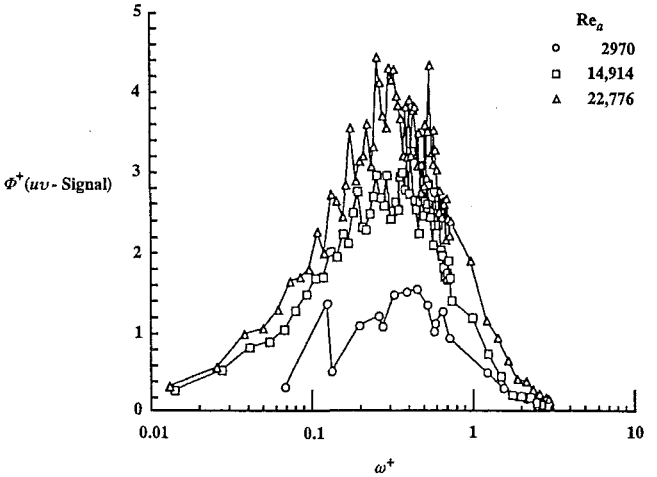

Fig 40. Power spectra of the Reynolds stress fluctuations at $y^+ = 125$. Channel flow data from Wei and Willmarth (1989).

space-averaging techniques (Blackwelder and Kaplan, 1976), respectively. The flatness factor, on the other hand, is always positive. Near the rotational/irrotational interface of a turbulent boundary layer and in the near-wall region where intermittent bursting events take place, the normalized fourth moment attains large values.

Profiles of the skewness factor of the streamwise velocity fluctuations in the boundary-layer flow of Andreopoulos *et al* (1984) are plotted in Fig 42 for four Reynolds numbers in the range of Re_θ = 3624-15,406. High positive values of S_u are observed in the viscous sublayer, indicating the skewed nature of the acceleration-dominated velocity fluctuations there. As a result of the arrival of high-speed fluid from regions away from the wall (sweep events), large positive values of u occur more frequently than large negative values in the near-wall region. In the log region, the skewness factor is only slightly different from that for a Gaussian probability density distribution. Farther away from the wall, the skewness is negative consistent with the arrival of low-speed fluid from the wall region (deceleration-dominated ejection events). Reynolds number effects are stronger in the wake region of the flow where the skewness is negative, although some effects penetrate all the way to the edge of the viscous sublayer. Figure 42 indicates strong Reynolds number effects on the streamwise flux of the longitudinal turbulence kinetic energy due to both sweep and ejection events.

Kline (1967) has proposed that the near-wall value of S_u is related to the width of the low-speed streaks (Section 7.1). In low-Reynolds number flows, the most probable location of the breakup stage of the bursting process is at y^+ = 15. According to the data in Fig 42, the value of S_u changes sign at that y^+ at Re_θ = 3624, but at the higher Reynolds number of $Re_\theta = 15.4\times10^3$, the skewness does not change sign till $y^+ \approx 200$.

Smits *et al* (1989) have compared the skewness factor S_u for subsonic low-Reynolds number (M_∞ = 0.1; $Re_\theta = 5\times10^3$) and supersonic high-Reynolds number (M_∞ = 2.9; $Re_\theta = 80\times10^3$) turbulent boundary layers. Since the effect of Mach number appears to be weak and can be taken into account by considering the local fluid properties, the comparison primarily shows the effect of Re_θ. It is interesting that in Smits *et al*'s experiments, S_u changes sign at y/δ = 0.17 for $Re_\theta = 5\times10^3$, but at y/δ = 0.68 for $Re_\theta = 80\times10^3$. Thus, the point of cross-over from the sweep- to the ejection-dominated motions moves outward as Re_θ increases and shows no sign of reaching an asymptote. Admittedly, the available data are scarce, but it is clear that Reynolds

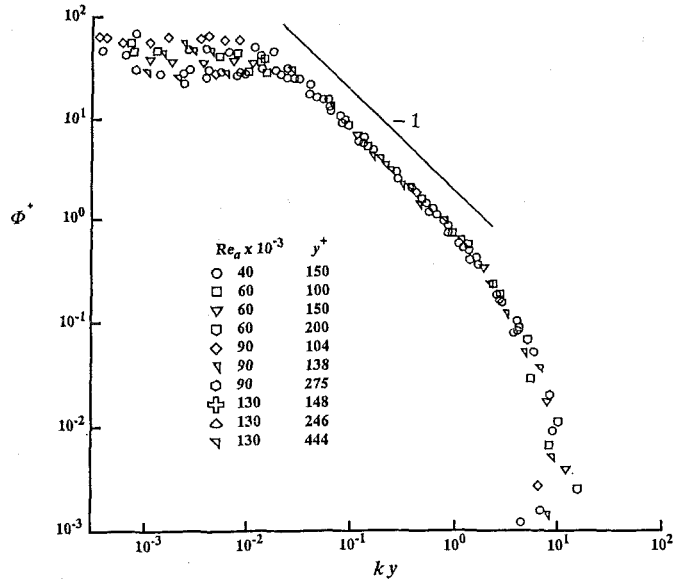

Fig 41. Normalized power spectra of the streamwise velocity fluctuations. Pipe flow data from Perry and Abell (1975) at different Reynolds numbers and different distances from the wall.

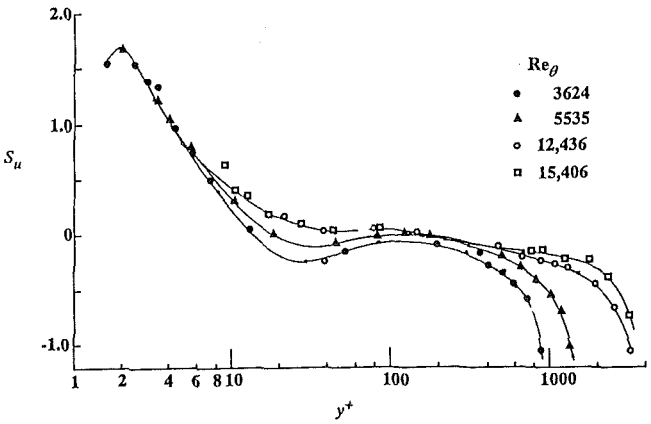

Fig 42. Profiles of skewness factor of streamwise velocity fluctuations at four Reynolds numbers (from Andreopoulos *et al*, 1984).

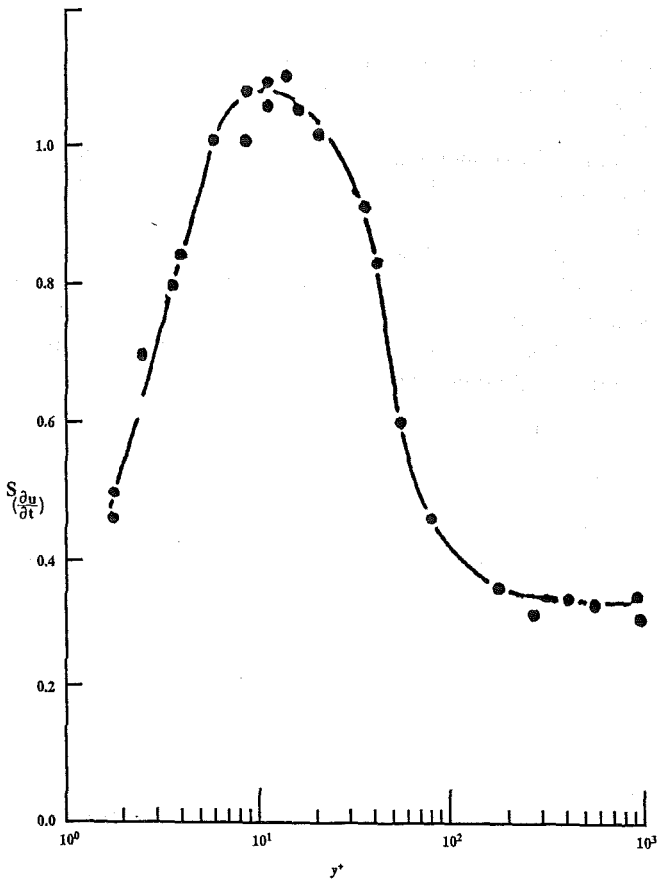

Fig 43. Skewness of the velocity derivative *du/dt* in the inner region of a pipe flow (from Elena and Dumas, 1978).

number effects on third- and higher-order moments are stronger than those on the first- and second-order moments.

In isotropic turbulence, the skewness of the velocity derivative du/dx signifies the inertial transfer of energy across the wavenumber domain and is proportional to the production of mean-square vorticity by vortex stretching. For the anisotropic wall-bounded flow, Sreenivasan (1989) argues that such interpretations may hold at least qualitatively. Figure 43 depicts $S_{(du/dt)}$ for the pipe flow data of Elena and Dumas (1978). In a high-shear flow, time derivative is very roughly related to space derivative through the Taylor's frozen flow hypothesis. The skewness profile in Fig 43 is typical and peaks at roughly $S_{(du/dt)} = 1$ around $y^+ = 12$, indicating strong nonlinear effects, or vortex stretching, in the same region where production of turbulence kinetic energy also reaches a maximum. The value of $S_{(du/dt)}$ drops to 0.4 in the outer layer and towards zero at the wall. Similar trends are observed in channel flows (Comte-Bellot, 1963) and boundary layers (Ueda and Hinze, 1975).

For the reasons indicated in Section 6.1, Andreopoulos *et al* (1984) measured the normal velocity fluctuations at the single low Reynolds number of $Re_\theta = 3624$. Their results for the skewness factor of the normal-velocity fluctuations are depicted in Fig 44. Unlike the skewness of the streamwise velocity fluctuations, the value of S_v is negative near the wall and positive in the outer flow region, signaling the more frequent occurrence of negative and positive normal velocity fluctuations in the inner and outer layer, respectively. The skewness is again near zero in the overlap region.

Andreopoulos *et al*'s (1984) data follows the general trends of those measured by Gupta and Kaplan (1972), but differ somewhat from the data of Kreplin and Eckelmann (1979) and more strongly from those due to Kutateladze and Khabakhpasheva (1978). The disagreements are particularly noticeable in the near-wall region. This is not surprising considering the spatial and temporal probe-resolution difficulties associated with the measurement of higher-order moments. The near-wall distribution of the skewness of the normal velocity fluctuations is compared for the four different experiments in Fig 45. Note that a linear scale is used for the abscissa in this figure. Except for the data of Kutateladze and Khabakhpasheva (1978), S_v is positive for $y^+ > 5$ and negative for $y^+ < 5$. It is intriguing that as the wall is approached, the increased viscous effects and wall constrain are incapable of damping the wall-ward component of the velocity fluctuations.

Profiles of the flatness factor of the streamwise velocity fluctuations in the boundary layer flow of Andreopoulos *et al* (1984) are plotted in Fig 46 for four different Reynolds numbers in the range of $Re_\theta = 3624$-15,406. The kurtosis has high values near the wall and in the outer layer, indicating that the turbulence is highly intermittent in both places. In the overlap region, F_u is nearly 3, and Reynolds number effects are weak. But Reynolds number effects are noticeable in the buffer layer penetrating all the way to the edge of the viscous sublayer and are much stronger in the outer layer, much the same as the corresponding effects on the skewness factor S_u depicted in Fig 42.

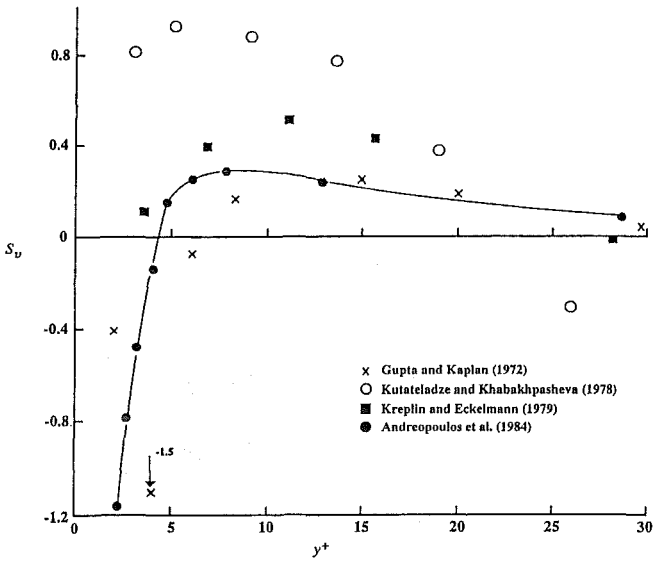

Fig 45. Distribution of skewness factor of velocity fluctuations normal to the wall. Near-wall region results from four different facilities. Adapted by Andreopoulos *et al* (1984).

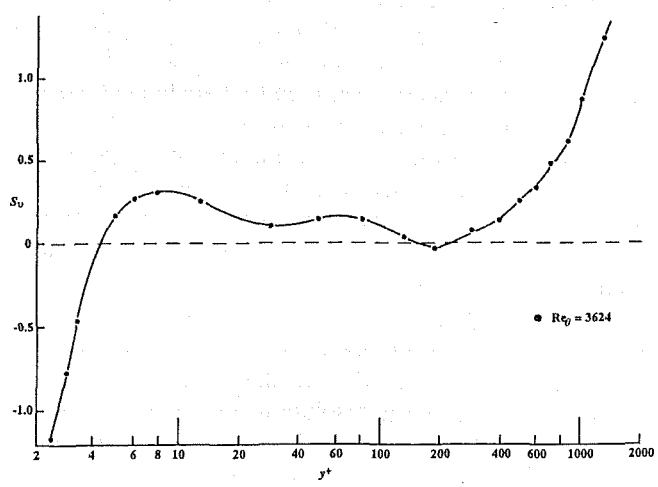

Fig 44. Distribution of skewness factor of velocity fluctuations normal to the wall (from Andreopoulos *et al*, 1984).

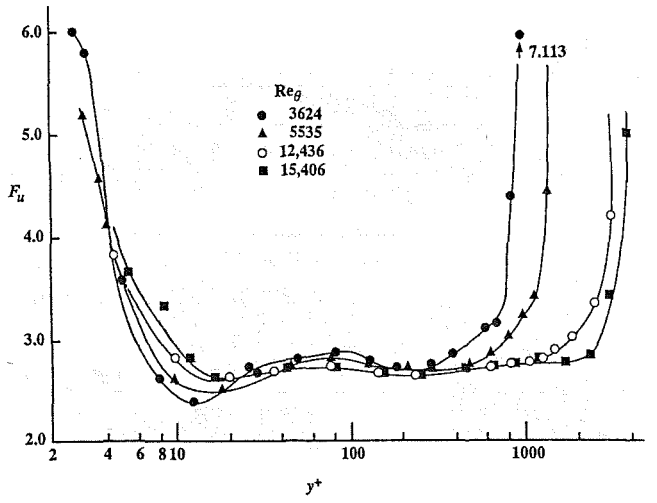

Fig 46. Profiles of flatness factor of streamwise velocity fluctuations at four Reynolds numbers (from Andreopoulos *et al*, 1984).

Table 1. Wall-pressure fluctuation statistics

a. Measurements					
p'_w/U_τ^2	2.3 - 2.6				3.38 (Average)
Re_θ	up to 4×10^4				$Re_x \sim 10^8$; $M \le 0.6$
	Laboratory Measurements (Willmarth, 1975b)				Flight: Boeing 737 forward (Bhatt, 1971)
b. Flat-Plate and Channel Simulations					
p'_w/U_τ^2	2.3 - 2.4	2.8	1.9	2.7	1.4
Re_θ	353 - 505	576	300	1410	$Re_D = 1.38 \times 10^4$
	LES (Tsai & Leslie, 1990)		DNS (Spalart, 1988)		DNS (Kim *et al*, 1987)
c. Structural Model (Bandyopadhyay and Balasubramanian, 1994)					
p'_w/U_τ^2	1.28		1.26	3.59	2.32
Re_Γ	200		100	200	100
Vortex Model	Ejection		Ejection	Sweep	Sweep

6.5 Wall-pressure fluctuations

Important physics of the turbulent wall-bounded flow can be learned from the measurements of the instantaneous pressure. Pressure fluctuations are often proposed as an important mechanism by which the outer region of a boundary layer could influence and even initiate dynamically significant events in the wall region. Additionally, pressure fluctuations in a wall-bounded flow induce structural vibrations on the surface and are believed to be responsible for radiated noise. Solving practical engineering problems that deal with reducing this flow-induced noise, for example to improve the performance of sonar domes on submarines or to suppress unpleasant noise in the interior of commercial aircraft, requires documenting the important statistics of the random pressure field, such as root mean square, spectrum, and cross correlation.

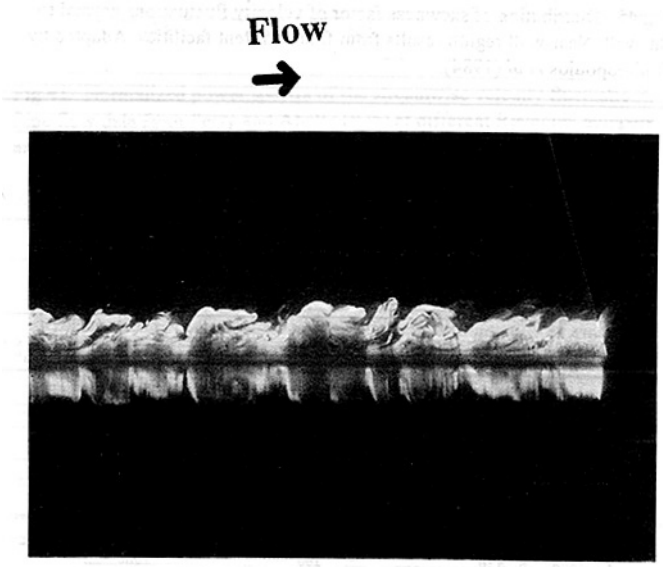

Fig 47. Side view of a low-Reynolds number turbulent boundary layer; Re_θ = 725. Flat plate towed in a weter channel. Large eddies are visualized using a sheet of laser and fluorescence dye (from Gad-el-Hak *et al*, 1984).

The local static pressure fluctuations across a shear flow cannot yet be measured. The only location where it can be measured is at the wall. This is often advantageous since information on convective structures within the boundary layer can be obtained nonintrusively by using wall-pressure sensors. The subject of wall-pressure measurements has been reviewed by Willmarth (1975b). Johansson *et al* (1987) and Farabee and Casarella (1991) describe the current status. The latter authors show that the applicable scaling laws change with the frequency range of the spectrum. As anticipated earlier by Panton and Lineberger (1974), the friction velocity and the boundary layer thickness are the appropriate scales at low wavenumbers. At high wavenumbers, the friction velocity and the viscous length-scale seem to collapse the data (Robert, 1993; Panton and Robert, 1993; 1994).

Reliable laboratory measurements of pressure fluctuations are particularly difficult since extraneous freestream turbulence and acoustic noise are unavoidably sensed by the wall-mounted microphones. To partially alleviate this problem, Panton *et al* (1980) conducted pressure measurements on the fuselage of a sail plane. Contributions from potential motion outside the boundary layer were measured and show a slight Reynolds number dependence.

The state of the art of probe resolution is a much more serious problem for wall pressure than it is in velocity-based variables. For example, pressure sensors as large as 450 wall units have been used in the past. Schewe (1983) used one of the smallest probes, having an effective diameter of $19\nu/U_\tau$ More recently, Lauchle and Daniels (1987) used sensors with diameters in the range of 0.7-1.5 wall units. However, the glycerin pipe-flow facility they utilized was acoustically noisy, and elaborate noise-removal techniques were used to process the pressure fluctuations data. The wall-pressure spectra measured by Lauchle and Daniels in the range of Reynolds numbers of Re_a = 7000-16,500 are consistent with the flow physics: higher Reynolds number flow supports smaller scales and hence higher-frequency pressure fluctuations. When non-dimensionalized with wall variables, however, the spectra, in that range of Reynolds numbers, seem to collapse.

Keith *et al* (1992) assert that attenuations resulting from inadequate spatial resolution of a sensor are of primary concern. Variations among different data sets are reduced at higher frequencies when resolution effects are accounted for. Keith *et al* clearly show the Reynolds number effects in the scaling of the low-frequency portion of wall-pressure spectra; while at low $Re_\theta (< 4.5\times10^3)$ a mixed scaling ap-

plies, outer scaling holds better at higher Re_θ ($> 4.5x10^3$). In their work, the outer scaling of the low-frequency end of the spectrum is related to the mixed scaling by the factor $(U_\tau/U_\infty)^4$, which decreases as Re_θ increases. This observed change in the scaling laws with Reynolds number is intriguing. Inner scaling seems to be effective, on the other hand, at the high-frequency portion of the spectra over the entire range of Reynolds numbers where reliable data are available.

Note that even a weak Reynolds number dependence in wavenumber space will be accentuated in frequency space. The reason being that a large eddy moving at a fast speed would produce the same frequency as a small eddy moving at a low speed. For that reason, Panton (1989) developed his inner/outer theory in wavenumber-phase velocity space and reasonable agreement with experimental data was observed (Panton and Robert, 1994).

Table 1, adapted from Bandyopadhyay and Balasubramanian (1994), is a summary of rms wall pressure, normalized with the square of the friction velocity, from measurements and simulations. Both the physical and numerical experiments indicate a slight increase with Reynolds number, a result that is also theoretically anticipated (Bradshaw, 1967). In the structural model of Bandyopadhyay and Balasubramanian, higher Reynolds number effects in p'_w are better simulated by higher vortex-Reynolds number sweep motions.

7. COHERENT STRUCTURES

The classical view that turbulence is essentially a stochastic phenomenon having a randomly fluctuating velocity field superimposed on a well-defined mean has been changed in the last few decades by the realization that the transport properties of all turbulent shear flows are dominated by quasi-periodic, large-scale vortex motions (Laufer, 1975; Townsend, 1976; Cantwell, 1981). Despite the extensive research work in this area, no generally accepted definition of what is meant by coherent motion has emerged. In physics, coherence stands for well-defined phase relationship. For the present purpose we adopt the rather restrictive definition given by Hussain (1986): *a coherent structure is a connected turbulent fluid mass with instantaneously phase-correlated vorticity over its spatial extent.* In other words, underlying the random, three-dimensional vorticity that characterizes turbulence, there is a component of large-scale vorticity which is instantaneously coherent over the spatial extent of an organized structure. The apparent randomness of the flow field is, for the most part, due to the random size and strength of the different type of organized structures comprising that field.

In a wall-bounded flow, a multiplicity of coherent structures have been identified mostly through flow visualization experiments, although some important early discoveries have been made using correlation measurements (*eg*, Townsend, 1961; 1970; Bakewell and Lumley, 1967). Although the literature on this topic is vast, no research-community-wide consensus has been reached particularly on the issues of the origin of and interaction between the different structures, regeneration mechanisms, and Reynolds number effects. What follow are somewhat biased remarks addressing those issues. At times diverse view points will be presented but for the most part particular scenarios, which in the present authors' opinion are most likely to be true, will be emphasized. The interested reader is referred to the large number of review articles available (*eg*, Kovasznay, 1970; Laufer, 1975; Willmarth, 1975a; 1975b; Saffman, 1978; Cantwell, 1981; Fiedler, 1986; 1988; Blackwelder, 1988; Robinson, 1991). The last reference in particular summarizes many of the different, sometimes contradictory, conceptual models offered thus far by different research groups. Those models are aimed ultimately at

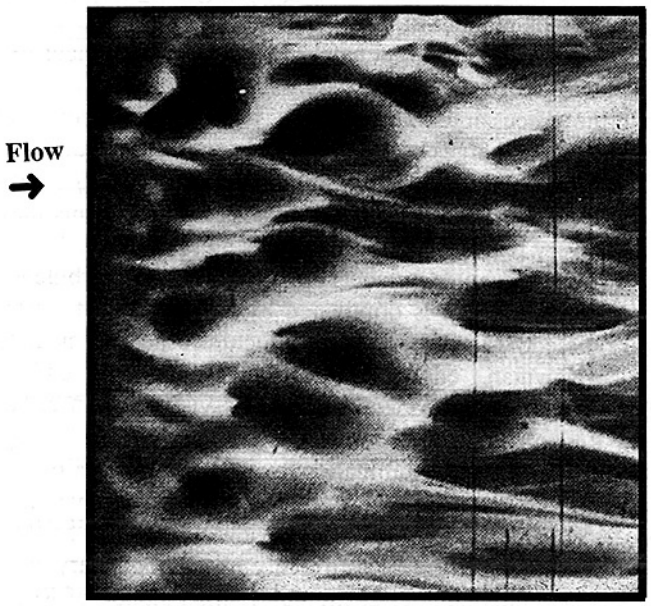

Fig 48. Top view of a low-Reynolds number turbulent boundary layer; Re_θ = 742. Wind tunnel experiment. Pockets, believed to be the fingerprints of typical eddies, are visualized using dense smoke (from Falco, 1980).

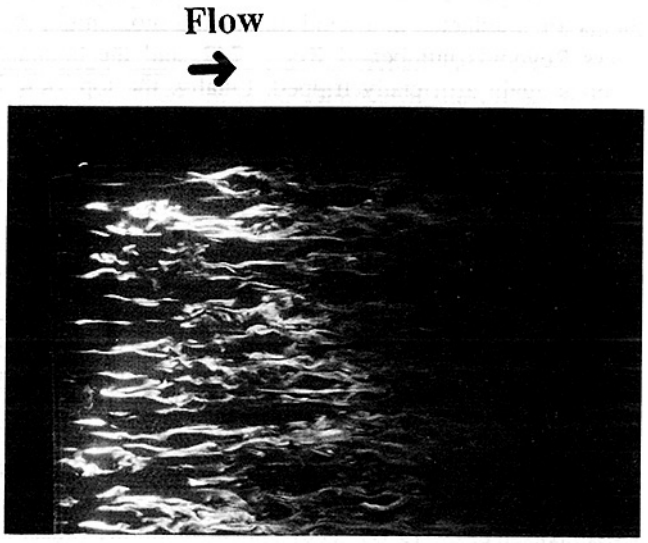

Fig 49. Top view of a low-Reynolds number turbulent boundary layer; Re_θ = 725. Flat plate towed in a water channel. Low-speed streaks are visualized using a sheet of laser and fluorescence dye (from Gad-el-Hak *et al*, 1984).

explaining how the turbulence maintains itself, and range from the speculative to the rigorous but none, unfortunately, is self-contained and complete. Furthermore, the structure research dwells largely on the kinematics of organized motion and little attention is given to the dynamics of the regeneration process.

7.1 Overview

With few exceptions, most of the available structural information on wall-bounded flows come from rather low-Reynolds number experiments and numerical simulations. Organized structures appear to be similar in all wall-bounded flows only in the inner layer. The outer region of a boundary layer is by necessity different from the core region of a pipe or channel flow. Before getting to the issue of Reynolds number effects, an overall view, whose source of information is predominately low-Reynolds number experiments, is first presented. As will become clear throughout the discussion following the present subsection, the picture that emerges at high Reynolds numbers is quite different, and structural information gleaned from low-Reynolds number physical and numerical experiments may not be very relevant to high-Reynolds number flows.

In (low-Reynolds number) external flows, the turbulence production process is dominated by three kinds of quasi-periodic eddies: the large outer structures, the intermediate Falco-Newman eddies,[12] and the near-wall eddies. Examples of these coherent structures visualized in rather low-Reynolds number boundary layers are depicted in Figs 47-49. Laser sheet illumination is used in all three photographs. The large eddies forming on a flat plate towed in a water channel are seen in the side view in Fig 47. The flow is from left to right. The artificially tripped boundary layer has a Reynolds number at the observation station of Re_θ = 725, and is marked with fluorescein dye. The smoke-filled boundary layer shown in top view in Fig 48 depicts the characteristic *pockets* believed to be induced by the motion of Falco-Newman eddies over the wall. In here, the experiments are conducted in a wind tunnel at a momentum thickness Reynolds number of Re_θ = 742, and the boundary layer is again artificially tripped. Finally, the top view in Fig 49 depicts the low-speed streaks in the near-wall region of the same turbulent boundary layer previously shown in side view in Fig 47. Flow direction is again from left to right.

The large, three-dimensional bulges (Fig 47) scale with the boundary layer thickness, δ, and extend across the entire layer (Kovasznay *et al*, 1970; Blackwelder and Kovasznay, 1972). These eddies control the dynamics of the boundary layer in the outer region, such as entrainment, turbulence production, etc. The large eddies are characterized by a sharp interface and a highly contorted surface which exhibits a significant amount of folding (Paiziz and Schwarz, 1974) and has a fractal dimension of close to 2.4 (Sreenivasan *et al*, 1989). They appear randomly (quasi-periodically) in space and time, and seem to be, at least for moderate Reynolds numbers, the residue of the transitional Emmons spots (Zilberman *et al*, 1977; Gad-el-Hak *et al*, 1981). Note, however, that at higher Reynolds numbers (Re_θ ~17,000) the very existence of the large eddy as an isolated coherent structure has been questioned by Head and Bandyopadhyay (1981), and this point will be revisited in Section 7.2.2.

The Falco-Newman eddies are also highly coherent and three-dimensional. Falco (1974; 1977) named them typical eddies because they appear in wakes, jets, Emmons spots, grid-generated turbulence, and boundary layers in zero, favorable and adverse pressure gradients. They have an intermediate scale of about 100 wall units. The Falco-Newman eddies appear to be an important link between the large structures and the near-wall events. In the plan view shown in Fig 48, smoke fills the near-wall region of a boundary layer and the roughly circular regions devoid of marked fluid are called pockets.[13] Falco (1980) asserts that these pockets are the *footprints* of some outer structures that induce fluid towards the wall. Robinson *et al* (1989) analyzed the data base generated from the direct numerical simulations of Spalart (1988). They concur that the pockets are the signature of local wall-ward motions, evidenced by spanwise divergence of streamlines, above regions of high wall-pressure. Low-pressure regions, on the other hand, occur along lines of converging streamlines associated with outward motion.

The third kind of eddies exists in the wall region ($0 \le y^+ \le 100$) where the Reynolds stress is produced in an intermittent fashion. Half of the total production of turbulence kinetic energy $-\overline{uv}\ (dU/dy)$ takes place near the wall in the first 5% of the boundary layer at typical laboratory Reynolds numbers (smaller fraction at higher Reynolds numbers), and the dominant sequence of intense organized motions there are collectively termed the bursting phenomenon. This dynamically significant process, identified during the 1960s by researchers at Stanford University (Kline and Runstadler, 1959; Runstadler *et al*, 1963; Kline *et al*, 1967; Kim *et al*, 1971; Offen and Kline, 1974; 1975), was reviewed by Willmarth (1975a) and Blackwelder (1978), and most recently by Robinson (1991).

Qualitatively, the process, according to at least one school of thought, begins with elongated, counter-rotating, streamwise vortices having diameters of approximately $40\nu/U_\tau$. This estimate for the diameter of the vortex is obtained from the conditionally averaged spanwise velocity profiles reported by Blackwelder and Eckelmann (1979). There is a distinction, however, between vorticity distribution and a vortex (Saffman and Baker, 1979; Robinson *et al*, 1989; Robinson, 1991), and the visualization results of Smith and Schwartz (1983) may indicate a much smaller diameter. In any case, the counter-rotating vortices exist in a strong shear and induce low- and high-speed regions between them. The vortices and the accompanying eddy

[12] Identified independently at about the same time by Falco (1974) and Newman (1974).

[13] These undulations are very similar to the so-called folds observed by Perry *et al.* (1981) in turbulent spots.

structures occur randomly in space and time. However, their appearance is sufficiently regular that an average spanwise wavelength of approximately 80 to $100\nu/U_\tau$ has been identified by Kline *et al* (1967) and others.

It might be instructive at this point to emphasize that the distribution of streak spacing is very broad. The standard of deviation is 30 - 40% of the more commonly quoted mean spacing between low-speed steaks of 100 wall units. Both the mean and standard deviation are roughly independent of Reynolds number in the rather limited range of reported measurements (Re_θ = 300-6500, see Smith and Metzler, 1983; Kim *et al*, 1987). Butler and Farrell (1993) have shown that the mean streak spacing of $100\nu/U_\tau$ is consistent with the notion that this is an optimal configuration for extracting "the most energy over an appropriate eddy turnover time." In their work, the streak spacing remains 100 wall units at Reynolds numbers, based on friction velocity and channel half-width, of a^+ = 180-360.

Kim *et al* (1971) observed that the low-speed regions (Fig 49) grow downstream, lift up and develop inflectional *U(y)* profiles. At approximately the same time, the interface between the low- and high-speed fluid begins to oscillate, apparently signaling the onset of a secondary instability. The low-speed region lifts up away from the wall as the oscillation amplitude increases, and then the flow rapidly breaks up into a completely chaotic motion. The streak oscillations commence at $y^+ \approx 10$, and the abrupt breakup takes place in the buffer layer although the ejected fluid reaches all the way to the logarithmic region. Since the breakup process occurs on a very short time scale, Kline *et al* (1967) called it a *burst*. Virtually all of the net production of turbulence kinetic energy in the near-wall region occurs during these bursts.

Corino and Brodkey (1969) showed that the low-speed regions are quite narrow, *ie*, $20\nu/U_\tau$, and may also have significant shear in the spanwise direction. They also indicated that the ejection phase of the bursting process is followed by a large-scale motion of upstream fluid that emanates from the outer region and cleanses (sweeps) the wall region of the previously ejected fluid. The sweep phase is, of course, required by the continuity equation and appears to scale with the outer-flow variables. The sweep event seems to stabilize the bursting site, in effect preparing it for a new cycle.

Considerably more has been learned about the bursting process during the last decade. For example, Falco (1980; 1983) has shown that when a typical eddy, which may be formed in part by ejected wall-layer fluid, moves over the wall it induces a high $u\upsilon$ sweep (positive u and negative υ). The wall region is continuously bombarded by *pockets* of high-speed fluid originating in the logarithmic and possibly the outer layers of the flow. These pockets appear to scale, at least in the limited Reynolds number range where they have been observed, Re_θ = O[1000], with wall variables and tend to promote and/or enhance the inflectional velocity profiles by increasing the instantaneous shear leading to a more rapidly growing instability. The relation between the pockets and the sweep events is not clear, but it seems that the former forms the highly irregular interface between the latter and the wall-region fluid. More recently, Klewicki *et al* (1994) conducted a four-wire hot-wire probe measurements in a low-Reynolds number canonical boundary layer to clarify the roles of velocity-spanwise vorticity field interactions regarding the near-wall turbulent stress production and transport.

Other significant experiments were conducted by Tiederman and his students (Donohue *et al*, 1972; Reischman and Tiederman, 1975; Oldaker and Tiederman, 1977; Tiederman *et al*, 1985) and Smith and his colleagues (Smith and Metzler, 1982; 1983; Smith and Schwartz, 1983). The first group conducted extensive studies of the near-wall region, particularly the viscous sublayer, of channels with Newtonian as well as drag-reducing non-Newtonian fluids. Smith's group, using a unique, two-camera, high-speed video system, was the first to indicate a symbiotic relationship between the occurrence of low-speed streaks and the formation of vortex loops in the near-wall region.

7.2 Open issues

There are at least four unresolved issues regarding coherent structures in wall-bounded flows, not all are necessarily independent: How does a particular structure originate; how do different structures, especially the ones having disparate scales, interact; how does the turbulence continue to regenerate itself; and does the Reynolds number affect the different structures in any profound way? The primary difficulty in trying to answer any of those queries stems from the existence of two scales in the flow that become rather disparate at large Reynolds numbers (Fig 2). The closely related issues of origin, inner/outer interaction and regeneration will be addressed in the following two subsections. Reynolds number effects on the coherent structures are reserved for the four subsections in Section 7.3.

7.2.1 Origin of different structures

Faced with the myriad of coherent structures existing in the boundary layer, a legitimate question is where do they all come from and which one is dynamically significant? Sreenivasan (1988) offers a glimpse of the difficulties associated with trying to answer this question. The structural description of a turbulent boundary layer may not be that complicated, however, and some of the observed structures might simply be a manifestation of the different aspects of a more basic coherent structure. For example, some researchers argue that the observed near-wall streamwise vortices and large eddies are, respectively, the legs and heads of the omnipresent hairpin vortices (Head and Bandyopadhyay, 1981). Nevertheless, that still leaves us with a minimum number of *building blocks* that must be dealt with.

If the large eddies are assumed to be dynamically significant, then how are they recreated? It is easy to argue that the conventional laminar-to-turbulent transition can not be responsible, because the same large eddies appear even in heavily tripped boundary layers where the usual transition routes are by-passed. Wall events can not be responsi-

ble for creating large eddies because of their extremely small relative scale at high Reynolds number. Furthermore, no hierarchical amalgamation of scales has been observed to justify such proposition.

If, alternatively, wall events are assumed to dominate, then where do the streamwise vortices or the low-speed streaks come from and what mechanism sustains the bursting cycle? Mechanisms that assume local instability can not be valid at large Reynolds numbers where the wall layer is, say, 0.1% of the boundary layer thickness,[14] and it is difficult to conceive that 99.9% of the boundary layer has no active role in the generation and maintenance of turbulence. On the other hand, assuming the bursting events are triggered by the large eddies brings us back to the original question of where do the latter come from.

The above difficulties explain the lack of a self-consistent model of the turbulent boundary layer, despite the enormous effort expended to establish one. None of the existing models is complete in the sense that none accounts for each aspect of the flow in relation to every other aspect. Developing a complete, self-consistent model is more than an academic exercise; for a proper conceptual model of the flow gives researchers the necessary tools to compute high-Reynolds number practical flows using the Reynolds-averaged Navier-Stokes equations and to devise novel flow control strategies as well as to extend known laboratory-scale control devices to field conditions.

7.2.2 Inner/outer interaction and regeneration mechanisms

There is no doubt that significant interactions between the inner and outer layers take place. On energy grounds alone, it is known that in the outer layer the dissipation is larger than the turbulence kinetic energy production (Townsend, 1976). It is therefore necessary for energy to be transported from the inner layer to the outer layer simply to sustain the latter. How that is accomplished and whether coherent structures are the only vehicle to transport energy is not clear, but two distinct schools of thought have emerged. In the first, the large-scale structures dominate and provide the strong buffeting necessary to maintain the low-Reynolds number turbulence in the viscous region ($Re \leq 30$). In the second view, rare, intense wall-events are assigned the active role and, through outward turbulent diffusion, provide the necessary energy supply to maintain the outer region. As mentioned in the previous subsection, both views have some loose ends.

Based on a large number of space-time two-point correlation measurements of u and υ, Kovasznay *et al* (1970) suggested that the outer region of a turbulent boundary layer is dominated by large eddies. The interface between the turbulent flow and the irrotational fluid outside the boundary layer is highly corrugated with a root-mean-square slope in the $(x\text{-}y)$-plane of roughly 0.5. The three-dimensional bulges are elongated in the streamwise direction with an aspect ratio of approximately 2:1, and have a characteristic dimension, in the wall-normal direction, of between 0.5δ and δ. They appear quasi-periodically and are roughly similar to each other. Kovasznay *et al* allowed that the large eddies are passive in the sense that the wall events and not these eddies are responsible for producing the Reynolds stress. Kovasznay (1970) advanced the hypothesis that wall bursting starts a chain reaction of some sort at all intermediate scales culminating into a sequence of amalgamations which eventually leads to the large structures. As mentioned earlier, such hierarchical amalgamation of scales has not been directly observed in the laboratory.

Head and Bandyopadhyay (1981), on the other hand, suggested that the very existence of the large eddies at high Reynolds numbers is in doubt. Their combined flow visualization/hot-wire probe experiments are unique in that an unusually large range of Reynolds number was investigated, Re_θ = 500-17,500, allowing them to clarify unambiguously Reynolds number effects on the structure of the boundary layer. Head and Bandyopadhyay maintained that a large structure seen in typical flow visualization experiments is nothing but the slow overturning of a random collection of smaller-scale hairpin vortices, just a few or even a single isolated vortex loop at low Reynolds numbers (say, $Re_\theta < 1000$) but a large number of them at high Reynolds numbers (say, $Re_\theta > 5000$). This is sketched for typical low- and high-Reynolds number boundary layers in Figs 50a and 50b, respectively. A brisker rate of rotation of the isolated (fat) vortex loop is observed at the lowest Reynolds number, consistent with prior observations of large eddies in low-speed experiments. The hairpins are inclined at around 45° to the plane of the flow over a major part of the layer thickness. In Head and Bandyopadhyay's (1981) view, the entire turbulent boundary layer consists very largely of vortex loops that become increasingly elongated as the Reynolds number increases (see Fig 3). The so-called large eddies, on the other hand, do not appear to exhibit any particular coherent motion beyond a relatively slow overturning or toppling due to shear.

Corroborative evidence for the hairpin angle of inclination of 45° comes from the simultaneous, multiple-point hot-wire measurements of Alving *et al* (1990) in both a canonical turbulent boundary layer and a boundary layer recovering from the effects of strong convex curvature. Their cross-correlation results are consistent with the observation of large-scale structures spanning the entire shear layer and inclined at angles in the range of 35°-45° near the outer edge of the boundary layer, but at continuously decreasing angles as the wall is approached.

The sketch in Fig 50b for a typical large eddy at high Reynolds number is consistent with the statistical findings of Brown and Thomas (1977), who have shown by using conditional averaging techniques that a typical large structure in a turbulent boundary layer has an upstream rotational/irrotational interface inclined at 18° to the flow direction. Head and Bandyopadhyay (1981) have observed such *individual* structures only at higher Re_θ (> 5000). It is possible to arrive precisely at this slope by modeling the large structure to be composed of hairpin vortices formed at

[14] This is the near-wall region of thickness $y = 30\nu/U_\tau$ as a percentage of the boundary layer thickness when the Reynolds number is $Re_\theta \approx 100{,}000$ (see Fig 6).

regular intervals (Bandyopadhyay, 1980). Such large structures composed of many hairpin vortices have not been observed in the low-Reynolds number DNS simulations.

Samples of Head and Bandyopadhyay's (1981) visualization experiments at three Reynolds numbers are depicted in Fig 51. A laser light sheet illuminates a section of the smoke-filled boundary layer making 45° with the downstream plane. The vortex loops seen in this figure at Re_θ = 600, 1700 and 9400 correspond roughly to the vortex loop, horseshoe vortex and hairpin vortex sketched previously in Fig 3 of the present paper. The increased elongation of the vortex loops as the Reynolds number increases over one order of magnitude is evident in the three photographs in Fig 51.

Robinson (1991) summarizes many of the conceptual models advanced by different researchers to explain how a wall-bounded turbulent flow maintains itself. Among those reviewed are the models advocated by Willmarth and Tu (1967), Black (1968), Offen and Kline (1975), Hinze (1975), Praturi and Brodkey (1978), Thomas and Bull (1983), Acarlar and Smith (1987a; 1987b), and Robinson (1990). Some of those conceptual models emphasize a particular aspect of the flow dynamics as for example the bursting cycle, while others are more ambitious and attempt to include both the inner and outer structures and their interaction.

Robinson (1991) also lists significant contributions that utilize structural information to predict statistical quantities or invoke a simplified form of the governing equations to model the dynamics of the near-wall turbulence-production process. Among the predictive models discussed are those by Landahl (1967; 1980; 1990), Townsend (1976), Perry and Chong (1982), Perry *et al* (1986; 1989), Walker and Herzog (1988), Aubry *et al* (1988), Hanratty (1989), and Berkooz *et al* (1991).

Other, potentially useful, predictive models not discussed by Robinson (1991) include those based on stability considerations (Malkus, 1956; 1979), based on the turbulence energy equation (Bradshaw *et al*, 1967), based on the u-v velocity-quadrant statistical description of the organized motions (Nagano and Tagawa, 1990), and based on a single hairpin-like vortex in a unit domain of turbulence production (Bandyopadhyay and Balasubramanian, 1993; 1994). These models account explicitly for Reynolds number effects and might, therefore, be useful for practical Reynolds numbers.

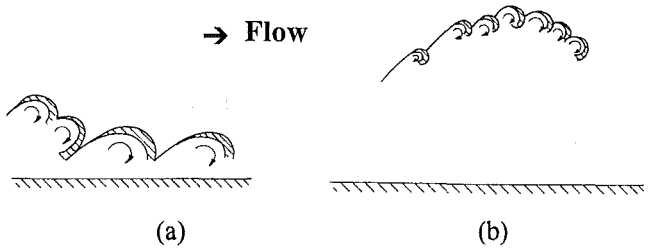

Fig 50. Sketch of large eddy structures as a collection of smaller-scale hairpin vortices (from Head and Bandyopadhyay, 1981): (a) Typical low-Reynolds number boundary layer; (b) Typical high-Reynolds number boundary layer.

Inevitably in almost all the conceptual models the omnipresent hairpin vortex (or horseshoe at low Re) plays a key role. Such a vortex has been proposed earlier by Theodorson (1952) on intuitive grounds as the primary structure responsible for turbulence production and dissipation in the boundary layer. His *tornado-like* vortices form astride near-wall, low-speed regions of fluid and grow outward with their heads inclined at 45° to the flow direction.

Black (1966; 1968) conducted a more rigorous analytical work to show the fundamental role of hairpin vortices in the dynamics of wall-bounded flows. His basic premise is that the primary role of the random turbulent motion is not to transfer mean momentum directly, but rather to excite strong, three-dimensional instability of the sublayer which is a *powerhouse* of vorticity. In Black's model, trains of discrete horseshoes are generated by repetitive, localized nonlinear instabilities within the viscous sublayer. The vortical structures are *shed* and outwardly migrate from the near-wall region in a characteristic, quasi-frozen spatial array.

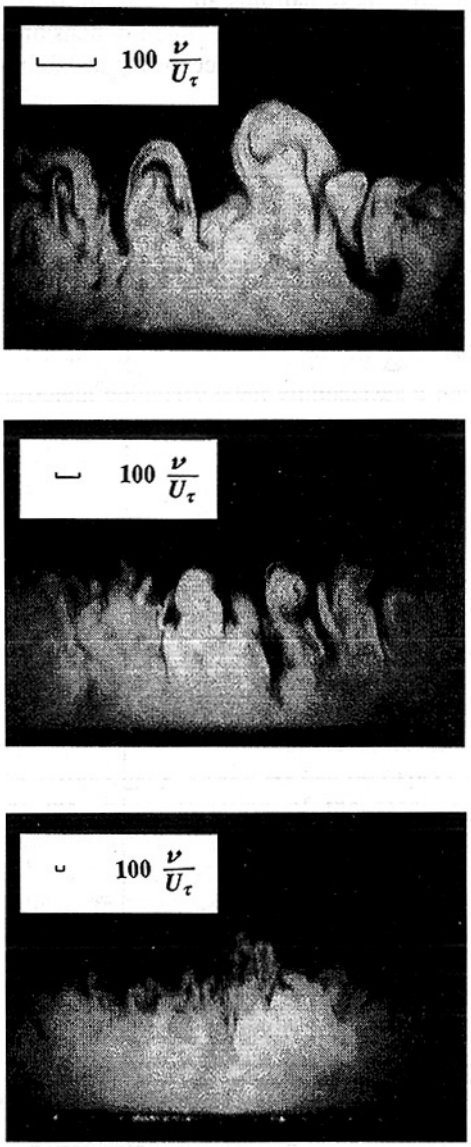

Fig 51. Hairpin structures in a smoke-filled turbulent boundary layer at three Reynolds numbers. Sheet of laser illuminates a section making 45° with downstream plane (from Head and Bandyopadhyay, 1981).

The horseshoes inviscidly induce an outflow of low-speed fluid from within the vortex loops, creating motions that would be seen by a stationary probe as sharp, intermittent spikes of Reynolds stress. Because of the continuous creation of new vortex loops that replace older elements, the lifetime of the vortical array is much longer than that for its individual members. According to Black (1968), such organized structures are responsible for the efficient mass and momentum transfer within a turbulent boundary layer.

Sreenivasan (1987) offers a similar model to that of Black (1968). The essential structures of the boundary layer, including the hairpin vortices, result from the instability of a *caricature* flow in which all the mean flow vorticity has been concentrated in a single fat sheet. Sreenivasan's conclusions were briefly discussed in Section 4 of the present article.

As a parting remark in this subsection, it might be instructive to recall that hairpin vortices play an important role also in the laminar-to-turbulent transition of boundary layer flows. Essentially, these hairpins are the result of the nonlinear tertiary instability of the three-dimensional peak/valley pattern which itself is the secondary instability of the primary Tollmien-Schlichting waves (Klebanoff *et al*, 1962).

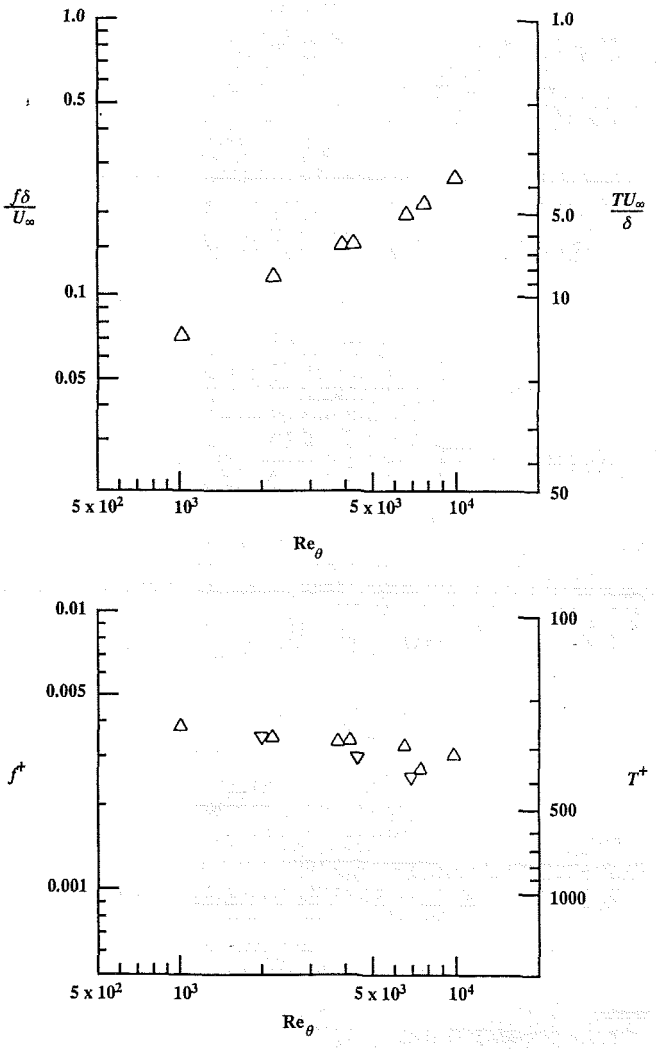

Fig 52. Mean bursting frequency versus Reynolds number (from Blackwelder and Haritonidis, 1983): (a) Outer-flow variables scaling; (b) Inner-flow variables scaling. The inverted triangles represent three additional data points from an untripped boundary layer.

7.3 Reynolds number effects

The last question to be discussed in this section relates to Reynolds number effects on the coherent structures in wall-bounded flows. There are several facets to that issue and the present section is divided into four subsections. To be addressed below are proper scaling for the period between bursts, possibility of profound structural changes after the well known Reynolds number limit of $Re_\theta = 6000$, small-structures existing in the outer layer, and Reynolds number effects on inner structures.

7.3.1 Bursting period

Because of the problems of threshold setting and probe resolution, bursting frequency and its scaling have become the source of continuing controversy. Cantwell (1981), based on a review of available literature, have concluded that this frequency scales on outer variables, thus establishing a strong link between the inner and outer regions of a wall-bounded flow. On the other hand, Blackwelder and Haritonidis (1983) have shown that the frequency of occurrence of these events scales with the viscous parameters consistent with the usual boundary layer scaling arguments. Their results obtained with a hot-wire probe whose length varied in the range of $\ell^+ = 4.5\text{-}20$[15] as the Reynolds number increased in the range of $Re_\theta = 1000\text{-}10{,}000$ are depicted in Fig 52. In Fig 52a, outer variables are used to normalize the bursting frequency (or its inverse, the period between bursts). The non-dimensional frequency increases with Reynolds number, thus clearly indicating that outer scaling is not applicable. On the other hand, the same data plotted in Fig 52b using the viscous time scale to normalize the frequency indicate the validity of inner scaling.[16] Thus, the properly non-dimensionalized bursting period is independent of the Reynolds number, in agreement with the observations of Kline *et al* (1967), Corino and Brodkey (1969), Donohue *et al* (1972), Achia and Thompson (1977), and Blackwelder and Eckelmann (1978). Blackwelder and Haritonidis (1983) have suggested that past erroneous results are caused by insufficient spatial resolution of the sensors used to detect the bursts.

Based on measurements in the atmospheric boundary layer where the Reynolds number is several orders of magnitude higher than in typical laboratory experiments, Narasimha and Kailas (1986; 1987; 1990) still maintain that bursting events scale on outer variables. To do otherwise, the insufficient time resolution of the atmospheric data would simply not have allowed the detection of any dynamically significant events. Narasimha and Kailas cite other laboratory experiments to support their position (*eg*,

[15] The upper end of this range might not provide sufficient probe resolution according to the criterion established earlier in the present paper.

[16] Three additional data points (inverted triangles) from an untripped boundary layer are also shown in Fig 52b.

Rao *et al*, 1977; Ueda and Hinze, 1975; Willmarth, 1975a; Shah and Antonia, 1989; Rajagopalan and Antonia, 1984).

Adding to the present confusion, Bandyopadhyay (1982) has shown that the bursting period is not a universal function and both inner and outer variables are involved in its scaling with Re_θ. He reviewed existing data and concluded that a universal value of the bursting frequency scaled with either inner or outer variables in various boundary layers ranging from relaminarized to separated does not exist. Since a turbulent boundary layer is characterized by three integral variables, C_f, H, and Re_θ, verification of universality with Re_θ alone is clearly inadequate, and the apparent confusion stems in part from the lack of experiments over a sufficiently wide range of shape factors H. Johansson and Alfredsson (1982) have also suggested that the bursting period scale with intermediate scaling proportional to the geometric mean of the inner and outer scales. It should be noted, however, that within the framework of an asymptotic theory mixed variables have little or no physical significance.

The arguments by both Blackwelder and Haritonidis (1983) and Narasimha and Kailas (1987) are compelling, and the issue of scaling of the bursting events must, for the moment at least, stay open. The laboratory experiments of the former group are well controlled but the range of Reynolds numbers and range of shape factors investigated are not large enough. The latter group experiments are conducted with sufficient probe resolution but the atmosphere can neither be controlled nor fully documented. Moreover, the effects of roughness on the scaling is simply not known. Controlled high-Reynolds number experiments using smooth walls and probes with sufficient resolution should settle the question.

7.3.2 High Reynolds number

Does the boundary layer structure change when $Re_\theta > 6x10^3$? The Reynolds number variations of due to Coles (1962) were reproduced in the present paper in Figs 13 and 14 up to values of $15x10^3$ and $50x10^3$, respectively. Fig 13 does suggest that an asymptotic state is reached approximately when $Re_\theta > 6x10^3$. But, the higher Reynolds number data in Fig 14 shows that beyond that limit, ΔU^+ drops, although very slowly compared to the rise rate for $Re_\theta < 6x10^3$. The gradual departure of ΔU^+ from the apparent low asymptote suggests that some new effects are appearing in the turbulence production process at approximately $Re_\theta > (6$ to $15)x10^3$. Experiments conducted in several different facilities are briefly described below and they show that profound changes in the coherent structures of different wall-bounded flows might indeed take place at very high Reynolds numbers.

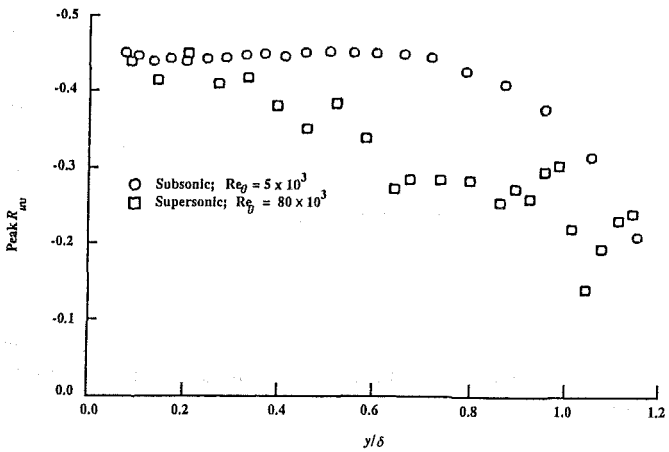

Fig 53. Comparison of the shear correlation coefficient in a high- and a low-Reynolds number boundary layers (from Smits, 1990).

Relevant to the issue of structural changes when $Re_\theta > 6x10^3$, is the recent assertion by Kailasnath (1993) that the skin friction, the pressure fluctuations and the mean-velocity profiles all show a distinct change of behavior at about the same Reynolds number. For example, a power-law fit to existing skin-friction data for both boundary layers and pipe flows[17] indicates a break point, at $Re_\theta \approx 5000$, that separates two ranges of Reynolds numbers. This and other evidence prompted Kailasnath (1993) to propose a *transitional* behavior for wall-bounded flows from a low- to a high-Reynolds number regime and to suggest further that the turbulence regeneration mechanism is different in the two regimes.

The results of Head and Bandyopadhyay (1981) discussed earlier indicate that the hairpin structures exhibit strong dependence on Reynolds number for $Re_\theta < 7000$, and hence the hairpins are atypical. At higher Reynolds numbers, on the other hand, the hairpin vortex is found unambiguously. In Head and Bandyopadhyay's view, Falco's (1977) *typical eddies* are merely the longitudinal cross-sections of the tips of the hairpins. Perry and Chong (1982) and Perry *et al* (1986) concur with this view. Their model of the turbulent boundary layer emphasizes a hierarchy of hairpin eddies as the essential structure of the outer region. In wavenumber space, the analogous idea of a hierarchy of interacting scales and energy transfer from large eddies to smaller ones is, of course, not new and has been proposed as early as 1920 by Richardson[18] and formalized by Kolmogorov (1941a).

Turbulent boundary layers ranging from relaminarized to separated cover the entire range of possible shape factor H. The statistical properties of the turbulent/irrotational fluid interface as well as the bursting period in such diverse layers can be described by H (Fiedler and Head, 1966; Bandyopadhyay, 1982). As can be expected, the location of the maximum deviation of the mean velocity from the logarithmic law also correlates with the mean location of the intermittent layer. Changes in the properties of the intermittent layer can take place when H drops below 1.3, that is approximately when $Re_\theta > 10x10^3$. This is supported by the flow visualization results of Head and Bandyopadhyay (1981) at $Re_\theta = 17.5x10^3$, which shows that the outer part of the boundary layer is noticeably sparser: fewer of the hair-

[17] The pipe Reynolds number based on its radius and the centerline velocity could be related to an equivalent Reynolds number based on the momentum thickness.

[18] Richardson's (1920; 1922) poetic description (widely recited but often misquoted) of the turbulent eddies within a cumulus cloud reads: Big whirls have little whirls that feed on their velocity, and little whirls have lesser whirls and so on to viscosity.

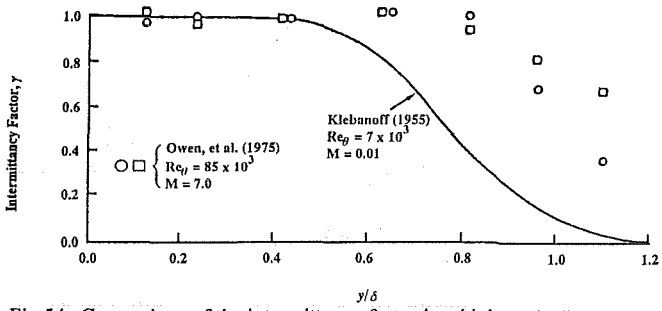

Fig 54. Comparison of the intermittency factor in a high- and a low-Reynolds number boundary layers (from Smits, 1990).

pin vortices reach δ although more of them are produced per unit (dimensional) wall area. Figure 53, which shows the variations of the shear correlation coefficient across a subsonic boundary layer and a supersonic one, seems also to echo that, as the Reynolds number is drastically increased, u- and v-fluctuations are not as well correlated in the outer layer. Note that the trends in this figure are primiraly due to changing the Reynolds number; the effect of varying the Mach number has already been accounted for by considering local fluid properties.

In high-speed, high-Reynolds number turbulent boundary layers, the mean location of the intermittent layer and its standard deviation change significantly according to the results of Owen *et al* (1975) at $M_\infty = 7.0$ and $Re_\theta = 85x10^3$. This is shown in Fig 54, where the supersonic data are compared to the low-Reynolds number, low-Mach number results of Klebanoff (1954). The intermittency profile for the supersonic boundary layer is clearly fuller. Furthermore, at these high Reynolds numbers, *the boundary layer structures do not exhibit much overturning motion which is typical of lower Reynolds numbers*. In the statistical measurements of conventional boundary layer properties at high Reynolds numbers these changes may not always seem dramatic, but their critical importance might lie in the efficiency of outer-layer or other control devices for drag reduction (Section 8.3.1).

Morrison *et al* (1971) compared the sublayer spectra, $P(k_z^+, \omega^+)$, at low- and high-Reynolds number pipe flows. Their results are depicted in Figs 55 and 56.[19] Over a sufficiently wide range of Reynolds numbers, the shape of the two-dimensional spectra expressed in wall-layer variables is not universal. This result contradicts the earlier low-Reynolds number, one- and two-dimensional spectral observations made by Bakewell and Lumley (1967) and Morrison (1969). *As the Reynolds number is increased from* Re_a = 10,000 to 100,000, more energy appears in the low-frequency, low-wavenumber region. The additional energy results from disturbances which convect at twice the characteristic velocity of the sublayer of $8U_\tau$. The high Reynolds numbers appear to have the effect of *randomizing* the phase velocity whereby the disturbances are no longer phase-correlated in the sublayer. This additional evidence also suggests much change in the turbulence production mechanism at very high Reynolds numbers. In fact, Morrison *et al* (1971) have strongly suggested that the low-speed streaks are unique to low-Reynolds number wall-bounded flows. Streaks would no longer appear at very high Reynolds numbers, where a phase-correlated, wave-like turbulence might not exist within the viscous sublayer.

Using a rake of X-wires and conditional averaging techniques, Antonia *et al* (1990) have examined the effects of Reynolds number on the topology of the large structures in the range $1360 \le Re_\theta \le 9630$. The instantaneous longitudinal sectional streamlines in a moving frame of reference contain many rotational structures O[$\delta/2$] at the lowest Reynolds number. Very significant Re_θ effects can be observed in the instantaneous frames (see their Fig 5). As Re_θ is gradually increased to 9630, the large rotational structures become much smaller and no longer dominate the outer layer. When the large structures are selectively sampled and averaged, their foci are found to be more circular at lower Reynolds numbers. As Re_θ is increased from 1360 to 9630, the location of the foci moves closer to the wall from 0.83δ to 0.78δ. This is consistent with the effect of Reynolds number on the mean location of the intermittent layer, for similar values of the shape factor H (Fiedler and Head, 1966).

7.3.3 Small structures in outer layer

In this subsection, a relation is developed relating the ratio of outer to inner scales to Reynolds number changes. Reynolds number effects on small structures existing in the outer layer are then discussed. Finally, brief remarks are made on vortex-vortex interaction in the outer region.

The boundary-layer thickness in wall units, δ^+,[20] is related to the Reynolds number Re_θ via the skin-friction coefficient and the ratio of boundary layer thickness to momentum thickness:

$$\delta^+ \equiv \frac{\delta U_\tau}{\nu} = \frac{U_\tau}{U_\infty} \cdot \frac{\delta}{\theta} \cdot Re_\theta \tag{35}$$

$$\delta^+ \equiv \left(\frac{C_f}{2}\right)^{\frac{1}{2}} \cdot \frac{\delta}{\theta} \cdot Re_\theta \tag{36}$$

For a smooth flat plate, an approximate empirical relation can be obtained by using the modified pipe resistance formula viz $c_f = 0.0296\ (Re_x)^{-1/5}$ and the $1/7^{th}$-power-law velocity profile. The ratio of the outer scale to inner scale is thus given by:

$$\delta^+ = 1.168\ (Re_\theta)^{0.875} \tag{37}$$

Figure 57, taken from Bandyopadhyay (1991), shows that Eq 37 describes the data over the entire Reynolds number range where measurements are available.

[19] Although the spectra in Fig 56 were measured outside the viscous sublayer (at $y^+ = 13.9$), Morrison *et al* (1971) argue that the energy distribution at the sublayer edge is not substantially different from the distribution within the viscous sublayer.

[20] The notation Re^* is also used as discussed in Section 3.

Falco (1977) used simultaneous hot-wire anemometry and flow visualization to measure the characteristic dimensions of the typical eddy in the outer region of a boundary layer (C_x and C_y; see insert in Fig 58). His conclusion is that while large eddies appear to be Reynolds number independent, the typical eddies do depend on the Reynolds number.

Figure 58, taken from Bandyopadhyay (1991), shows a compilation of data from widely different physical as well as numerical experiments. The emphasis is on Reynolds number effects on organized small scales in the outer layer. Equation 37 is used to rescale Bushnell *et al*'s (1975) compilation of the variation of the maximum mixing length (ℓ) with Reynolds number, shown by the shaded area in Fig 58. The streamwise and normal characteristic dimensions of the typical eddy, C_x and C_y, are obtained from Falco's (1977) experiments referenced above. This data is represented respectively by the broken and solid lines in Fig 58. Data for the Taylor's streamwise and normal micro-scales, λ_x and λ_y, are compiled by Falco (1974) and indicated here by the slanted dashes. Finally, the range of variation of the diameter, *d*, of the characteristic hairpin near the edge of the boundary layer is computed from Spalart's direct numerical simulations by Robinson (1990). This is indicated in Fig 58 at a single Reynolds number by the open circle and the *error bar*. The large variability of the vortex diameter in the simulations is intriguing. All scales are normalized with the appropriate boundary layer thickness, δ. At $Re_\theta > 10x10^3$, the characteristic size of all the organized small structures appear to asymptote to the value of the maximum mixing length:

$$\lambda_x/\delta \approx \lambda_y/\delta \approx C_x/\delta \approx C_y/\delta \approx (\ell/\delta)_{max} \qquad (38)$$

In the same range of Reynolds numbers, the above scales are probably also equal to λ_z/δ and C_z/δ. This does not necessarily imply an approach to isotropy, but rather that *x-y* and *x-z* sections of the same hairpin vortex are being observed.

Smits *et al* (1989) and Smits (1990) have compared a supersonic ($Re_\theta = 80x10^3$) and a subsonic ($Re_\theta = 5x10^3$) turbulent boundary layer, which comparison primarily reflects the effect of Re_θ and not M_∞ . In the high-Reynolds number flow, for $y/\delta > 0.25$, the peak value of the shear correlation coefficient $R_{u\upsilon}$ is lower than the corresponding value in the low-Reynolds number flow, for example by 40% at $y/\delta > 0.65$ (see Fig 53). Comparison of the probability density function shows that for $y/\delta > 0.25$, the vertical component of the Reynolds-stress-contributing motion is weaker in the Re_θ high case.

If the Reynolds-stress-production module is qualitatively unchanged, the drop in the coefficient $R_{u\upsilon}$, referred henceforth to the peak value, represents a disproportionate increase in the denominator. A large drop in the value of $R_{u\upsilon}$ could happen if the turbulence becomes partially stochastic whereby u and υ are decorrelated while the kinetic energy production continues to contribute to the rms values of u and υ. But since such a situation will come largely due to high-frequency components which do not have much energy, the decreased $R_{u\upsilon}$ must come from an increased contribution from the large scales which are energetic but are unable to produce turbulence. The growth, at higher Reynolds numbers, of an approximately flow-aligned, large-scale swirling motion in the cross-stream plane in the outer part of the boundary layer satisfies this requirement. Long time two-dimensionality requires that swirls of both signs be produced. The development of the swirl suggests an increase in the υ- and w-turbulence. Since the outer layer u-turbulence intensity in supersonic boundary layers still scales with y/δ exactly as at low Re_θ

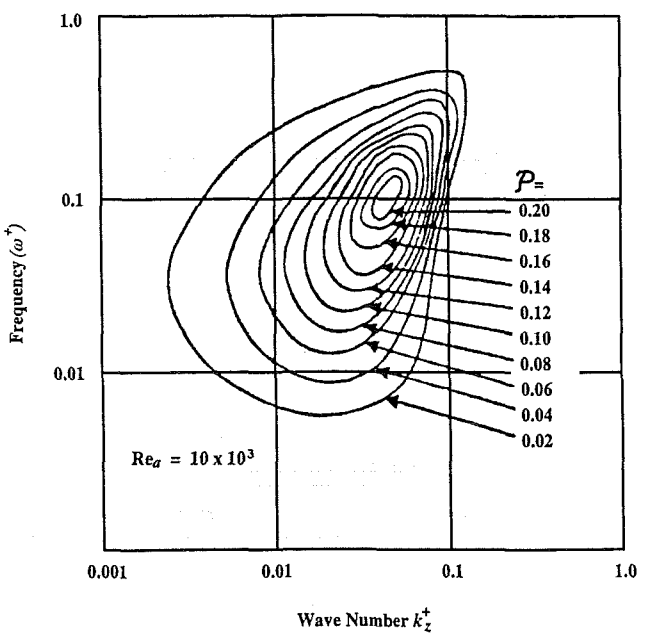

Fig 55. Two-dimensional spectra $P(k_z^+, \omega^+)$ for Re_a = 10,000; y^+ = 1.56 (from Morrison *et al*, 1971).

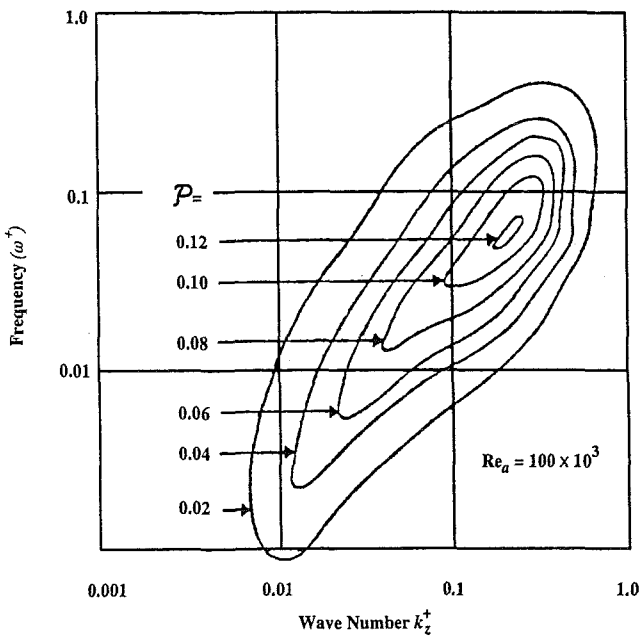

Fig 56. Two-dimensional spectra $P(k_z^+, \omega^+)$ for Re_a = 100,000; y^+ = 13.9 (from Morrison *et al*, 1971).

(Smits 1990), the lower $R_{u\upsilon}$ is attributable to increased υ-turbulence only. Accordingly, in the cross-stream plane, the υ- and w- motions must be correlated over distances O[δ] at high Reynolds numbers. With increasing Reynolds numbers, the vortex-vortex interactions in intra- and inter-hairpin vortices could lead to the formation of such new scales described as double helix and tornadoes, respectively, in Bandyopadhyay (1989).

The sequence of photographs in Fig 59 shows that double-helix spiraling of a hairpin vortex in a turbulent boundary layer can indeed take place. The smoke-filled flow is illuminated with a sheet of laser inclined upstream at 45° to the flow direction, and the Reynolds number is approximately $Re_\theta = 600$. At this low Reynolds number, a typical vortex loop has a relatively low aspect ratio and vortex stretching is not pronounced. Nevertheless, the photographs in Fig 59 adequately illustrate the phenomenon. Increased vortex stretching and vortex-vortex interaction could cause a hairpin vortex to first spiral around itself into a double helix and then onto further spiraling between neighboring double helixes. The process contributes to crinkling and increase in surface area of the vorticity layer. The hierarchies of spiraling leading to many miniature tornadoes continues as long as they contribute to enstrophy amplification. These special behaviors become more pronounced as the Reynolds number is increased. As the double helix crosses the static light plane, the cross-section moves wall-wards and the direction of the inner induced-flow rotates. In this example, the maximum vortex diameter happens to be the same as the maximum mixing length and it decreases in size both as $y \to 0$ and $y \to \delta$.

7.3.4 Inner structures

In this subsection, Reynolds number effects on the inner structures are discussed. It will be argued that vortex stretching is enhanced at higher Reynolds numbers, and that the low-speed streaks, commonly observed in low-Reynolds number experiments, might become less important at higher speeds.

Wei and Willmarth (1989) have argued that in turbulent channel flow literature where an inner-layer scaling has been claimed to hold errors have crept into measurements which are ascribable to large invasive probes, and that sometimes small but systematic variations with Reynolds number have been overlooked because such a scaling was assumed *a priori*. Their measurements, described previously in Section 6 of the present article, show that u_{rms}/U_τ turbulence intensity scales on inner variables only up to $y^+ \approx 10$ which is well inside the inner region. The υ_{rms}/U_τ turbulence intensity and the Reynolds shear stress $-\overline{u\upsilon}/U_\tau^2$ distributions do not scale on inner variables anywhere in the channel. Interestingly, the maximum normalized Reynolds stress and normal turbulence intensity increase with Reynolds number. This they attributed to the enhancement of the vortex-stretching mechanism in the inner region with increasing Reynolds number.

Since the Reynolds number Re_a or Re_θ is a dimensionless grouping of outer variables, failure of the turbulence quantities in the inner region to scale only on inner variables is an indication that the dynamics of the inner region structure are affected by outer as well as inner variables. Wei and Willmarth argue that these Reynolds-number dependencies are caused by *changes in the coherent structure of the turbulence close to the wall,* and that the turbulent

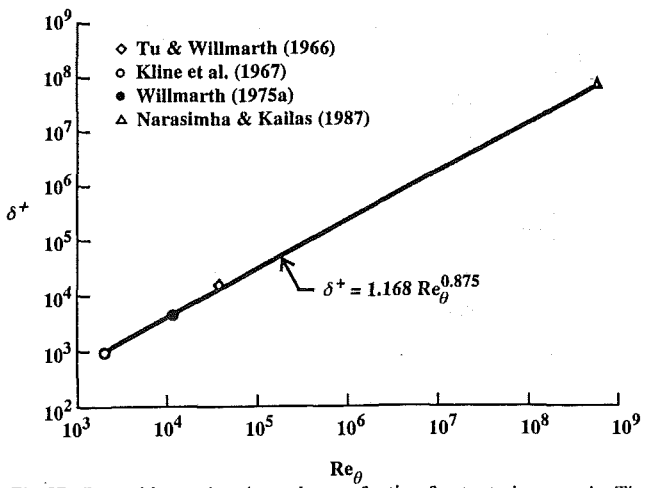

Fig 57. Reynolds number dependence of ratio of outer to inner scale. The straight line is computed from modified pipe resistence formula and power-law mean-velocity profile. Data compiled by Bandyopadhyay (1991) from different experiments.

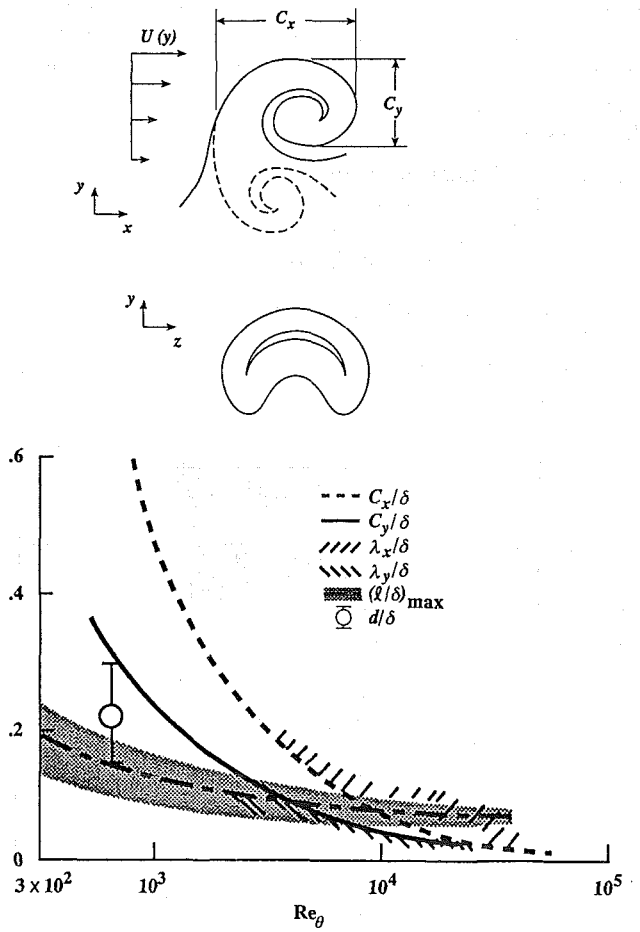

Fig 58. Reynolds number variation of maximum mixing length, typical eddy and Taylor's micro-scale lengths. The single data point in the figure indicates range of hairpin diameters detected at edge of directly simulated boundary layer. The curves are fairings of experimental results. Data compiled by Bandyopadhyay (1991).

flow structure at high Reynolds number near solid boundaries, *ie* the hairpin vortex structure and interactions, will differ significantly from lower-Reynolds number inner structures.

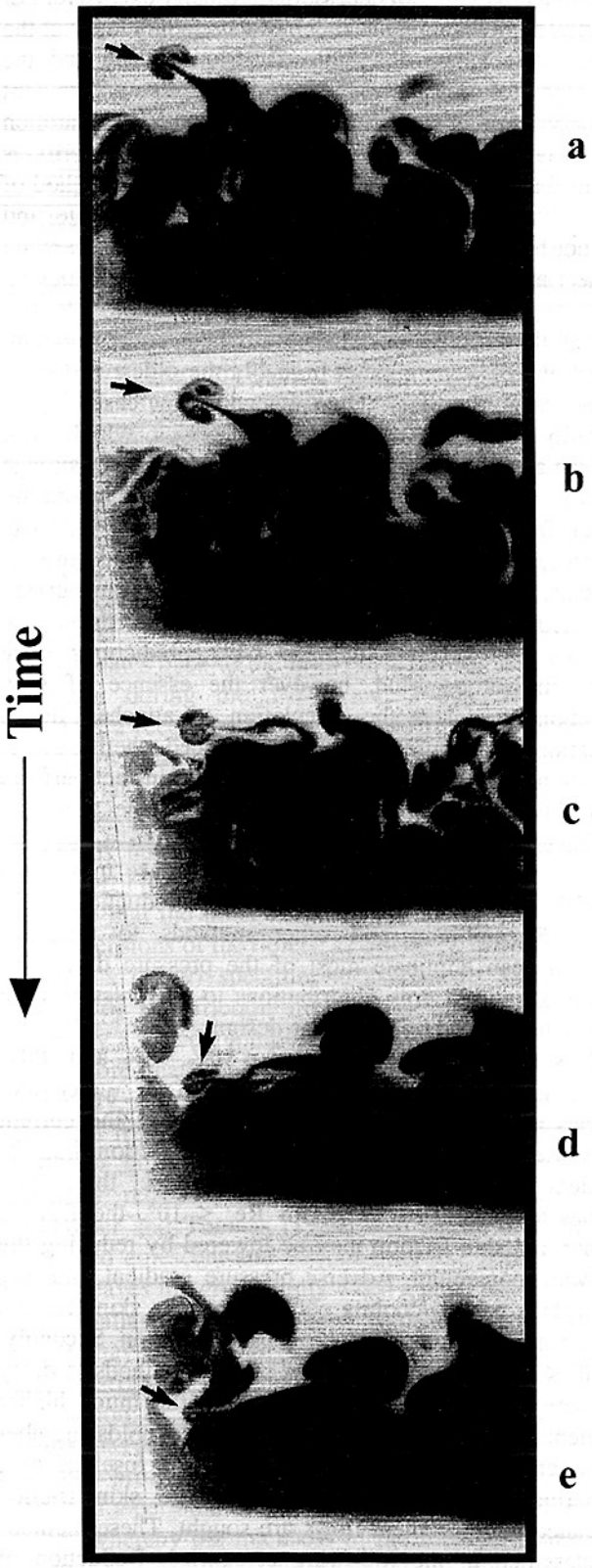

Fig 59. Smoke-filled turbulent boundary layer illuminated using a laser sheet inclined upstream at 45° to flow direction. Arrows in sequence of four photographs show double-helix spiraling of a hairpin vortex (from Bandyopadhyay, 1989).

Morrison *et al* (1971) have studied the organized motion in the sublayer region of a pipe flow. As discussed in Section 7.3.2, they have measured the two-dimensional frequency-wavenumber spectra of the longitudinal velocity fluctuations at $10.6\text{x}10^3 \le \text{Re}_a \le 96.5\text{x}10^3$. An appeal of this data lies in its long-time averaged statistical nature and the absence of any troublesome subjective threshold setting as used in VITA or VISA techniques. For $\text{Re}_a < 30\text{x}10^3$, the streamwise phase velocity c_x^+ in the sublayer is independent of wavenumber and remains a constant throughout the sublayer. Since this constant velocity co-ordinates the phase of the periodic motions at different wall-normal locations, Morrison *et al* concluded that the sublayer turbulence is wave-like and in fact at low Reynolds numbers it is likely that the sublayer consists of relatively periodic waves.

The critical-layer height is estimated to be $9\nu/U_\tau$ because at that location the average fluid velocity equals $c_x^+ = 8$. At $\text{Re}_a < \text{Re}_c = 30\text{x}10^3$, the characteristic spanwise wavelength λ_z^+ of 135 agrees with Kline *et al*'s (1967) streak-spacing estimate of 130. However, for $\text{Re}_a > \text{Re}_c$, the frequency-wavenumber spectra for the laterally spaced points loose their universal shape and the relative amount of low-frequency, low-wavenumber $\left(k_z^+\right)$ energy increases with Reynolds numbers (see Figs 55 and 56). This additional energy which becomes significant at higher Reynolds numbers results from disturbances which convect at velocities much greater (the average being $16U_\tau$) than the characteristic sublayer velocity of $8U_\tau$. This led Morrison *et al* (1971) to conclude that at higher Reynolds numbers, the character of the sublayer will be substantially altered, with an increasing amount of low-frequency, low-wavenumber energy being introduced. The disturbances responsible for this additional energy have propagation velocities much

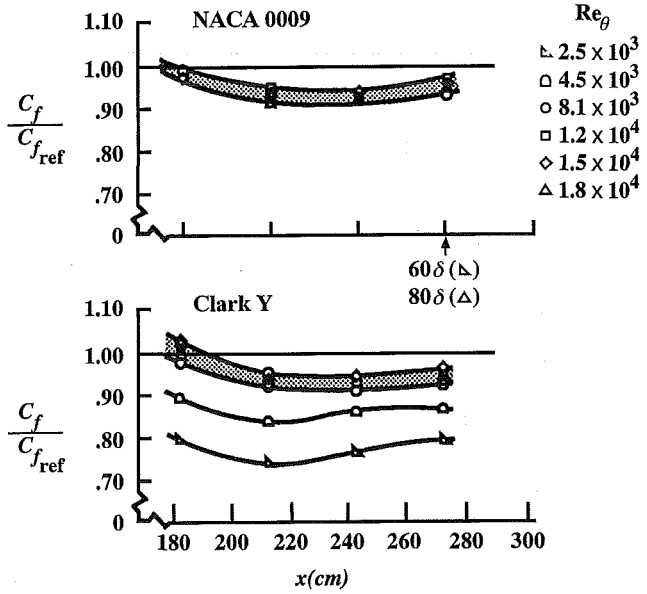

Fig 60. Reynolds number effects on viscous drag reduction due to OLD for $2500 \le \text{Re}_\theta \le 18{,}000$ (from Anders, 1990a).

larger than that which characterizes the sublayer at low Reynolds numbers. The "streaky" structure which has been assumed to be characteristic of the sublayer will become less important as the Reynolds number is increased and it is probable that the "streaks" may not be apparent at all at sufficiently large values.

By trial and error, Walsh (1990) has optimized the dimensions of drag reducing V-groove riblets ($h^+ = s^+ = 12$, where h and s are the riblet height and spanwise spacing, respectively) at low Reynolds numbers ($Re_\theta < 6\times10^3$). The value of s^+ does not scale with the spanwise mean-streak-spacing λ_z^+ (≈ 100). The findings of Walsh *et al* (1989) and Walsh (1990) that the riblet performance does not change at transonic speeds and high Reynolds numbers ($M_\infty = 0.7$; $20\text{x}10^3 \leq Re_\theta \leq 50\text{x}10^3$) does not, therefore, invalidate Morrison *et al*'s (1971) conclusion that the low-speed streaks will gradually become unimportant at high Reynolds numbers.

Grass (1971) investigated the nature of inner/outer interaction in smooth as well as rough wall-bounded flows. He maintains that the essential features of this interaction do not change despite the presence of three-dimensional roughness elements that protrude as much as 80 wall units into the inner layer, well outside the viscous region. Since low-speed streaks are not observed on walls with three-dimensional roughness, Grass' results minimize the importance of the streaks in the maintenance of turbulence.

A related issue is the importance of the intense but rare bursting events at high Reynolds numbers. A partial answer is given by Kailasnath (1993) who used a statistical approach to obtain useful information on the structure of the instantaneous momentum flux, thus sidestepping analysis conditioned on specific episodes and focusing instead on the contribution to the momentum flux associated with various magnitudes of velocity fluctuations. Kailasnath's non-episodic approach reveals that the contribution to the flux is dominated by medium amplitude velocity fluctuations in the range of $\pm 1.5u'$, which are not rare events. This implies a diminishing importance of the rare, intense events taking place in a progressively shrinking near-wall region as the Reynolds number increases.

8. FLOW CONTROL

8.1 Introductory remarks

The ability to actively or passively manipulate a flow field to effect a desired change is of immense technological importance. The term boundary layer control includes any mechanism or process through which the boundary layer of a fluid flow is made to behave differently than it normally would were the flow developing naturally along a smooth flat surface. The topic has been reviewed by, among others, Bushnell (1983), Bandyopadhyay (1986b), Wilkinson *et al* (1988), Bushnell and McGinley (1989), Gad-el-Hak (1989; 1990; 1993), Bushnell and Hefner (1990), Fiedler and Fernholz (1990), and Gad-el-Hak and Bushnell (1991). A boundary layer could be manipulated to achieve transition delay, separation postponement, lift enhancement, drag reduction, turbulence augmentation, or noise suppression. These objectives are not necessarily mutually exclusive. For example, by maintaining as much of a boundary layer in the laminar state as possible, the skin-friction drag and the flow-generated noise are reduced. However, a turbulent boundary layer is in general more resistant to separation than a laminar one. By preventing separation, lift is enhanced and the form drag is reduced. An ideal method of control that is simple, inexpensive to build and operate, and does not have any trade-off does not exist, and the skilled engineer has to make continuous compromises to achieve a particular goal.

Of all the various types of shear flow control now extant, control of flow separation is probably the oldest and most economically important. The tremendous increases in the capability of computational fluid dynamics, which have occurred as a direct result of increases in computer storage capacity and speed, are transforming flow separation control from an empirical art to a predictive science. Control techniques such as mitigation of imposed pressure gradients, blowing and suction are all readily parameterized via viscous CFD. Current inaccuracies in turbulence modeling can severely degrade CFD predictions once separation has occurred, however the essence of flow separation control is the calculation of attached flows, estimation of separation location, and indeed whether or not separation will occur, tasks which CFD can in fact perform reasonably well within the uncertainties of the transition location estimation.

Techniques to reduce the pressure drag are more well established than turbulent skin-friction reduction techniques. Streamlining and other methods to postpone separation can eliminate most of the pressure drag. The wave and induced drag contributions to the pressure drag can also be reduced by geometric design.

The skin friction constitutes about 50%, 90%, and 100% of the total drag on commercial aircraft, underwater vehicles and pipelines, respectively. Most of the current research effort concerns reduction of skin-friction drag for turbulent boundary layers. For that purpose, three flow regimes are identified. First, for $Re_x < 10^6$, the flow is laminar and skin friction may be lowered by reducing the near-wall momentum. Adverse pressure gradient, blowing and surface heating/cooling could lower the skin friction, but increase the risk of transition and separation. Secondly, for $10^6 < Re_x < 4\text{x}10^7$, active and passive methods to delay transition could be used, thus avoiding the much higher turbulent flow drag. Thirdly, at the Reynolds number encountered after the first few meters of a fuselage or a submarine, methods to reduce the large skin friction associated with turbulent flows are sought. These methods are classified in the following categories: Reduction of near-wall momentum; introduction of foreign substance; geometrical modification; relaminarization; and synergism.

The second category above leads to the most impressive results. Introduction of small concentration of polymers, surfactants, particles or fibers into a turbulent boundary layer leads to a reduction in the skin-friction coefficient of as much as 80%. Recently introduced techniques mostly fall under the third category above and seem to offer more modest net drag reduction. These methods are, however, still in the research stage and include riblets (~8%), large eddy breakup devices (or outer-layer devices, OLD) (~20%), and convex surfaces (~20%).

The knowledge of the Reynolds number effects is useful to flow control. This is because experimental investigations at low Reynolds numbers, *ie* lower speeds and/or smaller length scales, are less expensive. Most flow control devices are, therefore, developed and tested at rather low Reynolds numbers, say $Re_\theta = 1000$. Extrapolation to field conditions is not always straightforward though, and it often comes to grief. While the riblets results seem to extrapolate favorably to field conditions, the verdict on OLD is disappointing. These points will be discussed in Sections 8.2 and 8.3.

8.2 Riblets

Properly optimized, longitudinally grooved surfaces, called riblets, could lead to a modest skin-friction drag reduction, in the range of 5-10%, in turbulent boundary layers. The subject dates back to the mid 1960s but has attracted much attention during the 1970s and 1980s. Walsh (1990) provides a recent up-to-date review. The exact mechanism through which riblets achieve net drag reduction despite the substantial increase in wetted surface area is still controversial. For the present purpose, however, the issue of Reynolds number effects on riblets performance is more pertinent. Flight tests and transonic tunnel experiments all indicate that the inner variables are the proper scaling for the dimensions of the riblets, as discussed in Section 7.3.4.

Choi's (1989) spectrum measurements show that the energy of skin-friction fluctuations in the riblet groove drops by a decade compared to that of the smooth surface over more than a decade of the flow frequency range. Typically, over time expressed in wall units of $\ell^+ = 170$, the skin friction in the groove can remain below average and at a quiescent state as if the fluid in the groove is partially relaminarized. The dye flow visualization of Gallagher and Thomas (1984) also shows that the tracer remained quiescent and viscous-pool like between the ribs and it leaves the groove only when a burst passes overhead. Like Gallagher and Thomas, Narasimha and Liepmann (1988) have also suggested that the riblets create pools of slow viscous flow in the valleys, and thereby modify the interaction of the wall flow with the outer flow. Black (1968) has analytically described the dynamics of the mean-velocity profile of a canonical turbulent boundary layer in terms of a periodic competition between the wall and outer layers whereby the thickness of the sublayer changes with phase. The maximum thickness of the sublayer that the outer layer will allow can be obtained from the extrapolation of the log law to the sublayer profile. Consider the equality:

$$U^+ = y^+ = 2.41 \ln(y^+) + 5.4 \tag{39}$$

This is given by $y^+ = 11$, which is nearly the same as the optimized riblet height.

In a recent paper, Choi *et al* (1993) used direct numerical simulations to study the turbulent flow over a riblet-mounted surface. Quadrant analysis indicates that drag-reducing riblets mitigate the positive Reynolds-shear-stress-producing events. Choi *et al* suggest that riblets with sufficiently small spacing reduce viscous drag by restricting the location of the streamwise vortices above the wetted surface such that only a limited area of the riblets is exposed to the downwash of high-speed fluid induced by these vortices (see also the corroborating numerical results of Kravchenko *et al*, 1993).

Once it is accepted that the riblet performance is unrelated to streaks, it comes as no surprise that sand-grain roughness also has a drag-reducing behavior exactly like riblets. Tani (1987; 1988) has reanalyzed Nikuradse's (1933) experimental data on sand-grain roughness and has shown that its performance also changes from drag reducing to drag increasing with increasing h^+, where h is the characteristic roughness height. The skin friction remains lower than that of the smooth wall for $h^+ < 6$. Compared to the optimized riblets, the drag reduction is lower in magnitude, but is still of the same order. Tani has also suggested that the mechanism of drag reduction is likely to originate in the nearly quiescent regions of the flow within the interstices of the roughness elements, as observable deep within riblets.

Grass (1971) has shown in a channel flow that the inrush and outrush phases of the production cycle are also present when the wall has a three-dimensional roughness. Note, however, that walls with three-dimensional roughness elements do not have smooth, wave-like low-speed streaks, and although the outer-layer structure is similar to that in a smooth wall, the near-wall stress flux has a different behavior (Bandyopadhyay and Watson, 1988).

8.3 Recovery response

There are at least two modes of interaction between the inner and outer regions of a boundary layer. In the first, the outer structures obtain at least part of their energy by convection and turbulent transport from the inner region of the upstream part of the boundary layer. This view is supported by the near-constancy of the ratio between turbulence stress and twice the turbulence kinetic energy, $-\overline{uv}/\overline{q^2}$, across a major portion of the boundary layer. This is true even in the wake region, *ie*, $y/\delta \geq 0.2$, where both the Reynolds stress and the rms velocity fluctuations are rapidly decreasing. According to Townsend (1976), the turbulent fluid in that region has been sheared sufficiently long to attain its equilibrium structure. The second mode of inner/outer interaction involves the pressure effects of the inactive motion. Compared to the convective mode, the pressure mode is much less extended in the streamwise direction. In other words, the first mode points towards long

memory while the second is associated with short memory. This may be relevant to the performance of different control devices as discussed in the following two subsections.

8.3.1 Disturbances in outer layer

The long memory associated with the outer structure dependence on upstream conditions contrasts the short memory of the inner region. This was demonstrated by Clauser (1956) who has shown that in a turbulent boundary layer at a given Reynolds number, disturbances survive much longer in the outer layer ($y/\delta > 0.2$) than in the inner layer. He demonstrated this by placing a circular rod in the outer and inner regions of a fully-developed wall layer. For the rod placed at $y/\delta = 0.16$, the decay of the maximum deviation of the distorted mean-velocity profile from the equilibrium value was reduced to half of its initial value at a downstream distance of 2δ. In contrast, the outer-layer rod at $y/\delta = 0.6$ caused a distortion in the velocity profile that lasted four times longer, 8δ, and that did not completely disappear even at 16δ downstream of the rod (see Fig 13 of Clauser's article). Note that Clauser (1956) compared the response of the inner and outer layers at a low Reynolds number and did not consider any Reynolds number effect. Incidentally, some consider Clauser's demonstration as the predecessor of the modern day drag-reduction experiments employing modifications to the outer layer (Bushnell and Hefner, 1990).

In viscous drag reduction techniques where a device drag penalty is involved, as with outer-layer devices (OLD), a recovery length ~100δ is desirable to achieve a net gain. To date, drag reduction has been achieved only at low Reynolds numbers, $Re_\theta < 6x10^3$ (Anders, 1990a). However, when Anders examined his outer-layer devices at higher Reynolds numbers, to his surprise, the drag reduction performance was reduced and the device was no longer a viable candidate for viscous drag reduction. Anders' measurements in the range of Reynolds numbers of $2500 \leq Re_\theta \leq 18{,}000$ are depicted in Fig 60. The experiments were conducted by towing a slender, axisymmetric body in a water channel. The outer-layer device used in Fig 60a consists of two NACA-0009 airfoil-section rings placed in tandem 1.5 m downstream of the nose of the 3.7-meter-long body. The second device used in Fig 60b consists of two Clark Y low-Reynolds number airfoil-section rings, again placed in tandem. Both devices were optimized to yield lowest skin friction downstream. The figure depicts the downstream trends of the local skin friction, normalized with the skin friction at the same location but without the OLD.

Although both devices used by Anders (1990a) consistently lead to lower skin friction at all Reynolds numbers tested, net drag will, of course, be increased by the device drag penalty. This penalty depends on, among other factors, the thickness and angle of attack of the device, whether the boundary layer on the device itself is laminar, transitional or turbulent, and the presence and extent of any separation bubble that might form on the outer-layer ribbon/airfoil. Anders (1990a) reports a very modest net drag reduction for his airfoil devices of around 2% at the lowest Reynolds number but a net drag increase of 1-5% at higher Reynolds numbers.

Bandyopadhyay (1986a) used a large-area drag balance to investigate systematically the Reynolds number effects on both single- and tandem-ribbon devices. His Reynolds number range of $1300 \leq Re_\theta \leq 3600$ ($5x10^5 \leq Re_L \leq 1.8x10^6$) is lower than that of Anders' (1990a) but the loss-of-performance trends are the same as shown in Fig 61. In here, the net drag reduction as a percentage of the reference drag is plotted as a function of Reynolds number, Re_L, based on the freestream speed and the total length of the flat plate. Note that the drag penalty for the thin-ribbon devices used by Bandyopadhyay should be far smaller than that for the airfoil devices used by Anders. We conclude that for both low Re_θ ($< 6x10^3$) and high Re_θ ($> 6x10^3$), the effectiveness of OLD diminishes with the increase of Reynolds number.

The continued drop in the skin-friction reduction with Reynolds number comes as a surprise because the mean flow analysis of Coles (1962) indicates an asymptotic state of the outer layer to have been reached above $Re_\theta > 6x10^3$. The slow drop in ΔU^+ does not start until $Re_\theta > 15{,}000$ (see Figs 13 and 14). Anders (1990a) attributed the irreproducibility of the low-Reynolds number behavior at higher values to a significant change in the turbulence structure at higher Re_θ as discussed by Head and Bandyopadhyay (1981). The structural changes as the Reynolds number increases provide a simple explanation for the performance deterioration of outer-layer devices. These devices presumably work by selectively suppressing the normal velocity fluctuations and thus *decorrelating* the streamwise and normal velocities. As discussed in Section 7, at high Reynolds numbers, fewer hairpin vortices reach the edge of the boundary layer because of increased interactions among these vortices. The overturning motion of the large eddies observed at low Reynolds numbers is less at higher Reynolds numbers, which reduces the υ-turbulence suppression role for the OLD.

8.3.2 Disturbances close to wall

It is clear from the preceding subsection that knowledge of Reynolds number effects on the mean turbulent flow alone

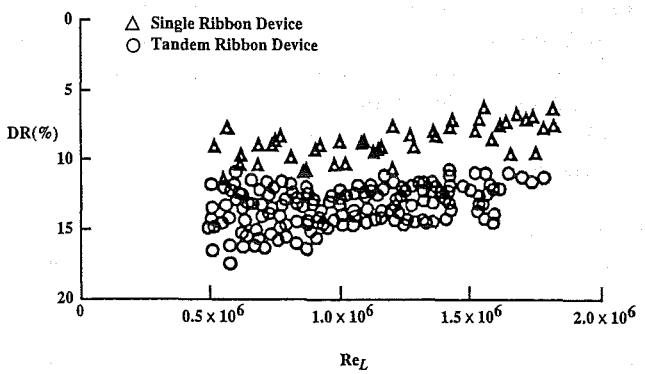

Fig 61. Large-area drag balance measurements showing Reynolds number effects on viscous drag reduction due to outer layer devices for $1300 \leq Re_\theta \leq 3600$ (from Bandyopadhyay, 1986a).

does not allow one to address all practical problems. This can be further demonstrated in the post-transition unexpected result alluded to in Section 2.3. Klebanoff and Diehl (1952) have made measurements on artificially thickened boundary layers at zero pressure gradient. The first 60 cm of their splitter plate was covered with No. 16 floor sanding paper. The measurements were carried out over a length of 320 cm at freestream velocities of 11, 17 and 33 m/s, giving three ranges of Reynolds numbers and producing a maximum Re_θ of 14,850. The Reynolds number Re_θ at the end of the sand roughness (at x = 60 cm) was 2640, 4050, and 7990 at the three above mentioned speeds, respectively. Figure 62 shows the recovery response of the turbulent boundary layer to the same wall disturbance (meaning the same sand roughness) at the three different reference Reynolds numbers (that is freestream speeds). One normally expects the recovery from wall disturbances to be the quickest (in x) at the highest Reynolds numbers. Therefore, it comes as a surprise that, in contrary, the return to the apparent "equilibrium" state (given by the broken line in Fig 62) is clearly slowed down as the reference Reynolds number is increased and not decreased! Note that at U_∞ = 33 m/s, δ = 2.54 cm at x = 60 cm, that is immediately after the sand roughness. Figure 62 shows that even at the last station where x = 320 cm and $\Delta x/\delta$ = 100, the recovery is not yet complete. The recovery length in the figure for an incoming Re_θ of about $8x10^3$ for the near-wall disturbance case is similar to the *outer-layer* disturbance case shown in Fig 60 at a similar Reynolds number. This puzzling behavior leads to the question: *why are the near-wall transition-trip disturbances surviving even beyond an x/δ of 100 at such high Reynolds numbers as* $15x10^3$ *much like it is known for outer-layer devices at much lower Reynolds numbers?* This question is clearly important to model testing in wind tunnels and code validation data, where roughness is used to trip and thicken the boundary layer to simulate high Reynolds numbers or flight conditions (Bushnell *et al*, 1993).

8.4 Control of high-Reynolds number flows

The above discussion indicates that post-transition memory is longer at higher Reynolds numbers for certain trips. Wall-layer control may, therefore, have a long-lasting effect, say O[100δ], if applied during transition. On the other hand, as per Clauser (1956), if the wall control is applied in the fully-developed turbulent region of the flow, the effect does not last long. The relevance of Reynolds number effects to flow control is particularly telling in case of full numerical simulation because it is currently limited to Reynolds numbers that are not that far from transitional values.

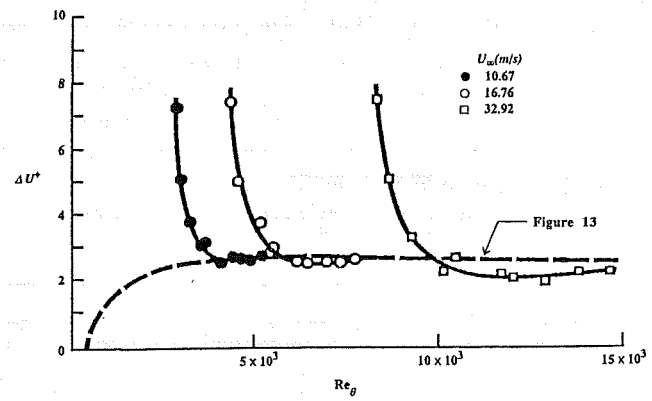

Fig 62. Approach to equilibrium after tripping device at moderately high Reynolds numbers (from Coles, 1962).

It is instructive to recall in here typical Reynolds numbers encountered in the laboratory and in the field. Other than a handful of large-scale facilities (see Section 5.4), boundary layers generated in wind tunnels and water tunnels typically have Reynolds numbers of Re_θ = O[1000]. A commercial aircraft traveling at a speed of 300 m/s at an altitude of 10 km would have a unit Reynolds number of 10^7/m. Due to the much smaller kinematic viscosity of water, a nuclear submarine moving at a modest speed of 10 m/s (≈ 20 knots) would have the same unit Reynolds number of 10^7/m. This unit Reynolds number translates to a momentum thickness Reynolds number near the end of either vehicle of roughly Re_θ = 300,000. The Reynolds number on the space shuttle is as high as Re_θ = 430,000, on an aircraft carrier can have a maximum of $Re_\theta = 1.5x10^6$, and in the atmospheric boundary layer is typically $Re_\theta = 10^6$-10^7. These ranges of Reynolds numbers together with the scopes of operation of typical wind and water tunnels, direct numerical simulations and three large-scale facilities, the National Transonic Tunnel, NASA-Langley towing tank and the super-pipe, are schematically shown in Fig 1.

It is clear from the discussion thus far in this section and from the strong Reynolds number effects on the mean flow, higher-order statistics and coherent structures demonstrated in Sections 5-7, that control devices developed and tested in the laboratory can not in general be readily extrapolated to field conditions. Detailed knowledge of high-Reynolds number consequences is required prior to attempting to control practical wall-bounded flows.

9. NUMERICAL SIMULATIONS

9.1 General remarks

The principles of conservation of mass, momentum and energy govern all fluid motions. In general, a set of partial, nonlinear differential equations expresses these principles and together with appropriate boundary and initial conditions constitute a well-posed problem. For a turbulent flow, the dependent variables are random functions of space and time, and no straightforward method exists for analytically obtaining stochastic solutions to nonlinear differential equations. Hence, the increased reliance on large-memory, high-speed digital computers to integrate the equations of motion. Large number of articles that specifically review turbulence computations are available (*eg*, Launder and Spalding, 1974; Reynolds, 1976; Lumley, 1978; 1983; Rogallo and Moin, 1984; Speziale, 1991). Understanding and modeling of turbulence via numerical

simulations can solve a variety of engineering problems and lead to important technological advances.

A distinguishable characteristic of high-Reynolds number turbulent flows is their large range of excited space and time scales. In homogeneous turbulence, for example, the energy-containing eddies are $O\left[Re_t^{3/4}\right]$ times larger than the length scale of the smallest eddies (Kolmogorov length-scale), where $Re_t = u'L/\nu$ is the turbulence Reynolds number (see, for example, Landau and Lifshitz, 1987). In order to resolve the flow adequately, a computer storage (at each time step) of $O\left[Re_t^{9/4}\right]$ and a total number of arithmetic operations of at least Re_t^3 are needed.

Direct numerical simulations (DNS) attempt to integrate the instantaneous equations and resolve *all scales* for which there is an appreciable kinetic energy, but are limited to simple geometries and Reynolds numbers well below the values encountered in most practical situations. The reason being the enormous computer capacity needed to resolve the necessarily time-dependent, three-dimensional velocity and pressure fields (as well as density and temperature fields if the flow is compressible). As indicated above the number of active degrees of freedom in an incompressible turbulent flow is on the order of $Re_t^{9/4}$ per unit volume. At Reynolds number of 10^8, modest by geophysical standards, there are on the order of 10^{18} active degrees of freedom per L^3, where L is the characteristic length of the flow (Frisch and Orszag, 1990). This colossal number challenges the capabilities of both algorithms and fastest supercomputers available now or in the foreseeable future.

Even if it can be carried out, the brute-force numerical integration of the equations of motion using the supercomputer is prohibitively expensive even at modest Reynolds numbers. For example, a single direct numerical simulation of a canonical wall-bounded flow at $Re_\theta = O[1000]$ requires about 1000 CPU hours and costs, at commercial supercomputer rates, close to $1 million. This requirement increases roughly by an order of magnitude if the Reynolds number is doubled.

For now and the foreseeable future, a statistical approach, where a temporal, spatial or ensemble mean is defined and the equations of motion are written for the various moments of the fluctuations about this mean, is the only route available to get meaningful engineering results. Unfortunately, the nonlinearity of the Navier-Stokes equations guarantees that the process of averaging to obtain moments results in an open system of equations, where the number of unknowns is always greater than the number of equations, and more or less heuristic modeling is used to close the equations. Such modeling can take a variety of forms and levels of sophistication, including the simple one-point first and second moments, the two-point closures or spectral models, the subgrid-scale models for large-eddy simulations, and models based on the joint probability density function.

In the simplest kind of turbulence modeling, the Reynolds stress is related to the mean-velocity gradient via a suitably assumed eddy viscosity, which may depend on position. Calculations of one-point first and second moments, such as mean velocity, mean pressure and turbulence kinetic energy, are then possible. Although gradient-transport models produce reasonable results in very few simple cases, they are in principle faulty (see, for example, Corrsin, 1974). Lumley (1992) summarizes the potential pitfalls in using first-order closure schemes. These are basically local models which, on introducing the Prandtl's (1925) concept of mixing length, make direct analogy between turbulent transport processes and molecular ones, an ill-fated assumption considering the lack of a clear-cut separation of scales in the former kind of transport.

A turbulent flow is by necessity nonlocal in nature. Conditions at a point depend on the history of all fluid particles that arrive at that point. This is due to the hyperbolicity of the Navier-Stokes equations (Bradshaw *et al*, 1967). Ideally, therefore, a turbulence model should be nonlocal depending on the weighted integral, with fading memory and progressively broadening domain of integration, back over the mean path through the point in question. Second-order closure models essentially do that for second-order quantities, but the approximations used there for third-order quantities are again local, and so on. The structural models also satisfy this non-local requirment well.

Second-order models attempt to close the Reynolds-stress transport equations. Since these models are based on the two-point velocity correlation tensor, they provide more detailed information about the turbulence structure. The original idea for second-order closure schemes is due to Rotta (1951), but the massive computational requirement for solving six additional transport equations delayed its practical implementation for over two decades.

An alternative approach to conventional closure schemes utilizes the renormalization group (RNG) theory. The dynamic RNG method, first developed for use in the quantum field theory, together with a correspondence principle have been formalized for the turbulence problem by Yakhot and Orszag (1986). The method uses dynamic scaling and invariance together with iterated perturbation techniques to evaluate the transport coefficients and transport equations for the large-scale modes. RNG computations have been shown to produce better comparisons with experiments for complex situations where conventional closure methods often fail; for example, for separated flows, swirling flows, etc. A major advantage of the RNG analysis is its independence of any experimentally adjustable parameters.

Perhaps the next best computational strategy to direct numerical simulations is large-eddy simulations (LES), where the energy-containing eddies are directly computed but the more universal small scales are modeled. LES uses

a fixed spatial resolution and the effects of eddies not resolved are modeled using gradient transport ideas (Galperin and Orszag, 1993) or the more sophisticated dynamic localization models. The two approaches are contrasted below.

Inertial transfer of energy over a wide range of spatial scales is a distinguishing characteristic of turbulent flows and one which strongly influences their evolution. This energy transfer originates from the nonlinear convective derivative term in the Navier-Stokes equation and gives rise to the familiar closure problem. The use of large-eddy simulation as a tool to explore the physics of complex turbulent flows is limited by current subgrid-scale (SGS) models (Rogallo and Moin, 1984). Implicit in each SGS model currently in use are fairly simplistic assumptions regarding the nature of inertial energy transfer over the subgrid wavenumber range. For example, the simple Smagorinsky (1963) model lumps the effect of the subgrid eddies into an effective subgrid viscosity in the Heisenburg sense. The effect of shear at subgrid scales is neglected and the validity of the Smagorinsky model has been questioned by Kim *et al* (1987). Such a model encounters particular difficulty when applied to complex nonequilibrium flows with extra strain rates. In the more recent *dynamic SGS model* (Germano *et al*, 1991), the eddy viscosity concept is retained but a space-time dependent Smagorinsky constant is computed which allows the constant to adjust to the local flow dynamics. A disadvantage of dynamic localization SGS models with regard to their application in wall-bounded turbulent flows lies in the failure to include effects associated with the anisotropy of small scales. The models can also predict energy backscatter which is too large and consequently gives rise to negative eddy viscosity values.

9.2 Direct numerical simulations

Notwithstanding the colossal computer requirement, it is clear that integrating the instantaneous equations of motion is physically more sound than the heuristic closure required for any of the alternative approaches discussed above. DNS is not, however, without its detractors. A legitimate question is what exactly is being simulated? It is not clear

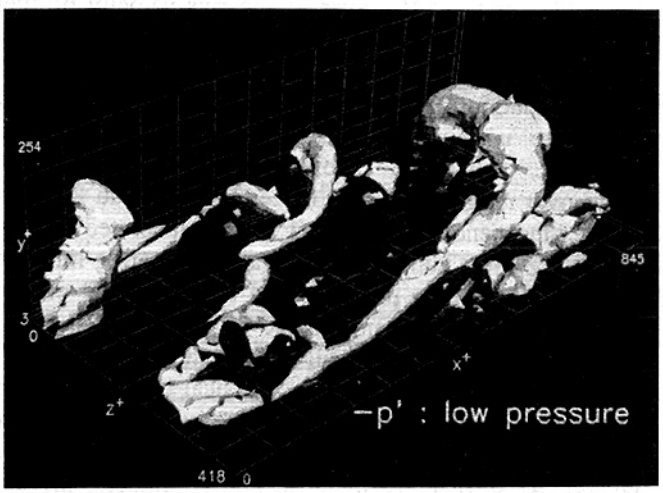

Fig 63. Vortical structures in turbulent boundary layer. Direct numerical simulation results from Robinson *et al* (1989).

that DNS and a corresponding physical experiment at the same Reynolds number are simulating the same flow. When the numerical results are compared to experiments, at first glance many points of agreement become evident. But some subtle disagreements remain, for example in higher-order statistics. Admittedly, such quantities are not easy to measure in the laboratory either, and the observed differences might be fairly blamed on the experimentalists. However, notwithstanding that the full Navier-Stokes equations are being integrated, there are several potential pitfalls that are unique to DNS. These include the imposed periodic boundary conditions, the unnatural way by which a boundary layer becomes turbulent (it is neither properly tripped nor evolving through natural transition), and the sterilized environment in which the calculations progress (perfectly smooth wall and precisely irrotational, disturbance-free freestream). None of these conditions is possible in a physical experiment, and their detailed effects on the computed flow remain unknown. Two specific discrepancies between physical and numerical experiments will be elaborated later in this section.

More to the main topic of the present article is the ability to extrapolate low-Reynolds number physical or numerical experiments to practical situations. Reynolds-averaged Navier-Stokes simulations model all the turbulent fluctuations, and is not limited to low Reynolds numbers. The problem is to figure out the proper model to use for each range of Reynolds numbers. DNS, on the other hand, is by necessity a viable tool only at very modest Reynolds numbers. Without knowing Reynolds number effects on the mean and turbulence quantities, DNS results can not be readily extended to engineering applications.

Now let us return to the subtle discrepancies between DNS and experiments. In the channel-flow direct numerical simulations of Moin and Kim (1982), the ratio of rms spanwise vorticity fluctuations to rms streamwise vorticity fluctuations computed at the wall is less than half of that computed from the near-wall velocity measurements of Kreplin and Eckelmann (1979) or the fluctuating shear stress right at the wall as measured by Fortuna and Hanratty (1971) and Sreenivasan and Antonia (1977). It seems that this discrepancy is a consequence of insufficient resolution in the viscous sublayer in the numerical simulations.

The second discrepancy concerns vortical structures, admittedly very difficult to detect experimentally. It has been shown in this paper that in a turbulent boundary layer, for $Re_\theta < 10^3$, Reynolds number affects the mean flow in the outer layer and the turbulence even down to $y^+ = 4$. In spite of that, the Direct Numerical Simulation (DNS) studies of the flat-plate boundary layers (Robinson *et al* 1989) give us information on the organized turbulence structures which would be valuable at higher Reynolds numbers. In the following, the simulation structure at $Re_\theta = 670$ is compared with the experimentally observed structure at $600 \le Re_\theta \le 17.5 \times 10^3$ (Head and Bandyopadhyay, 1981).

Figure 63 shows the numerically obtained vortical structures in a volume of several δ^3 (Robinson *et al* 1989). The fact that vortex cores are always associated with

regions of low pressure is utilized in here to identify the vortical structures. This way regions of significant vorticity are not confused with vortices, a potentially serious problem when dealing with unsteady viscous flows (Saffman and Baker, 1979; Robinson *et al*, 1989; Robinson, 1991). Compared to flow visualization experiments at Re_θ = 600 (Head and Bandyopadhyay, 1978), the immediate impression is that the number of structures per unit wall area is less and it is not difficult to track a structure all the way to the wall much like in the transitional layer. This gives credence to the criticism that what is being simulated numerically is not a fully-developed turbulent flow but more like a transitional boundary layer.

A large structure can be defined as an agglomeration of successively forming hairpin vortices creating a linear upstream interface. However, Theodorsen (1952) and most others consider only one horseshoe vortex and not any agglomerations of them to describe a turbulent boundary layer. This causes a paucity of scales and restricts the models in their ability to better describe the turbulent boundary layer at high Reynolds numbers.

A longitudinal section of Fig 63 contains one or two structures. In the constant-mixing-length region of the simulated boundary layer ($\delta^+ = 280 > y^+ > 150$), $d^+ \approx 60 \pm 20$ where d is the vortex diameter (Robinson 1990; Bushnell *et al* 1975). This gives a small range of δ^+ / d^+_{max}, viz 3.5 to 7.0, which means there is a paucity of scales and that the overturning in the individual structures dominates the entire boundary layer. The overturning in the boundary layer diminishes with Re_θ (Head and Bandyopadhyay, 1981). The value in the constant-mixing-length layer, viz $d^+/\delta^+ = 0.21^{.29}_{.14}$ compares with the mean value of Falco's (1974) typical-eddy[21] length scale $C_y/\delta = 0.31$ at this Re_θ (see Fig 58).

It has been argued elsewhere (Bandyopadhyay, 1989) that increased vortex stretching and vortex-vortex interaction could lead the hairpin vortices to first spiral around itself into a double helix and then onto further spiraling between neighboring double helixes. Such process at Re_θ = 600 was depicted in Fig 59 of the present paper. Vortex-vortex interactions are not present, however, in the direct numerical simulations at approximatley the same Reynolds number (Re_θ = 670).

The previously cited high-resolution velocity and vorticity measurements by Klewicki *et al* (1994) also indicate some disagreement with the numerical results of Spalart (1988). The experimental profile of turbulence kinetic energy production is consistently lower, predominately resulting from differences in the Reynolds stress profiles. Both their turbulent diffusion and viscous diffusion terms peak closer to the wall than the computational profiles. In the experiment, the negative peak in the diffusion profile occurs closer to the wall than the positive peak in the production profile. In contrast, an opposite situation is observed in the numerical simulations, where the diffusion term exhibits its negative peak further from the wall and crosses zero near the positive peak in the production profile (Fig 8 of Klewicki *et al'* s paper).

10. NON-CANONICAL BOUNDARY LAYERS

Thus far in this article the focus has been on the canonical, turbulent wall-bounded flow. The incompressible, isothermal, zero-pressure-gradient boundary layer developing over a smooth, rigid, semi-infinite flat plate, or the closely related two-dimensional channel flow, is the "simplest" problem to study analytically, experimentally or numerically. Practical wall-bounded flows, however, have one or more complicating influences such as freestream turbulence, pressure gradient, compressibility, roughness, surface curvature, three-dimensionality, wall compliance, heat transfer, stratification, change of phase, presence of side-walls and corners, etc (Bushnell *et al*, 1993). Such flows are naturally more difficult to deal with analytically, experimentally or numerically, but are nevertheless important to study for at least two reasons. Firstly, their behavior is often quite different from that of the canonical problem and therefore must be determined prior to rational design of practical devices. Secondly, as suggested by Clauser (1956) who in turn was inspired by Maxwell's concept of *black box*, the physical understanding of a canonical turbulent flow (the black box) could be improved by observing the response of the flow to different external influences. In other words, studying a boundary layer over a rough wall, for example, might shed more light on the smooth-wall flow.

From the point of view of Reynolds number effects on the non-canonical wall-bounded flows, it is intuitively appealing to conclude that these effects are at least as strong as those reviewed in the bulk of the present paper for the canonical flow. Corroborating data one way or the other are, unfortunately, not available. The few existing experiments dealing with complex wall-bounded flows were not specifically designed to search for Reynolds number effects. In other words, such experiments were carried out at a particular Reynolds number or at a rather narrow range of Reynolds numbers. However, if the rms-velocity profiles, for example, do not scale with inner variables in the canonical flow, there is little reason to believe that the corresponding profiles in the non-canonical case would do so. There is, however, one notable exception to this argument. Unlike the canonical problem, wall-bounded flows over rough walls may indeed achieve true Reynolds number-independence. This trait will be elaborated below.

In the present authors opinion, a complicating influence which is particularly useful to add to the arsenal of tools available to better understand the canonical wall-bounded flow is the non-smooth wall perturbation. Roughness is simple to implement, at least in physical experiments, and its effect on the flow is pronounced (see Raupach *et al*, 1990, for a recent review of rough-wall turbulent boundary layers). At sufficiently high Reynolds numbers, the skin friction becomes independent of viscosity and depends

[21] Which is the cross-section of the hairpin vortices according to Head and Bandyopadhyay (1981) and Klewicki *et al* (1994).

solely on the relative roughness scale. In this so-called fully-rough regime, the constant skin-friction coefficient contrasts the ever decreasing skin friction for a smooth wall. This has important consequences on the flow equilibrium as illustrated below.

According to Clauser (1954), an equilibrium turbulent boundary layer is characterized by similarity of its velocity-defect profile in the course of its downstream development. True equilibrium is achieved when the velocity-defect ratio becomes a function of (y/δ) only and, therefore, independent of Reynolds number. Tani and Motohashi's (1985a; 1985b) results of analyzing available data seem to negate the existence of equilibrium state for smooth, zero-pressure-gradient boundary layers. Tani (1986; 1987), on the other hand, show that equilibrium is possible for boundary layers in favorable pressure gradient over smooth as well as k-type rough surfaces. For a roughness height which increases linearly with the streamwise direction, equilibrium is achieved in zero pressure gradient. For d-type roughness, equilibrium exists for a certain range of pressure gradients, from favorable to adverse. These useful properties of rough walls may be exploited to better understand Reynolds number effects on smooth-wall boundary layers.

There is at least one more argument in favor of studying wall-bounded flows over rough walls. As discussed by Kailasnath (1993), changes in the wall-bounded flow physics are due to changing the scale ratio, δ^+ or a^+, and not the Reynolds number per se. While the mean flow is primarily influenced by Re_θ, δ^+ may be the more significant parameter for the turbulence and the coherent structures. Such assertion is difficult to prove for the canonical flow case since a change in Reynolds number leads to a corresponding change in the scale ratio. However, this is not the case for fully-rough walls, making them particularly useful to study. In that case, the scale ratio at a given Reynolds number could be simply changed by systematically varying the roughness height.

A glimpse of the complexity of Reynolds number effects in non-canonical turbulent boundary layers can be had by examining such effects in the presence of freestream turbulence (Blair, 1983; Hancock and Bradshaw, 1983; Castro, 1984; Bandyopodhyay, 1992). This is a complicating factor that is particularly important for turbomachinery blades where the Reynolds number is low ($Re_\theta <$ 5000) and the freestream turbulence is high. The effect of freestream turbulence is to increase the skin friction.

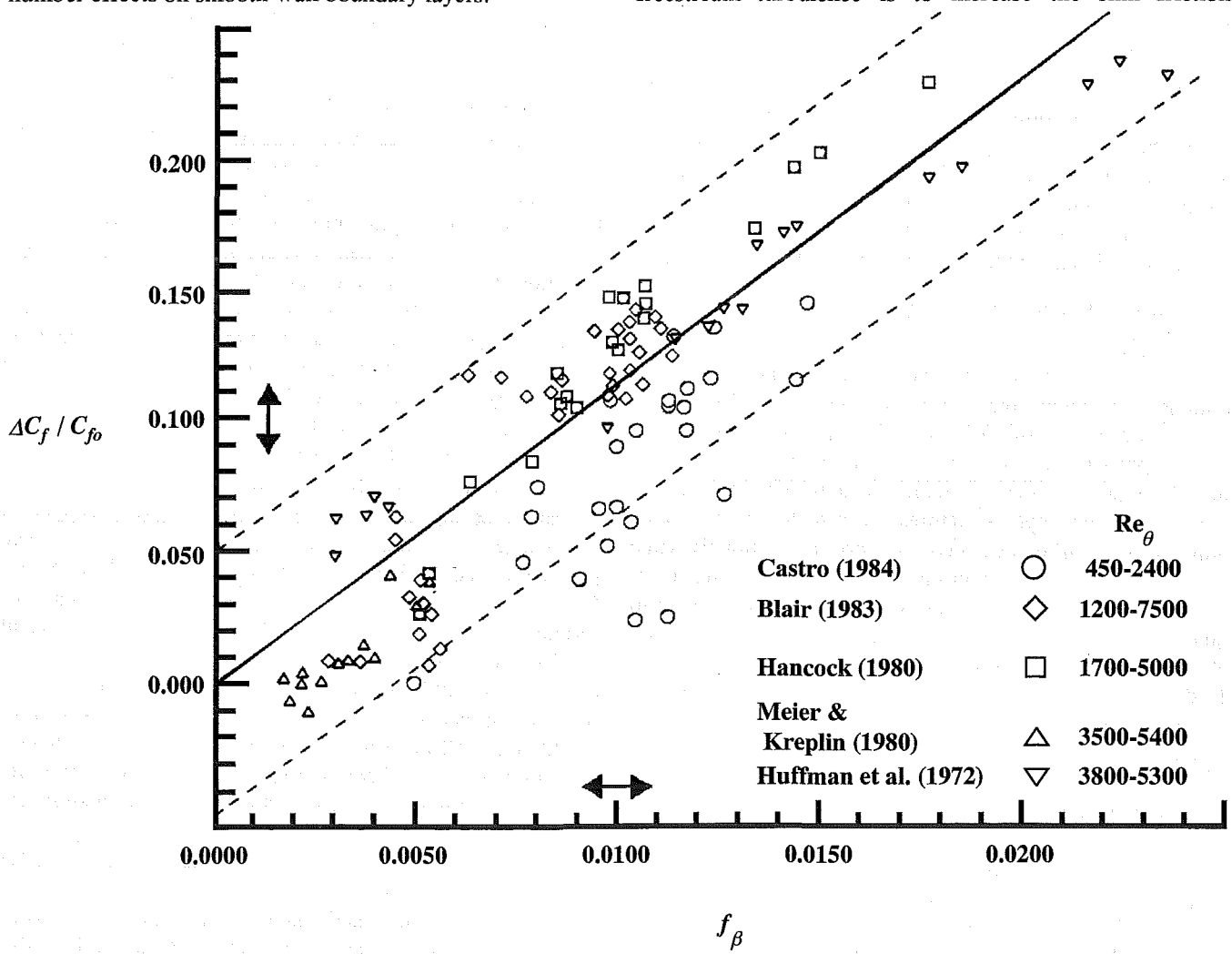

Fig 64. Reynolds number dependence of the fractional increase in skin friction due to freestream turbulence. Variable Reynolds number effects are included in the damped freestream turbulence parameter f_β. Dashed lines indicate a ±5% scatter band about the least-square-fit solid line, and the arrows indicate uncertainties (from Bandyopadhyay, 1992).

However, as Hancock (1980) have shown, freestream turbulence cannot be measured by turbulence intensity (u'/U_o) alone, but also jointly with the ratio of the dissipation length-scale in the freestream and the boundary layer thickness, (L_o/δ). The freestream turbulence parameter that combines these two effects is defined as:

$$f = \left\{ \left[\frac{u'}{U_o} \right] \Big/ \left[\left(\frac{L_o}{\delta} \right) + 2 \right] \right\} \tag{40}$$

The simultaneous involvement of the scale ratio greatly complicates the Reynolds number dependence of the freestream turbulence effects (Bandyopodhyay, 1992). For example, due to freestream turbulence in the range of $f >$ 0.0115, the wake component ΔU^+ increases with Re_θ, and in the range of $0.0025 < f < 0.0095$, ΔU^+ drops with Re_θ. On the other hand, in the two ranges of $f \leq .0025$ and $0.0095 \leq f \leq 0.0115$, there is no apparent dependence on Re_θ.

To account for low-Reynolds number effects, Blair (1983) empirically arrived at the following damping factor:

$$\beta = \left[1 + 3 \; e^{-(Re_\theta / 425)} \right] \tag{41}$$

According to Bandyopodhyay (1992), the fractional increase in skin friction is then a function of only $f_\beta = f \cdot \beta^n$, where the exponent n takes the values -1, 1, or 0 depending on wheter ΔU^+ respectively increases, decreases or remains constant with increasing Re_θ. Figure 64 is a summary of the increase in skin friction due to freestream turbulence when the just mentioned dependence on Re_θ is taken into account.

11. CONCLUDING REMARKS

In the present article, we attempted to assimilate the considerable volume of experimental and numerical boundary-layer data that have been accumulated since the mean flow review of Coles (1962). Attention is drawn to some aspects of the emerging description of the structure of high-Reynolds number turbulent boundary layers. Both the inner- and outer-layer structures are affected by Reynolds number. The turbulence quantities do not accurately scale with wall-layer variables in the inner layer. The outer-layer turbulence structure (S_u, peak R_{uv}, intermittency, u-v quadrant distributions, streamwise scales) is greatly changed at extremely high Reynolds numbers (Smits *et al*, 1989; Smits, 1990) and new structures probably evolve due to vortex-vortex interactions. As aptly illustrated by Kailasnath (1993), the classical similarity theory of wall-bounded flows that asserts a universal description for the near-wall flow is found to be increasingly deficient as the questions become more detailed.

The numerically simulated low-Reynolds number, flat-plate turbulent boundary layers are characterized by a paucity of scale and a lack of vortex-vortex interaction. Studies of the very low-Reynolds number turbulent boundary layer structure might not inherently involve several aspects of the high-Reynolds number structure which may be crucial to flow control through turbulence manipulation.

Why does the mean flow scale, at least approximately, with wall-layer variables in the inner layer yet turbulence quantities do not? At a relatively low Reynolds number, say $Re_\theta = 500$, the inner-layer mean flow appears to be already universal; so why should not the low-Re_θ structure be universal? These questions erroneously imply that there is a first-order direct connection between the mean flow and turbulence in a wall-bounded flow as in a free-shear flow. In a mixing layer, for example, the experimentally observed two-dimensional rollers are the direct result of an inviscid instability of the mean-velocity profile. Their characteristic dimension is equal to the layer thickness, and they contain almost all of the mean-flow vorticity. In a wall-bounded flow, on the other hand, the three-dimensional hairpin vortices are the result of a secondary or a tertiary instability, and their diameters are typically much smaller than the boundary layer thickness. The hairpins contain only a portion of the mean flow vorticity--that is, they are further removed from the mean flow.

Experience with turbulence modeling also suggest that the turbulence in a wall-bounded flow is not derived directly from the mean flow. In the earliest turbulence models, shear stress is derived from the mean-velocity profile. Such models have not been widely successful. Townsend (1976) and Bradshaw *et al* (1967) have argued that instead there is a much closer connection between the shear stress and the turbulence structure. Townsend's work was limited to the near-wall region, while Bradshaw *et al* have extended the argument to the entire shear layer. Direct measurements of typical eddies have supported their assertion (Falco, 1974; Newman, 1974).

It should be realized that ensemble averaging is a useful mathematical tool for computing typical characteristics as long as the variability in the quantities of interest is sufficiently low. The large variability in the measurements of streak spacing (standard deviation ~ 0.3 to 0.4 of mean) and of vortex diameter even in full simulation at one low Re_θ of 670 (maximum diameter about twice minimum one) is disturbing and this issue has not been addressed yet. It raises the following questions: (1) Is the turbulence production mechanism independent of Reynolds number? (2) Even at one Re_θ, is there only one mechanism of turbulence production? (3) Can there be several mechanisms simultaneously in play each of which has a different Reynolds number dependence? In the context of these questions the conclusion arrived at by Keith *et al* (1992) for wall-pressure spectra that the scaling changes from mixed to outer layer as Re_θ is increased, is intriguing. The answer to question (1) seems no longer an unequivocal affirmative.

We may summarize our conclusions of the Reynolds number effects as follows:

1. The widely accepted "asymptotic" state of the wake component is present only in the range of $6\text{x}10^3 < Re_\theta < 1.5\text{x}10^4$. At higher values, it drops although at a much slower rate than that in the range of $Re_\theta < 6\text{x}10^3$.

2. The Clauser's shape parameter is strongly Reynolds number dependent at $Re_\theta<10^3$, and weakly above that.
3. Alternatives to the logarithmic mean-velocity profile have been periodically proposed. Such *heretical* ideas deserve further scrutiny. Independent confirmation via well-controlled experiments that cover a wide range of Reynolds numbers, resolve the linear region and directly measure the wall-shear stress is needed.
4. The freestream turbulence effect is dependent on Reynolds number.
5. Turbulence measurements with probe lengths greater than the viscous sublayer thickness (~ 5 wall units) appear to be unreliable, particularly near the wall.
6. Unlike the mean flow, the statistical turbulence quantities do not scale accurately with the wall-layer variables over the entire inner layer. Such scaling applies over only a very small portion of the inner layer adjacent to the wall.
7. At low Reynolds numbers, the peak u-turbulence intensity increases slightly with Reynolds number in both channels and flat plates.
8. The distance from the wall where the streamwise turbulence intensity peaks appears to scale with inner variables.
9. In contrast, the corresponding distances, expressed in wall units, for both the normal fluctuations and the Reynolds stress move away from the wall as the Reynolds number increases. At high Re, the peak normal turbulence intensity and the peak Reynolds stress occur substantially outside the viscous region.
10. The wall-pressure rms increases slightly with Reynolds number.
11. Systematic changes in the mean and higher-order statistics as the Reynolds number varies could be considered as proper first-order trends within the framework of an asymptotic theory. At finite Reynolds numbers, the additive composite expansion formed from the inner and outer expansions of any turbulence quantity provides the only uniformly valid approximation in the matched region.
12. In flat plates, trip memory can survive the statistical turbulence quantities at even $Re_\theta > 6x10^3$, where the mean flow is said to have reached an asymptotic state.
13. The Reynolds number dependence of the post-transition relaxation length of both the mean and turbulence quantities is not well understood.
14. In pipe flows, the wave nature of the viscous sublayer, which is observable at low Reynolds numbers, gives way to a poorly understood random process at high Reynolds numbers.
15. While the variously defined (small) length scales differ greatly from each other at low Reynolds numbers, they all asymptote to the mixing length at much higher Reynolds numbers ($Re_\theta > 1.0x10^4$).
16. The outer-layer structure changes continuously with Reynolds numbers, and very little is known about the structure of very high-Reynolds number turbulent boundary layers.
17. The aspect ratio of the hairpin vortices increases with Reynolds number as they also become skinnier. In a large structure, the number of constituent hairpin vortices per unit wall area increases with Reynolds number.
18. Changes in the wall-bounded flow physics could be described as due to changing the scale ratio, δ^+ or a^+, and not the Reynolds number per se. In a given boundary layer, δ^+ changes downstream at a rate slightly lower than Re_θ. The influence of the wall changes from non-local to local as this scale ratio increases.
19. There is a dire need for high-resolution, reliable measurements of mean and statistical turbulence moments at high Reynolds numbers in smooth, flat-plate turbulent boundary layers.
20. Reynolds number effects in canonical flows can not always be extrapolated to non-canonical cases in a simple straightforward manner.

In closing, the present article is a modest attempt to investigate critically the effects of Reynolds number on the mean velocity, higher-order statistics and coherent structures of the canonical wall-bounded flow. Not surprisingly, our work has provided more questions than answers. It is clear that the present knowledge of Reynolds number effects is basically phenomenological and a good theoretical understanding is largely lacking. Real progress in the field and resolution of its many existing controversies can only be achieved, however, when well-controlled, well-resolved physical and numerical experiments are combined with at least a semblance of analytical foundation.

ACKNOWLEDGMENT

During the writing of this manuscript, the first author was a Distinguished Faculty Fellow at the Newport Division of the Naval Undersea Warfare Center, Newport, Rhode Island. M G wishes to acknowledge the financial support from the Office of Naval Research. The authors are grateful to Dr Kenneth Lima of NUWC Division Newport for providing funding for the graphics work in this paper. We would also like to express our gratitude to Professors Peter Bradshaw and Ronald L Panton for commenting on the manuscript, and to Professors Ron F Blackwelder, William K George, Alexander J Smits and Katepalli R Sreenivasan for providing us with difficult-to-obtain publications.

REFERENCES

Acarlar MS and Smith CR (1987a) "A Study of Hairpin Vortices in a Laminar Boundary layer. Part 1. Hairpin Vortices Generated by a Hemisphere protuberance," *J Fluid Mech* **175**, pp 1-41.

Acarlar MS and Smith CR (1987b) "A Study of Hairpin Vortices in a Laminar Boundary layer. Part 2. Hairpin Vortices Generated by Fluid Injection," *J Fluid Mech* **175**, pp 43-83.

Achia BU and Thompson DW (1977) "Structure of the Turbulent Boundary Layer in Drag-Reducing Pipe Flow," *J Fluid Mech* **81**, pp 439-464.

Afzal N (1976) "Millikan's Argument at Moderately Large Reynolds Number," *Phys Fluids* **1**, pp 600-602.

Afzal N and Bush WB (1985) "A Three-Layer Asymptotic Analysis of Turbulent Channel Flow," *Proc Indian Acad Sci (Math Sci)* **94**, pp 135-148.

Alfredsson PH and Johansson AV (1984) "On the Detection of Turbulence-Generating Events," *J Fluid Mech* **139**, pp 325-345.

Allan JF and Cutland RS (1953) "Wake Studies of Plane Surfaces," *Trans of the North East Coast Inst of Eng and Shipbuilders* **69**, pp 245-266.

Alving AE, Smits AJ, and Watmuff JH (1990) Turbulent Boundary Layer Relaxation from Convex Curvature," *J Fluid Mech* **211**, pp 529-556.

Anders JB (1990a) "Boundary Layer Manipulators at High Reynolds Numbers," in *Structure of Turbulence and Drag Reduction*, ed A Gyr, pp 475-482, Springer-Verlag, Berlin.

Anders JB (1990b) "Outer-Layer Manipulators for Turbulent Drag Reduction," in *Viscous Drag Reduction in Boundary Layers* , eds DM Bushnell and JN Hefner, pp 263-284, *AIAA Progress in Astronautics and Aeronautics*, Vol 123, Washington, DC.

Andreopoulos J, Durst F, Zaric Z, and Jovanovic J (1984) "Influence of Reynolds Number on Characteristics of Turbulent Wall Boundary Layers," *Exp Fluids* **2**, pp 7-16.

Antonia RA, Bisset DK, and Browne LWB (1990) "Effect of Reynolds Number on the Topology of the Organized Motion in a Turbulent Boundary Layer," *J Fluid Mech* **213**, pp 267-286.

Antonia RA, Rajagopalan S, Subramanian CS, and Chambers AJ (1982) "Reynolds-Number Dependence of the Structure of a Turbulent Boundary Layer," *J Fluid Mech* **121**, pp 123-140.

Antonia RA, Teitel M, Kim J, and Browne LWB (1992) "Low-Reynolds-Number Effects in a Fully Developed Turbulent Channel Flow," *J Fluid Mech* **236**, pp 579-605.

Ashkenas HI, and Riddell FR (1955) "Investigation of the Turbulent Boundary Layer on a Yawed Flat Plate," *NACA Tech Note* No TN-3383, Washington DC.

Aubrey N, Holmes P, Lumley JL, and Stone E (1988) " The Dynamics of Coherent Structures in the Wall Region of a Turbulent Boundary Layer," *J Fluid Mech* **192**, pp 115-173.

Bakewell HP and Lumley JL (1967) "Viscous Sublayer and Adjacent Wall Region in Turbulent Pipe Flow," *Phys Fluids* **10**, pp 1880-1889.

Bandyopadhyay PR (1980) "Large Structure with a Characteristic Upstream Interface in Turbulent Boundary Layers," *Phys Fluids* **23**, pp 2326-2327.

Bandyopadhyay PR (1982) "Period Between Bursting in Turbulent Boundary Layers," *Phys Fluids* **25**, pp 1751-1754.

Bandyopadhyay PR (1983) "Turbulent Spot-Like Features of a Boundary Layer," *Annals New York Acad Sci* **404**, pp 393-395.

Bandyopadhyay PR (1986a) "Drag Reducing Outer-Layer Devices in Rough Wall Turbulent Boundary Layers," *Exp Fluids* **4**, pp 247-256.

Bandyopadhyay PR (1986b) "Review–Mean Flow in Turbulent Boundary Layers Disturbed to Alter Skin Friction," *J Fluids Eng* **108**, pp 127-140.

Bandyopadhyay PR (1987) "Rough-Wall Turbulent Boundary Layers in the Transition Regime," *J Fluid Mech* **180**, pp 231-266.

Bandyopadhyay PR (1989) "Effect of Abrupt Pressure Gradients on the Structure of Turbulent Boundary Layers," *Proc 10 th Australasian Fluid Mech Conf*, eds AE Perry *et al*, Vol I, pp 1.1-1.4, Univ of Melbourne, Australia.

Bandyopadhyay PR (1990) "Convex Curvature Concept of Viscous Drag Reducion," in *Viscous Drag Reduction in Boundary Layers*, eds DM Bushnell and JN Hefner, pp 285-324, *AIAA Progress in Astronautics and Aeronautics*, Vol 123, Washington DC.

Bandyopadhyay PR (1991) "Comments on Reynolds Number Effects in Wall-Bounded Shear Layers," *AIAA Paper* No 91-0231, New York.

Bandyopadhyay PR (1992) "Reynolds Number Dependence of the Freestream Turbulence Effects on Turbulent Boundary Layers," *AIAA J* **30**, pp 1910-1912.

Bandyopadhyay PR and Ahmed A (1993) "Turbulent Boundary Layers Subjected to Multiple Curvatures and Pressure Gradients," *J Fluid Mech* **246**, pp 503-527.

Bandyopadhyay PR and Balasubramanian R (1993) "A Vortex Model for Calculating Wall Pressure Fluctuations in Turbulent Boundary Layers," *ASME Symposium on Flow Noise Modeling, Measurement and Control*, eds TM Farabee, WL Keith and RM Lueptow, NCA-Vol 15/FED-Vol 168, pp 13-24, ASME, New York.

Bandyopadhyay PR and Balasubramanian R (1994) "On the Role of Vortex Reynolds Number in Turbulent Boundary Layers," *Theor Comput Fluid Dyn*, in press.

Bandyopadhyay PR and Hussain AKMF (1984) "The Coupling between Scales in Shear Flows," *Phys Fluids* **27**, pp 2221-2228.

Bandyopadhyay PR and Watson RD (1988) "Structure of Rough-Wall Turbulent Boundary layers," *Phys Fluids* **31**, pp 1877-1883.

Barenblatt GI (1979) *Similarity, Self-Similarity, and Intermediate Hypothesis*, Plenum Press, New York.

Barenblatt GI (1993) "Scaling Laws for Fully Developed Turbulent Shear Flows. Part 1. Basic Hypothesis and Analysis," *J Fluid Mech* **248**, pp 513-520.

Barenblatt GI and Prostokishin VM (1993) "Scaling Laws for Fully Developed Turbulent Shear Flows. Part 2. Processing of Experimental Data," *J Fluid Mech* **248**, pp 521-529.

Berkooz G, Holmes P, and Lumley JL (1991) "Intermittent Dynamics in Simple Models of the Turbulent Boundary Layer," *J Fluid Mech* **230**, pp 75-95.

Bhatt WV (1971) "Flight Test Measurement of Exterior Turbulent Boundary Layer Pressure Fluctuations on Boeing Model 737 Airplane," *J Sound Vib* **14**, pp 439-457.

Black TJ (1966) "Some Practical Applications of a New Theory of Wall Turbulence," *Proc 1966 Heat Transfer and Fluid Mech Inst*, eds MA Saad and JA Miller, pp 366-386, Stanford Univ Press, Stanford CA.

Black TJ (1968) "An Analytical Study of the Measured Wall Pressure Field under Supersonic Turbulent Boundary Layers," *NASA Contractor Report* No CR-888, Washington DC.

Blackwelder RF (1978) "The Bursting Process in Turbulent Boundary Layers," in *Workshop on Coherent Structure of Turbulent Boundary Layers*, eds CR Smith and DE Abbott, pp 211-227, Lehigh Univ, Bethlehem PA.

Blackwelder RF (1988) "Coherent Structures Associated with Turbulent Transport," in *Transport Phenomena in Turbulent Flows*, eds M Hirata and N Kasagi, pp 69-88, Hemisphere, New York.

Blackwelder RF and Eckelmann H (1978)"The Spanwise Structure of the Bursting Phenomenon," in *Structure and Mechanisms of Turbulence I*, ed H Fiedler, pp 190-204, *Lecture Notes in Physics*, Vol 75, Springer-Verlag, Berlin.

Blackwelder RF and Eckelmann H (1979) "Streamwise Vortices Associated with the Bursting Phenomenon," *J Fluid Mech* **94**, pp 577-594.

Blackwelder RF and Haritonidis JH (1983) "Scaling of the Bursting Frequency in Turbulent Boundary Layers," *J Fluid Mech* **132**, pp 87-103.

Blackwelder RF and Kaplan RE (1976) "On the Wall Structure of the Turbulent Boundary Layer," *J Fluid Mech* **76**, pp 89-112.

Blackwelder RF and Kovasznay LSG (1972) "Time-Scales and Correlations in a Turbulent Boundary Layer," *Phys Fluids* **15**, pp 1545-1554.

Blair MF (1983) "Influence of Free-Stream Turbulence on Turbulent Boundary Layer Heat Transfer and Mean Profile Development, Part II--Analysis of Results," *J Heat Transfer* **105**, pp 41-47.

Blair MF and Werle MJ (1980) "The Influence of Free-Stream Turbulence on the Zero Pressure Gradient Fully Turbulent Boundary Layer," *United Tech Res Center Report* No R80-914388-12, Hartford CT.

Bradshaw P (1967) "'Inactive' Motion and Pressure Fluctuations in Turbulent Boundary Layers," *J Fluid Mech* **30**, pp 241-258.

Bradshaw P, Ferriss DH, and Atwell NP (1967) "Calculations of Boundary-Layer Development Using the Turbulent Energy Equation," *J Fluid Mech* **28**, pp 593-616.

Bremhorst K and Walker TB (1974) "Spectral Measurements of Turbulent Momentum Transfer in Fully Developed Pipe Flow," *J Fluid Mech* **61**, pp 173-186.

Brown GL and Thomas ASW (1977) "Large Structure in a Turbulent Boundary Layer," *Phys Fluids* **20**, pp S243-S252.

Bushnell DM (1983) "Turbulent Drag Reduction for External Flows," *AIAA Paper* No 83-0227, New York.

Bushnell DM and Greene GC (1991) "High-Reynolds-Number Test Requirements in Low-Speed Aerodynamics," in *High Reynolds Number Flows Using Liquid and Gaseous Helium*, ed RJ Donnelly, pp 79-85, Springer-Verlag, New York.

Bushnell DM and Hefner JN (eds) (1990) *Viscous Drag Reduction in Boundary Layers, AIAA Progress in Astronautics and Aeronautics*, Vol 123, Washington DC.

Bushnell DM and McGinley CB (1989) "Turbulence Control in Wall Flows," *Annu Rev Fluid Mech* **21**, pp 1-20.

Bushnell DM, Cary AM, and Holley BB (1975) "Mixing Length in Low Reynolds Number Compressible Turbulent Boundary Layers," *AIAA J* **13**, pp 1119-1121.

Bushnell DM, Yip LP, Yao C-S, Lin JC, Lawing PL, Batina JT, Hardin JC, Horvath TJ, Fenbert JW, and Domack CS (1993) "Reynolds Number Influences in Aeronautics," *NASA Tech Memorandum* No TM-107730, Washington DC.

Butler KM and Farrell BF (1993) "Optimal Perturbations and Streak Spacing in Wall-Bounded Shear Flow," *Phys Fluids A* **5**, pp 774-777.

Cantwell BJ (1990) "Organized Motion in Turbulent Flow," *Annu Rev Fluid Mech* **13**, pp 457-515.

Castro IP (1984) "Effects of Free Stream Turbulence on Low Reynolds Number Boundary Layers," *J Fluids Eng* **106**, pp 298-306.

Chiwanga SC and Ramaprian BR (1993) "The Effect of Convex Wall Curvature on the Large-Scale Structure of the Turbulent Boundary Layer," *Exp Thermal Fluid Sci* **6**, pp 168-176.

Choi H, Moin P, and Kim J (1993) "Direct Numerical Simulations of Turbulent Flow over Riblets," *J Fluid Mech* **255**, pp 503-539.

Choi K-S (1989) "Near-Wall Structure of a Turbulent Boundary Layer with Riplets," *J Fluid Mech* **208**, pp 417-458.

Clauser FH (1954) "Turbulent Boundary Layers in Adverse Pressure Gradient," *J Aeronaut Sci* **21**, pp 91-108.

Clauser FH (1956) "Turbulent Boundary Layer," *Adv Appl Mech* **4**, pp 1-51.

Coles D (1956) "The Law of the Wake in the Turbulent Boundary Layer," *J Fluid Mech* **1**, pp 191-226.
Coles D (1978) "A Model for Flow in the Viscous Sublayer," in *Workshop on Coherent Structure of Turbulent Boundary Layers,* eds CR Smith and DE Abbott, pp 462-475, Lehigh University, Bethlehem PA.
Coles DE (1962) "The Turbulent Boundary Layer in a Compressible Fluid," *Rand Corp Report* No R-403-PR, Santa Monica CA.
Coles DE (1969) "The Young Person's Guide to the Data," *Proc 1968 AFOSR-IFP-Stanford Conference on Computation of Turbulent Boundary Layers,* eds DE Coles and EA Hirst, Vol 2, pp 1-45, Thermosci Div, Stanford Univ, CA.
Comte-Bellot G (1963) "Contribution à l'Étude de la Turbulence de Conduite," Doctoral Thesis, Univ of Grenoble, France.
Comte-Bellot G (1965) "Ecoulement Turbulent entre Deux Parois Paralleles," *Publications Sci et Tech du Ministere de l' Air* No 419, Paris.
Corino ER and Brodkey RS (1969) "A Visual Investigation of the Wall Region in Turbulent Flow," *J Fluid Mech* **37**, pp 1-30.
Corrsin S (1957) "Some Current Problems in Turbulent Shear Flow," in *Symposium on Naval Hydrodynamics,* ed FS Sherman, pp 373-400, *Natl Acad of Sci/Natl Res Council Publication* No 515, Washington DC.
Corrsin S (1974) "Limitations of Gradient Transport Models in Random Walks and Turbulence," in *Turbulent Diffusion in Environmental Pollution,* eds FN Frenkiel and RE Munn, pp 25-60, *Adv in Geophys,* Vol 18A, Academic Press, New York.
Dimotakis PE (1991) "Turbulent Free Shear Layer Mixing and Combustion," in *High-Speed Flight Propulsion Systems,* eds SNB Murthy and ET Curran, pp 265-340, *AIAA Progress in Astronaut and Aeronaut,* Vol 137, Washington DC.
Dimotakis PE (1993) "Some Issues on Turbulent Mixing and Turbulence," *Guggenheim Aeronautical Lab Report* No FM93-1a, Pasadena, CA.
Donnelly RJ (1991) *High Reynolds Number Flows Using Liquid and Gaseous Helium,* Springer-Verlag, New York.
Donohue GL, Tiederman WG, and Reischman MM (1972) "Flow Visualization of the Near-Wall Region in a Drag-Reducing Channel Flow," *J Fluid Mech* **56**, pp 559-575.
Dutton RA (1955) "Experimental Studies of the Turbulent Boundary Layer on a Flat Plate with and without Distributed suction," PhD Dissertation, Cambridge Univ, UK.
Eckelmann H (1974) "The Structure of the Viscous Sublayer and the Adjacent Wall Region in a Turbulent Channel Flow," *J Fluid Mech* **65**, pp 439-459.
Elena M and Dumas R (1978) "Champs Dynamique et Thermique d'un Ecoulement Turbulent en Conduite avec Aspiration a la Paroi," *6th Int Heat Transfer Conf,* Vol 5, pp 239-244, Hemisphere, Washington DC.
Erm LP, Smits AJ, and Joubert PN (1987) "Low Reynolds Number Turbulent Boundary Layers on a Smooth Flat Surface in a Zero Pressure Gradient," *5th Symp on Turbulent Shear Flows,* eds F Durst *et al*, pp 2.13-2.18, Springer-Verlag, Berlin.
Falco RE (1974) "Some Comments on Turbulent Boundary Layer Structure Inferred from the Movements of a Passive Contaminant," *AIAA Paper* No 74-99, New York.
Falco RE (1977) "Coherent Motions in the Outer Region of Turbulent Boundary Layers," *Phys Fluids* **20**, pp S124-S132.
Falco RE (1980) "The Production of Turbulence Near a Wall," *AIAA Paper* No 80-1356, New York.
Falco RE (1983) "New Results, a Review and Synthesis of the Mechanism of Turbulence Production in Boundary Layers and its Modification," *AIAA Paper* No 83-0377, New York.
Falco RE (1991) "A Coherent Structure Model of the Turbulent Boundary Layer and its Ability to Predict Reynolds Number Dependence," *Phil Trans R Soc London A* **336**, pp 103-129.
Farabee TM and Casarella MJ (1991) "Spectral Features of Wall Pressure Fluctuations Beneath Turbulent Boundary Layers," *Phys Fluids A* **3**, pp 2410-2420.
Fiedler HE (1986) "Coherent Structures," in *Advances in Turbulence,* eds G Comte-Bellot and J Mathieu, pp 320-336, Springer-Verlag, Berlin.
Fiedler HE (1988) "Coherent Structures in Turbulent Flows," *Prog Aerospace Sci* **25**, pp 231-269.
Fiedler HE and Fernholz H-H (1990) "On Management and Control of Turbulent Shear Flows," *Prog Aerospace Sci* **27**, pp 305-387.
Fiedler HE and Head MR (1966) "Intermittency Measurements in the Turbulent Boundary Layer," *J Fluid Mech* **25**, pp 719-735.
Fortuna G and Hanratty TJ (1971) "The Influence of Drag-Reducing Polymers on Turbulence in the Viscous Sublayer," *J Fluid Mech* **53**, pp 575-586.
Frisch U and Orszag SA (1990) "Turbulence: Challenges for Theory and Experiment," *Phys Today* **43**, No 1, pp 24-32.
Gad-el-Hak M (1989) "Flow Control," *Appl Mech Rev* **42**, pp 261-293.
Gad-el-Hak M (1990) "Control of Low-Speed Airfoil Aerodynamics," *AIAA J* **28**, pp 1537-1552.
Gad-el-Hak M (1993) "Innovative Control of Turbulent Flows," *AIAA Paper* No 93-3268, Washington DC.
Gad-el-Hak M and Bushnell DM (1991) "Separation Control: Review," *J Fluids Eng* **113**, pp 5-30.
Gad-el-Hak M, Blackwelder RF, and Riley JJ (1981) "On the Growth of Turbulent Regions in Laminar Boundary Layers," *J Fluid Mech* **110**, pp 73-95.
Gad-el-Hak M, Blackwelder RF, and Riley JJ (1984) "On the Interaction of Compliant Coatings with Boundary-Layer Flows," *J Fluid Mech* **140**, pp 257-280.
Gallagher JA and Thomas ASW (1984) "Turbulent Boundary Layer Characteristics over Streamwise Grooves," *AIAA Paper* No 84-2185, New York.
Galperin B and Orszag SA (eds) (1993) *Large Eddy Simulations of Complex Engineering and Geophysical Flows,* Cambridge Univ Press, London.
George WK and Castillo L (1993) "Boundary Layers with Pressure Gradient: Another Look at the Equilibrium Theory," in *Near-Wall Turbulent Flows,* eds RMC SO *et el*, pp 901-910, Elsevier, Amsterdam.
George WK, Castillo L, and Knecht P (1992) "The Zero-Pressure Gradient Turbulent Boundary Layer Revisited," in *13th Symp on Turbulence,* ed XB Reed, Univ of Missouri, Rolla, 21-23 April.
George WK, Castillo L, and Knecht P (1993) "The Zero-Pressure Gradient Turbulent Boundary Layer," in *William C Reynolds Anniversary Symp on Turbulence,* Asilomar, California, 22-23 March.
George WK, Castillo L, and Knecht P (1994) "The Zero-Pressure Gradient Turbulent Boundary Layer," submitted to *Phys Fluids.*
Germano M, Piomelli U, Moin P, and Cabot W H (1991) "A Dynamic Subgrid-Scale Eddy Viscosity Model," *Phys Fluids A* **3**, pp 1760-1765.
Gillis JC (1980) "Turbulent Boundary Layer on a Convex, Curved Surface," PhD Dissertation, Stanford University, Stanford CA.
Grant HL (1958) "The large Eddies of Turbulent Motion," *J Fluid Mech* **4**, pp 149-190.
Granville PS (1977) "Drag and Turbulent Boundary Layer of Flat Plates at Low Reynolds Numbers," *J Ship Res* **21**, pp 30-39.
Grass AJ (1971) "Structural Features of Turbulent Flow over Smooth and Rough Boundaries," *J Fluid Mech* **50**, pp 233-255.
Grigson CWB (1992) "An Accurate Smooth Friction Line for Use in Performance Prediction," *Proc Roy Inst Naval Arch* **W5**, pp 1-9.
Gupta AK and Kaplan RE (1972) "Statistical Characteristics of Reynolds Stress in a Turbulent Boundary Layer," *Phys Fluids* **15**, pp 981-985.
Hama FR (1947) "The Turbulent Boundary Layer along a Flat Plate, Parts I and II," *Reports of the Inst of Sci and Tech* **1**, pp 13-16 and 49-50, Univ of Tokyo, Japan.
Hama FR (1954) "Boundary-Layer Characteristics for Smooth and Rough Surfaces," *Trans Soc Nav Arch Marine Eng* **62**, pp 333-358.
Hancock PE (1980) "The Effect of Free-stream Turbulence on Turbulent Boundary Layers," PhD Dissertation, Imperial College, London.
Hancock PE and Bradshaw P (1983) "The Effect of Free-stream Turbulence on Turbulent Boundary Layers," *J Fluids Eng* **105**, pp 284-289.
Hanratty TJ (1989) "A Conceptual Model of the Viscous Wall Region," in *Near Wall Turbulence,* eds SJ Kline and NH Afgan, pp 81-103, Hemisphere, New York.
Harder KJ and Tiederman WG (1991) "Drag Reduction and Turbulent Structure in Two-Dimensional Channel Flows," *Phil Trans R Soc Lond A* **336**, pp 19-34.
Head MR and Bandyopadhyay PR (1978) "Combined Flow Visualization and Hot-Wire Measurements," in *Coherent Structure of Turbulent Boundary Layers,* eds CR Smith and DE Abbott, pp 98-129, Lehigh Univ, Bethlehm PA.
Head MR and Bandyopadhyay PR (1981) "New Aspects of Turbulent Boundary-Layer Structure," *J Fluid Mech* **107**, pp 297-338.
Hinze JO (1975) *Turbulence,* second edition, McGraw-Hill, New York.
Hopkins EJ, Keener ER, and Polek TE (1972) "Hypersonic Turbulent Skin Friction and Boundary Layer Profiles on Nonadiabatic Flat Plates," *AIAA J* **10**, pp 40-48.
Huffman GD and Bradshaw P (1972) "A Note on von K_rm_n's Constant in Low Reynolds Number Turbulent Flows," *J Fluid Mech* **53**, pp 45-60.
Hussain AKMF (1983) "Coherent Structures--Reality and Myth," *Phys Fluids* **26**, pp 2816-2850.
Hussain AKMF (1986) "Coherent Structures and Turbulence," *J Fluid Mech* **173**, pp 303-356.
Hussain AKMF and Reynolds WC (1975) "Measurements in Fully Developed Turbulent Channel Flow," *J Fluids Eng* **97**, pp 568-580.
Izakson A (1937) "Formula for the Velocity Distribution Near a Wall," *Zh Eksper Teor Fiz* **7**, pp 919-924.
Johansson AV and Alfredsson PH (1982) "On the Structure of Turbulent Channel Flow," *J Fluid Mech* **122**, pp 295-314.
Johansson AV and Alfredsson PH (1983) "Effects of Imperfect Spatial Resolution on Measurements of Wall-Bounded Turbulent Shear Flows," *J Fluid Mech* **137**, pp 409-421.

Johansson AV, Her J-Y, and Haritonidis JH (1987) "On the Generation of High-Amplitude Wall-Pressure Peaks in Turbulent Boundary Layers and Spots," *J Fluid Mech* **175**, pp 119-142.

Kailasnath P (1993) "Reynolds Number Effects and the Momentum Flux in Turbulent Boundary Layers," PhD Thesis, Yale Univ, New Haven CT.

Karlsson RI and Johansson TG (1986) "LDV Measurements of Higher Order Moments of Velocity Fluctuations in a Turbulent Boundary Layer," *Proc 3rd Int Symp on Appl of Laser Anemometry to Fluid Mech*, eds DFG Durão *et al*, Paper No 12.1, July 7-9, Lisbon, Portugal.

Karniadakis GEm and Orszag SA (1993) "Nodes, Modes and Flow Codes," *Phys Today* **46**, No 3, pp 34-42.

Kastrinakis EG and Eckelmann H (1983) "Measurement of Streamwise Vorticity Fluctuations in a Turbulent Channel Flow," *J Fluid Mech* **137**, pp 165-186.

Keith WL, Hurdis DA, and Abraham BM (1992) "A Comparison of Turbulent Boundary Layer Wall-Pressure Spectra," *J Fluids Eng* **114**, pp 338-347.

Kim HT, Kline SJ, and Reynolds WC (1971) "The Production of Turbulence Near a Smooth Wall in a Turbulent Boundary Layer," *J Fluid Mech* **50**, pp 133-160.

Kim J and Moin P (1986) "The Structure of the Vorticity Field in Turbulent Channel Flow. Part 2. Study of Ensemble-Averaged Fields," *J Fluid Mech* **162**, pp 339-363.

Kim J, Moin P, and Moser RD (1987) "Turbulence Statistics in Fully-Developed Channel Flow at Low Reynolds Number," *J Fluid Mech* **177**, pp 133-166.

Klebanoff PS (1954) "Characteristics of Turbulence in a Boundary Layer with Zero Pressure Gradient," *NACA Report* No R-1247, Washington DC.

Klebanoff PS and Diehl ZW (1952) "Some Features of Artificially Thickened Fully Developed Turbulent Boundary Layers with Zero Pressure Gradient," *NACA Report* No 1110, Washington DC.

Klebanoff PS, Tidstrom KD, and Sargent LM (1962) "The Three-Dimensional Nature of Boundary-Layer Instability," *J Fluid Mech* **12**, pp 1-34.

Klewicki JC, Murray JA, and Falco RE (1994) "Vortical Motion Contributions to Stress Transport in Turbulent Boundary Layers," *Phys Fluids* **6**, pp 277-286.

Kline SJ (1967) "Observed Structure Features in Turbulent and Transitional Boundary Layers," in *Fluid Mechanics of Internal Flow*, ed G Sovran, pp 27-79, Elsevier, Amsterdam.

Kline SJ and Runstadler PW (1959) "Some Preliminary Results of Visual Studies of the Flow Model of the Wall Layers of the Turbulent Boundary Layer," *J Appl Mech* **26**, pp 166-170.

Kline SJ, Reynolds WC, Schraub FA, and Runstadler PW (1967) "The Structure of Turbulent Boundary Layers," *J Fluid Mech* **30**, pp 741-773.

Kolmogorov AN (1941a) "The Local Structure of Turbulence in Incompressible Viscous Fluid for Very Large Reynolds Numbers," *Comp Rend Acad Sci URSS* **30**, pp 301-305.

Kolmogorov AN (1941b) "On Degeneration of Isotropic Turbulence in an Incompressible Viscous Liquid," *Comp Rend Acad Sci URSS* **31**, pp 538-542.

Kolmogorov AN (1941c) "Dissipation of Energy in Locally Isotropic Turbulence," *Comp Rend Acad Sci URSS* **32**, pp 16-18.

Kolmogorov AN (1962) "A Refinement of Previous Hypothesis Concerning the Local Structure of Turbulence in a Viscous Incompressible Fluid at High Reynolds Number," *J Fluid Mech* **13**, pp 82-85.

Koskie JE and Tiederman WG (1991) "Turbulence Structure and Polymer Drag Reduction in Adverse Pressure Gradient Boundary Layers," *Purdue Univ, Sch Mech Eng Report* No PME-FM-91-3, W Lafayette IN.

Kovasznay LSG (1970) "The Turbulent Boundary Layer," *Annu Rev Fluid Mech* **2**, pp 95-112.

Kovasznay LSG, Kibens V, and Blackwelder RF (1970) "Large-Scale Motion in the Intermittent Region of a Turbulent Boundary Layer," *J Fluid Mech* **41**, pp 283-325.

Kravchenko AG, Choi H, and Moin P (1993) "On the Relation of Near-Wall Streamwise Vortices to Wall Skin Friction in Turbulent Boundary Layers," *Phys Fluids A* **5**, pp 3307-3309.

Kreplin H-P and Eckelmann H (1979) "Behaviour of the Three Fluctuating Velocity Components in the Wall Region of a Turbulent Channel Flow," *Phys Fluids* **22**, pp 1233-1239.

Kudva AK and Sesonske A (1972) "Structure of Turbulent Velocity and Temperature Fields in Ethylene Glycol Pipe Flow at Low Reynolds Number," *Int J Heat Mass Transfer* **15**, pp 127-145.

Kutateladze SS and Khabakhpasheva EM (1978) "Structure of Wall Boundary Layer (Forced Flow, Thermal Convection)," Institute of Thermodynamics, Siberian Branch of the USSR Academy of Science, Novosibirsk, USSR.

Landahl MT (1967) "A Wave-Guide Model for Turbulent Shear Flow," *J Fluid Mech* **29**, pp 441-459.

Landahl MT (1972) "Wave Mechanics of Breakdown," *J Fluid Mech* **56**, pp 775-802.

Landahl MT (1977) "Dynamics of Boundary Layer Turbulence and the Mechanism of Drag Reduction," *Phys Fluids* **20**, pp S55-S63.

Landahl MT (1980) "A Note on an Algebraic Instability of Inviscid Parallel Shear Flows," *J Fluid Mech* **98**, pp 243-251.

Landahl MT (1990) "On Sublayer Streaks," *J Fluid Mech* **212**, pp 593-614.

Landau LD and Lifshitz EM (1987) *Fluid Mechanics*, second edition, Pergamon Press, Oxford, United Kingdom.

Landweber L (1953) "The Frictional Resistance of Flat Plates at Zero Pressure Gradient," *Trans Soc Nav Arch Mar Eng* **61**, pp 5-32.

Landweber L and Siao TT (1958) "Comparison of Two Analyses of Boundary-Layer Data on a Flat Plate," *J Ship Res* **1**, pp 21-33.

Lauchle GC and Daniels MA (1987) "Wall-Pressure Fluctuations in Turbulent Pipe Flow," *Phys Fluids* **30**, pp 3019-3024.

Laufer J (1951) "Investigation of Turbulent Flow in a Two-Dimensional Channel," *NACA Report* No R-1053, Washington DC.

Laufer J (1954) "The Structure of Turbulence in Fully Developed Pipe Flow," *NACA Report* No R-1174, Washington DC.

Laufer J (1975) "New Trends in Experimental Turbulence Research," *Annu Rev Fluid Mech* **7**, pp 307-326.

Launder BE and Spalding DB (1974) "The Numerical Computation of Turbulent Flows," *Comput Methods Appl Mech Eng* **3**, pp 269-289.

Lee RE, Yanta WJ, and Leonas AC (1969) "Velocity Profile, Skin Friction Balance and Heat Transfer Measurements of the Turbulent Boundary Layer at M 5 and Zero Pressure Gradient," *Nat Ordnance Lab Report* No NOL-TR69-106, White Oak MD.

Lewkowicz AK (1982) "An Improved Universal Wake Function for Turbulent Boundary layers and Some of its Consequences," *Z Flugwiss Weltraumforsch* **6**, pp 261-266.

Ligrani PM and Bradshaw P (1987) "Spatial Resolution and Measurements of Turbulence in the Viscous Sublayer Using Subminiature Hot-Wire Probes," *Exp Fluids* **5**, pp 407-417.

Löfdahl L, Stemme G, and Johansson B (1989) "A Sensor Based on Silicon Technology for Turbulence Measurements," *J Phys E Sci Instum* **22**, pp 391-393.

Löfdahl L, Stemme G, and Johansson B (1991) "Reynolds Stress Measurements Using Direction Sensitive Double-Chip Silicon Sensors," *Meas Sci Tech* **2**, pp 369-373.

Löfdahl L, Stemme G, and Johansson B (1992) "Silicon Based Flow Sensors Used for Mean Velocity and Turbulence Measurements," *Exp Fluids* **12**, pp 270-276.

Long RR and Chen T-C (1981) "Experimental Evidence for the Existence of the 'Mesolayer' in Turbulent Systems," *J Fluid Mech* **105**, pp 19-59.

Lucik TS and Tiederman WG (1986) "Effect of Spanwise Probe Volume Length on Laser Velocimeter Measurments in Wall Bounded Turbulent Flows," *Exp Fluids* **3**, pp 339-341.

Lumley JL (1978) "Computational Modeling of Turbulent Flows," *Adv Appl Mech* **18**, pp 123-176.

Lumley JL (1983) "Turbulence Modeling," *J Appl Mech* **50**, pp 1097-1103.

Lumley JL (1992) "Some Comments on Turbulence," *Phys Fluids A* **4**, pp 203-211.

Mabey DG (1979) "Influence of the Wake Component on Turbulent Skin Friction at Subsonic and Supersonic Speeds," *Aeronaut Quart* **30**, pp 590-606.

Mabey DG, Meier HU, and Sawyer WG (1976) "Some Boundary Layer Measurements on a Flat Plate at Mach Numbers from 25 to 45," *Royal Aeronaut Est Tech Report* No RAE-74127, London.

Malkus WVR (1956) "Outline of a Theory of Turbulent Shear Flow," *J Fluid Mech* **1**, pp 521-539.

Malkus WVR (1979) "Turbulent Velocity Profiles from Stability Criteria," *J Fluid Mech* **90**, pp 401-414.

Mansour NN, Kim J, and Moin P (1988) "Reynolds-Stress and Dissipation-Rate Budgets in a Turbulent Channel Flow," *J Fluid Mech* **194**, pp 15-44.

Mickley HS and Davis RS (1957) "Momentum Transfer for Flow over a Flat Plate with Blowing," *NACA Tech Note* No TN-4017, Washington DC.

Millikan CB (1939) "A Critical Discussion of Turbulent Flows in Channels and Circular Tubes," *Proc 5th Int Cong Appl Mech*, eds JP Den Hartog and H Peters, pp 386-392, Wiley, New York.

Moin P and Kim J (1982) "Numerical Investigation of Turbulent Channel Flow," *J Fluid Mech* **118**, pp 341-377.

Moin P and Kim J (1985) "The Structure of the Vorticity Field in Turbulent Channel Flow Part 1 Analysis of Instantaneous Fields and Statistical Correlations," *J Fluid Mech* **155**, pp 441-464.

Monin AS and Yaglom AM (1971) *Statistical Fluid Mechanics*, Vol I, MIT Press, Cambridge, MA.

Morrison WRB (1969) "Two-Dimensional Frequency-Wavenumber Spectra and Narrow-Band Shear Stress Correlations in Turbulent Pipe Flow," PhD Thesis, University of Queensland, Queensland, Australia.

Morrison WRB, Bullock KJ, and Kronauer RE (1971) "Experimental Evidence of Waves in the Sublayer," *J Fluid Mech* **47**, pp 639-656.

Murlis J, Tsai HM, and Bradshaw P (1982) "Structure of Turbulent Boundary Layers at Low Reynolds Numbers," *J Fluid Mech* **122**, pp 13-56.

Nagano Y and Tagawa M (1990) "A Structural Turbulence Model for Triple Products of Velocity and Scalar," *J Fluid Mech* **215**, pp 639-657.

Naguib AM and Wark CE (1992) "An Investigation of Wall-Layer Dynamics Using a Combined Temporal Filtering and Correlation Techniques," *J Fluid Mech* **243**, pp 541-560.

Naguib AM and Wark CE (1994) "Inner- and Outer-Layer Effects on the Dynamics of a Turbulent Boundary Layer," submitted to *J Fluid Mech.*

Narasimha R and Kailas SV (1986) "Energy Events in the Atmospheric Boundary Layer," *Indian Inst of Sci Report* No 86-AS-8, Bangalore, India.

Narasimha R and Kailas SV (1987) "Energy Events in the Atmospheric Boundary Layer," in *Perspectives in Turbulent Studies,* eds HU Meier and P Bradshaw, pp 188-222, Springer-Verlag, Berlin.

Narasimha R and Kailas SV (1990) "Turbulent Bursts in the Atmosphere," *Atmospheric Environment* **24A**, pp 1635-1645.

Narasimha R and Liepmann HW (1988) "Introduction," in *Turbulence Management and Relaminarisation,* eds HW Liepmann and R Narasimha, pp xii-xx, Springer-Verlag, Berlin.

Narasimha R and Sreenivasan KR (1988) "Flat Plate Drag Reduction by Turbulence Manipulation," *Sadhana* **12**, pp 15-30.

Newman GR (1974) "An Experimental Study of Coherent Structures in the Turbulent Boundary Layer, Post-Graduate Study Dissertation, Cambridge Univ, Cambridge, UK.

Nikuradse J (1932) "Gesetzmässigkeit der turbulenten Strömung in glatten Rohren," *Forschg Arb Ing-Wes* No 356, Germany.

Nikuradse J (1933) "Strömungsgesetze in rauhen Rohren," *Forschg Arb Ing-Wes* No 361, Germany.

Offen GR and Kline S J (1974) "Combined Dye-Streak and Hydrogen-Bubble Visual Observations of a Turbulent Boundary Layer," *J Fluid Mech* **62**, pp 223-239.

Offen GR and Kline S J (1975) "A Proposed Model of the Bursting Process in Turbulent Boundary Layers," *J Fluid Mech* **70**, pp 209-228.

Oldaker DK and Tiederman WG (1977) "Spatial Structure of the Viscous Sublayer in Drag-Reducing Channel Flows," *Phys Fluids* **20**, pp S133-144.

Owen FK and Horstman CC (1972) "On the Structure of Hypersonic Turbulent Boundary Layers," *J Fluid Mech* **53**, pp 611-636.

Owen FK, Horstman CC, and Kussoy MI (1975) "Mean and Fluctuating Flow Measurements of a Fully-Developed, Non-Adiabatic, Hypersonic Boundary Layer," *J Fluid Mech* **70**, pp 393-413.

Paiziz ST and Schwarz WH (1974) "An Investigation of the Topography and Motion of the Turbulent Interface," *J Fluid Mech* **63**, pp 315-343.

Panton RL (1989) "Inner-Outer Structure of the Wall-Pressure Correlation Function," in *Near-Wall Turbulence,* eds SJ Kline and NH Afgan, pp 381-396, Hemisphere, New York.

Panton RL (1990a) "Scaling Turbulent Wall layers," *J Fluid Eng* **112**, pp 425-432.

Panton RL (1990b) "The Role of Dimensional Analysis in Matched and Composite Asymptotic Expansions," in *Ocean Waves Mechanics, Computational Fluid Dynamics and Mathematical Modelling,* ed M Rahman, pp 363-379, Comput Mech Publications, Boston.

Panton RL (1991) "The Effects of Reynolds Number on Turbulent Wall Flows," *Proc 8th Symp on Turbulent Shear Flows,* Paper No I-15, Tech Univ of Munich, 9-11 September.

Panton RL and Linebarger JH (1974) "Wall Pressure Spectra Calculations for Equilibrium Boundary Layers," *J Fluid Mech* **65**, pp 261-287.

Panton RL and Robert G (1993) "The Wall-Pressure Spectrum under a Turbulent Boundary Layer: Part 2, Theory and Results," *ASME Fluid Eng Conf,* eds MJ Morris and BF Carrol, FED-Vol 155, pp 43-48, ASME, New York.

Panton RL and Robert G (1994) "The Wavenumber-Phase Velocity Representation for the Turbulent Wall-Pressure Spectrum," *J Fluids Eng,* in press.

Panton RL, Goldman AL, Lowery RL, and Reischman MM (1980) "Low-Frequency Pressure Fluctuations in Axisymmetric Turbulent Boundary Layers," *J Fluid Mech* **97**, pp 299-319.

Perry AE and Abell CJ (1975) "Scaling Laws for Pipe-Flow Turbulence," *J Fluid Mech* **67**, pp 257-271.

Perry AE and Abell CJ (1977) "Asymptotic Similarity of Turbulence Structures in Smooth- and Rough-Walled Pipes," *J Fluid Mech* **79**, pp 785-799.

Perry AE and Chong MS (1982) "On the Mechanism of Wall Turbulence," *J Fluid Mech* **119**, pp 173-217.

Perry AE, Henbest SM, and Chong MS (1986) "A Theoretical and Experimental Study of Wall Turbulence," *J Fluid Mech* **165**, pp 163-199.

Perry AE, Li JD, Henbest S, and Marusic I (1989) "The Attached Eddy Hypothesis in Wall Turbulence," in *Near Wall Turbulence,* eds SJ Kline and NH Afgan, pp 715-735, Hemisphere, New York.

Perry AE, Lim TT, and Teh EW (1981) "A Visual Study of Turbulent Spots," *J Fluid Mech* **104**, pp 387-405.

Peters H (1938) "A Study in Boundary Layers," *Proc 5th Int Cong Appl Mech,* eds JP Den Hartog and H Peters, pp 393-395, Wiley, New York.

Phillips WRC (1987) "The Wall Region of a Turbulent Boundary Layer," *Phys Fluids* **30**, pp 2354-2361.

Phillips WRC and Ratnanather JT (1990) "The Outer Region of a Turbulent Boundary Layer," *Phys Fluids A* **2**, pp 427-434.

Prandtl L (1925) "Bericht über Untersuchungen zur ausgebildeten Turbulenz," *Z angew Math Mech* **5**, pp136-139.

Praturi AK and Brodkey RS (1978) "A Stereoscopic Visual Study of Coherent Structures in Turbulent Shear Flows," *J Fluid Mech* **89**, pp 251-272.

Preston JH (1958) "The Minimum Reynolds Number for a Turbulent Boundary Layer and the Selection of a Transition Device," *J Fluid Mech* **3**, pp 373-384.

Preston JH and Sweeting NE (1944) "The Velocity Distribution in the Boundary Layer of a Plane Wall at High Reynolds Numbers with Suggestions for Further Experiments," *Aeronaut Res Council Report* No ARC-FM-671, London.

Purtell LP, Klebanoff PS, and Buckley FT (1981) "Turbulent Boundary Layer at Low Reynolds Number, *Phys Fluids* **24**, pp 802-811.

Rajagopalan S and Antonia RA (1984) "Conditional Averages Associated with the Fine Structure in a Turbulent Boundary Layer," *Phys Fluids* **27**, pp 1966-1973.

Rajagopalan S and Antonia RA (1993) "RMS Spanwise Vorticity Measurements in a Turbulent Boundary Layer," *Exp Fluids* **14**, pp 142-144.

Rao KN, Narasimha R, and Badri Narayanan MA (1971) "The 'Bursting' Phenomenon in a Turbulent Boundary Layer," *J Fluid Mech* **48**, pp 339-352.

Raupach MR, Antonia RA, and Rajagopalan S (1991) "Rough-Wall Turbulent Boundary Layers," *Appl Mech, Rev* **44**, pp 1-25.

Reischman MM and Tiederman WG (1975) "Laser-Doppler Anemometer Measurements in Drag-Reducing Channel Flows," *J Fluid Mech* **70**, pp 369-392.

Reynolds O (1883) "An Experimental Investigation of the Circumstances which Determine whether the Motion of Water shall be Direct or Sinuous, and of the Law of Resistence in Parallel Channels," *Phil Trans Roy Soc Lond Ser A* **174**, pp 935-982.

Reynolds O (1895) "On the Dynamical Theory of Incompressible Viscous Fluids and the Determination of the Criterion," *Phil Trans Roy Soc Lond Ser A* **186**, pp 123-164.

Reynolds WC (1976) "Computation of Turbulent Flows," *Annu Rev Fluid Mech* **8**, pp 183-208.

Richardson LF (1920) "The Supply of Energy from and to Atmospheric Eddies," *Proc R Soc Lond A* **97**, pp 354-373.

Richardson LF (1922) *Weather Prediction by Numerical Process,* Cambridge University Press, London.

Robert G (1993) "The Wall-Pressure Spectrum under a Turbulent Boundary Layer: Part 1, Experiments," *ASME Fluid Engineering Conference,* eds MJ Morris and BF Carrol, FED-Vol 155, pp 37-42, ASME, New York.

Robinson SK (1990) "A Review of Vortex Structures and Associated Coherent Motions in Turbulent Boundary layers," in *Structure of Turbulence and Drag Reduction,* ed A Gyr, pp 23-50, Springer-Verlag, Berlin.

Robinson SK (1991) "Coherent Motions in the Turbulent Boundary Layer," *Annu Rev Fluid Mech* **23**, pp 601-639.

Robinson SK, Kline SJ, and Spalart PR (1989) "A Review of Quasi-Coherent Structures in a Numerically Simulated Turbulent Boundary Layer," *NASA Technical Memorandum* No TM-102191.

Rogallo RS and Moin P (1984) "Numerical Simualtion of Turbulent Flows," *Annu Rev Fluid Mech* **16**, pp 99-137.

Roshko A (1992) "Bluff-Body and Other Shear Flows," *Proc NUWC Div Newport Seminar Series on Turbulence and Its Control,* compiled by PR Bandyopadhay and JCS Meng, pp 41-434, *Naval Undersea Warfare Center Tech Memorandum* No NUWC-NPT TM 922089, Newport RI.

Rotta JC (1951) "Statistische Theorie nichthomogener Turbulenz," *Z Phys* **129**, pp 547-572.

Rotta JC (1962) "Turbulent Boundary Layers in Incompressible Flow," *Prog Aeronautical Sci* **2**, pp 1-219.

Runstadler PG, Kline SJ, and Reynolds WC (1963) "An Experimental Investigation of Flow Structure of the Turbulent Boundary Layer," *Stanford Univ Dept of Mech Eng Report* No MD-8, Stanford CA.

Saddoughi SG and Veeravalli SV (1994) "Local Isotropy in Turbulent Boundary Layers at High Reynolds Number," submitted to *J Fluid Mech.*

Saffman PG (1978) "Problems and Progress in the Theory of Turbulence," in *Structure and Mechanisms of Turbulence II,* ed H Fiedler, pp 273-306, *Lecture Notes in Physics,* Vol 76, Springer-Verlag, Berlin.

Saffman PG and Baker GR (1979) "Vortex Interactions," *Annu Rev Fluid Mech* **11**, pp 95-122.

Sasaki K and Kiya M (1991) "Three-Dimensional Vortex Structure in a Leading-Edge Separation Bubble at Moderate Reynolds Numbers," *J Fluids Eng* **113**, pp 405-410.

Schewe G (1983) "On the Structure and Resolution of Wall-Pressure Fluctuations Associated with Turbulent Boundary-Layer Flow," *J Fluid Mech* **134**, pp 311-328.

Schildknecht M, Miller JA, and Meir GEA (1979) "The Influence of Suction on the Structure of Turbulence in Fully Developed Pipe Flow," *J Fluid Mech* **90**, pp 67-107.

Schlichting H (1979) *Boundary-Layer Theory,* seventh edition, McGraw-Hill, New York.

Shah DA and Antonia RA (1989) "Scaling of the 'Bursting' Period in Turbulent Boundary Layer and Duct Flows," *Phys Fluids A* **1**, pp 318-325.

Simpson RL (1970) "Characteristics of Turbulent Boundary Layers at Low Reynolds Numbers with and without Transpiration," *J Fluid Mech* **42**, pp 769-802.

Simpson RL (1976) "Comment on 'Prediction of Turbulent Boundary Layers at Low Reynolds Numbers'," *AIAA J* **14**, pp 1662-1663.

Smagorinsky J (1963) "General Circulation Experiments with the Primitive Equations," *Mon Weather Rev* **91**, pp 99-164.

Smith CR and Metzler SP (1982) "A Visual Study of the Characteristics, Formation, and Regeneration of Turbulent Boundary Layer Streaks," in *Developments in Theoretical and Applied Mechanics,* Vol XI, eds TJ Chung and GR Karr, pp 533-543, University of Alabama, Huntsville.

Smith CR and Metzler SP (1983) "The Characteristics of Low-Speed Streaks in the Near-Wall Region of a Turbulent Boundary Layer," *J Fluid Mech* **129**, pp 27-54.

Smith CR and Schwartz SP (1983) "Observation of Streamwise Rotation in the Near-Wall Region of a Turbulent Boundary Layer," *Phys Fluids* **26**, pp 641-652.

Smith DW and Walker JH (1959) "Skin-Friction Measurements in Incompressible Flow," *NACA Report* No R-26, Washington DC.

Smith RW (1994) "Effect of Reynolds Number on the Structure of Turbulent Boundary Layers," PhD Thesis, Princeton Univ, Princeton NJ.

Smits AJ (1990) "New Developments in Understanding Supersonic Turbulent Boundary Layers," *Proc 12th Symp on Turbulence,* eds XB Reed Jr, *et al,* pp IL41-IL419, University of Missouri, Rolla.

Smits AJ, Spina EF, Alving AE, Smith RW, Fernando EM, and Donovan JF (1989) "A Comparison of the Turbulence Structure of Subsonic and Supersonic Boundary Layers," *Phys Fluids A* **1**, pp 1865-1875.

Spalart PR (1986) "Direct Simulation of a Turbulent Boundary Layer up to $R_\theta = 1410$," *NASA Tech Memorandum* No TM-89407, Washington DC.

Spalart PR (1988) "Direct Simulation of a Turbulent Boundary Layer up to $R_\theta = 1410$," *J Fluid Mech* **187**, pp 61-98.

Speziale CG (1991) "Analytical Methods for the Development of Reynolds-Stress Closures in Turbulence," *Annu Rev Fluid Mech* **23**, pp 107-157.

Spina EF, Donovan JF, and Smits AJ (1991) "On the Structure of High-Reynolds-Number Supersonic Turbulent Boundary Layers," *J Fluid Mech* **222**, pp 293-327.

Sreenivasan KR (1988) "A Unified View of the Origin and Morphology of the Turbulent Boundary Layer Structure," in *Turbulence Management and Relaminarisation,* eds HW Liepmann and R Narasimha, pp 37-61, Springer-Verlag, Berlin.

Sreenivasan KR (1989) "The Turbulent Boundary Layer," in *Frontiers in Experimental Fluid Mechanics,* ed M Gad-el-Hak, pp 159-209, *Lecture Notes in Engineering,* Vol 46, Springer-Verlag, Berlin.

Sreenivasan KR and Antonia RA (1977) "Properties of Wall Shear Stress Fluctuations in a Turbulent Duct," *J Appl Mech* **44**, pp 389-395.

Sreenivasan KR, Ramshankar R, and Meneveau C (1989) "Mixing, Entrainment and Fractal Dimensions of Surfaces in Turbulent Flows," *Proc R Soc Lond A* **421**, pp 79-108.

Tani I (1986) "Some Equilibrium Turbulent Boundary Layers," *Fluid Dyn Res* **1**, pp 49-58.

Tani I (1987) "Turbulent Boundary Layer Development over Rough Surfaces," in *Perspectives in Turbulent Studies,* eds HU Meier and P Bradshaw, pp 223-249, Springer-Verlag, Berlin.

Tani I (1988) "Drag Reduction by Riblet Viewed as Roughness Problem," *Proc Japan Acad B* **64**, pp 21-24.

Tani I and Motohashi T (1985a) "Non-Equilibrium Behavior of Turbulent Boundary Layer Flows Part I Method of Analysis," *Proc Japan Acad B* **61**, pp 333-336.

Tani I and Motohashi T (1985b) "Non-Equilibrium Behavior of Turbulent Boundary Layer Flows Part II Results of Analysis," *Proc Japan Acad B* **61**, pp 337-340.

Theodorsen Th (1952) "Mechanism of Turbulence," *Proc 2nd Midwestern Conf on Fluid Mechanics,* pp 1-18, Ohio State Univ, Columbus OH.

Theodorson Th (1955) "The Structure of Turbulence," in *50 Jahre Grenzschichtsforschung (Ludwig Prandtl Anniversal Volume),* eds H Görtler and W Tollmien, pp 55-62, Friedr Vieweg und Sohn, Braunschweig, Germany.

Thomas ASW and Bull MK (1983) "On the Role of Wall-Pressure Fluctuations in Deterministic Motions in the Turbulent Boundary Layer," *J Fluid Mech* **128**, pp 283-322.

Tiederman WG, Luchik TS, and Bogard DG (1985) "Wall-Layer Structure and Drag Reduction," *J Fluid Mech* **156**, pp 419-437.

Townsend AA (1961) "Equilibrium Layers and Wall Turbulence," *J Fluid Mech* **11**, pp 97-120.

Townsend AA (1970) "Entrainment and the Structure of Turbulent Flow," *J Fluid Mech* **41**, pp 13-46.

Townsend AA (1976) *The Structure of Turbulent Shear Flow,* second edition, Cambridge Univ Press, London.

Tsai HM and Leslie DC (1990) "Large Eddy Simulation of a Developing Turbulent Boundary Layer at Low Reynolds Number," *Int J Num Methods in Fluids* **10**, pp 519-555.

Tu BJ and Willmarth WW (1966) "An Experimental Study of the Structure of Turbulence Near the Wall through Correlation Measurements in a Thick Turbulent Boundary Layer," *Univ of Michigan Dept of Aerospace Eng Report* No 02920-3-T, Ann Arbor MI.

Ueda H and Hinze JO (1975) "Fine Structure Turbulence in the Wall Region of a Turbulent Boundary Layer," *J Fluid Mech* **67**, pp 125-143.

Ueda H and Mizushina T (1979) "Turbulence Structure in the Inner Part of the Wall Region in a Fully Developed Turbulent Flow," *Proc 5th Biennial Symp on Turbulence,* eds GK Patterson and JL Zakin, pp 357-366, Science Press, Princeton NJ.

Van Dyke M (1964) *Perturbation Methods in Fluid Mechanics,* Academic Press, New York.

Von Kármán Th (1930) "Mechanische Ähnlichkeit und Turbulenz," *Nachr Ges Wiss Göttingen, Math-Phys Klasse,* pp 58-76.

Walker JDA and Herzog S (1988) "Eruption Mechanisms for Turbulent Flows Near Walls," in *Transport Phenomena in Turbulent Flows,* eds M Hirata and N Kasagi, pp 145-156, Hemisphere, New York.

Walsh MJ (1990) "Riblets," in *Viscous Drag Reduction in Boundary Layers,* eds DM Bushnell and JN Hefner, pp 203-261, *AIAA Progress in Astronautics and Aeronautics,* Vol 123, Washington DC.

Walsh MJ, Sellers III WL, and McGinley CB (1989) "Riblet Drag at Flight Conditions," *J Aircraft* **26**, pp 570-575.

Wark CE and Nagib HM (1991) "Experimental Investigation of Coherent Structures in Turbulent Boundary Layers," *J Fluid Mech* **230**, pp 183-208.

Wei T and Willmarth WW (1989) "Reynolds-Number Effects on the Structure of a Turbulent Channel Flow," *J Fluid Mech* **204**, pp 57-95.

Wieghardt K (1943) "Über die Wandschubspannung in turbulenten Reibungsschichten bei veränderlichem Aussendruck," *Kaiser Wilhelm Inst für Strömungsforschung,* No U&M-6603, Göttingen, Germany.

Wilkinson SP, Anders JB, Lazos BS, and Bushnell DM (1988) "Turbulent Drag Reduction Research at NASA Langley: Progress and Plans," *Int J Heat and Fluid Flow* **9**, pp 266-277.

Willmarth WW (1959) "Space-Time Correlations and Spectra of Wall Pressure in a Turbulent Boundary Layer," *NASA Memorandum* No 3-17-59W, Washington DC.

Willmarth WW (1975a) "Structure of Turbulence in Boundary Layers," *Adv Appl Mech* **15**, pp 159-254.

Willmarth WW (1975b) "Pressure Fluctuations Beneath Turbulent Boundary Layers," *Annu Rev Fluid Mech* **7**, pp 13-37.

Willmarth WW and Bogar TJ (1977) "Survey and New Measurements of Turbulent Structure Near the Wall," *Phys Fluids* **20**, pp S9-S21.

Willmarth WW and Sharma LK (1984) "Study of Turbulent Structure with Hot Wires Smaller than the Viscous Length," *J Fluid Mech* **142**, pp 121-149.

Willmarth WW and Tu BJ (1967) "Structure of Turbulence in the Boundary Layer Near the Wall," *Phys Fluids* **10**, pp S134-S137.

Yajnik KS (1970) "Asymptotic Theory of Turbulent Shear Flows," *J Fluid Mech* **42**, pp 411-427.

Yakhot V and Orszag SA (1986) "Renormalization Group Analysis of Turbulence I Basic Theory," *J Sci Comput* **1**, pp 3-51.

Zakkay V, Barra V, and Hozumi K (1980) "Turbulent Boundary Layer Structure at Low and High Subsonic Speeds," in *Turbulent Boundary Layers - Experiments, Theory and Modeling, AGARD Conf Proc* No 271, pp 41-420.

Zaric Z (1972) "Wall Turbulence Studies," *Adv Heat Transf* **8**, pp 285-350.

Zilberman M, Wygnanski I, and Kaplan RE (1977) "Transitional Boundary Layer Spot in a Fully Turbulent Environment," *Phys Fluids* **20**, pp S258-S271.

Mohamed Gad-el-Hak *received his BSc (summa cum laude) in mechanical engineering from Ain Shams University in 1966 and his PhD in fluid mechanics from Johns Hopkins University in 1973. He has since taught and conducted research at the University of Virginia, University of Southern California, Institut National Polytechnique de Grenoble and Université de Poitiers, and has lectured extensively at seminars in the US and overseas. Gad-el-Hak is currently Professor of Aerospace and Mechanical Engineering at the University of Notre Dame. Prior to that, he was a Senior Research Scientist and Program Manager at Flow Research Co in Seattle, WA. Professor Gad-el-Hak has developed several novel measurement techniques for turbulent flows, and he holds two patents: one for a drag-reducing method for airplanes and underwater vehicles and the other for a lift-control device for delta wings. Gad-el-Hak has published over 190 articles and has presented 100 invited lectures in the basic and applied research areas of isotropic turbulence, boundary layer flows, stratified flows, compliant coatings, unsteady aerodynamics, biological flows, non-Newtonian fluids, and flow control. He is the editor of two volumes in Springer-Verlag's* Lecture Notes in Engineering *entitled* "Frontiers in Experimental Fluid Mechanics," *and* "Advances in Fluid Mechanics Measurements." *Gad-el-Hak is a member of the American Chemical Society, an associate fellow of the American Institute of Aeronautics and Astronautics, a life member of the American Physical Society, and a member of the American Society of Mechanical Engineers. From 1988 to 1991, he served as Associate Editor for the* AIAA Journal. *He is currently serving as Associate Editor for* Applied Mechanics Reviews *as well as a Contributing Editor for Springer-Verlag's* Lecture Notes in Engineering *and for* McGraw-Hill Year Book of Science and Technology. *Gad-el-Hak served as a consultant to the US Government, the Government of Egypt, the United Nations, and several industrial organizations During the 1991-1992 academic year, Gad-el-Hak was a visiting professor at Institut de Mécanique de Grenoble, France. During the summers of 1993 and 1994, he was, respectively, a distinguished faculty fellow at the Naval Undersea Warfare Center, Newport RI, and a visiting exceptional professor at Université de Poitiers, France.*

Promode R Bandyopadhyay *received his BS in mechanical engineering in 1968 from the University of North Bengal, MS in ME in 1970 from the University of Calcutta, PhD in applied mechanics in 1974 from IIT, Madras, and PhD in aerodynamics in 1978 from Cambridge University. He was a Post-Doctoral Research Assistant at the Cambridge University Engineering Department ('78-'79), a Senior Design Engineer at Hindustan Aeronautics, Bangalore ('79-'81), a Research Scientist at the University of Houston ('81-'83), a Research Scientist (in-house contractor) at NASA Langley Research Center ('83-'91), and an Adjunct Professor of the ME Department, Old Dominion University ('89-'91). Soon after naturalization, in 1991, he joined the Naval Undersea Warfare Center, division Newport, RI. He was a National Scholar for Study Abroad in ME of the Government of India, was elected a Fellow of Wolfson College, University of Cambridge, and has received several awards from NASA, NUWC, and ASME. He is a member of ASME, a life member of APS, and an Associate Fellow of AIAA He has published over 90 articles, about 30 in refereed journals. He has written several review articles in journals and holds several patents. He has conducted experimental research on the coherent structures in turbulent and transitional boundary layers, on curved and rough-wall flows, on trailing vortex, and on drag reduction and flow control. In the late seventies, with Dr MR Head (deceased) in Cambridge, UK, he showed experimentally the effects of Reynolds number on the constituent hairpin vortices of a turbulent boundary layer. He is currently working on the application of microfabricaton to turbulence control, separation of gas from liquids, and the structural modeling of a turbulent boundary layer.*